REFERENCE ONLY

UNIVERSITY OF LONDON THESIS

Degree PhD Year 2006 Name of Author DREW, C.M.

Pharmacological Characterisation of the $hP2Y_{11}$ and $XlP2Y_{11}$ receptors.

Christian M. Drew

Thesis submitted to University College London
for the degree of Doctor of Philosophy.
November 2005

Department of Biochemistry and Molecular Biology,
University College London,
Gower Street,
London.
WC1E 6BT

ProQuest LLC
789 East Eisenhower Parkway
P.O. Box 1346
Ann Arbor, MI 48106-1346

ABSTRACT

Extracellular nucleotides and nucleosides are important signalling molecules that exert a diverse range of physiological responses throughout the body. These chemical messengers often transduce their effects through interaction with specific cell surface receptors called purinoceptors. The P2Y purinoceptor family binds extracellular nucleotides, principally ATP, ADP, UTP and UDP. Conformational change of the P2Y purinoceptors upon ligand binding conveys a signal to intracellular heterotrimeric G proteins, which are activated, transducing the signal further downstream by acting at different effector enzymes to influence second messenger production.

In this thesis I present the first pharmacological characterisation of a non-mammalian $P2Y_{11}$ receptor orthologue, Xenopus laevis $P2Y_{11}$ ($XlP2Y_{11}$), and extend the pharmacological profile of the human $P2Y_{11}$ receptor ($hP2Y_{11}$). Second messenger assays were employed to record the intracellular cyclic AMP (cAMP) accumulation and Ca^{2+} mobilisation generated by both the human and *Xenopus laevis* P2Y receptors in response to various P2Y agonists and antagonists. In a manner similar to its human orthologue, I have shown that $XlP2Y_{11}$ is activated by nucleotides and nucleotide analogues, mobilising calcium from intracellular stores, and increasing cAMP production through the activation of adenylyl cyclase. When compared to previously published data, $XlP2Y_{11}$ exhibits a novel rank order of agonist and antagonist potency, revealing a receptor functionally similar but pharmacologically distinct from both the human and canine $P2Y_{11}$ receptor orthologues ($hP2Y_{11}$ and $cP2Y_{11}$).

ACKNOWLEDGEMENTS

I would firstly like to thank my supervisor Andrea, for being an excellent boss over the years, always being on hand to point me in the right direction, and allowing me to use her $hP2Y_{11}$ Ca^{2+} assay data.

I would also like to thank all of my friends, especially Emma, Jack, Nick, Rob, Nicola, Richard, Chris Chudziak and anyone that I've happened to live with at some point. I would like to thank past and present members of the lab, including Magdalene, Monica, Rob (again), Dahna, and 'people I've shared the lab with' (John and Frank - who also gets a mention for suggesting the word 'canonical' on page 22).

Family, of course, deserve a huge thank you. I'd like to thank Mam, Dad, Rachael, Marcus, Henry, Gran, Malcolm, Jenny, and all other members of the various clans and tribes that have given me support over the last few years.

CONTENTS

LIST OF FIGURES

LIST OF TABLES

ABBREVIATIONS

α,β-MeATP	α,β-Methyleneadenosine 5′-triphosphate
aa	amino acid
AC	adenylyl cyclase
AMP	adenosine 5′-monophosphate
ADP	adenosine 5′-diphosphate
ATP	adenosine 5′-triphosphate
β,γ-MeATP	β,γ-Methyleneadenosine 5′-triphosphate
bp	base pairs
BSA	bovine serum albumen
BzATP	2′-3′-O-(4-Benzoyl-benzoyl) adenosine 5′-triphosphate
$CaCl_2$	calcium chloride
cAMP	cyclic adenosine 3′,5,-monophosphate
CCD	charged coupled device
cDNA	complementary DNA
CsCl	caesium chloride
dH_20	distilled water
DMSO	dimethyl sulphoxide
DNA	deoxyribonucleic acid
dNTPs	deoxynucleotide triphosphates
EC_{50}	half effective agonist-concentration
E.coli	*Escherichia coli*
EDTA	ethylene diamine tetraacetic acid
EtOH	ethanol
FBS	foetal bovine serum
IC_{50}	half inhibitory concentration
IP	inositol (3,4,5-)triphosphate
IP_3	inositol (3,4,5-)triphosphate
KAc	potassium acetate
LASER	light amplicifaction by stimulated emission of radiation
LB	Luria-Bertani broth
M	molar
mg	milligrams

ABBREVIATIONS CONTINUED.

mL	millilitres
mM	millimolar
mm²	millimetres squared
NaAc	sodium acetate
NaCl	sodium chloride
NaOH	sodium hydroxide
nM	nanomolar
nm	nanometres
OD	optical density
PBS	phosphate buffered saline
PCR	polymerase chain reaction
PKA	protein kinase A
PKC	protein kinase C
PLC	phospholipase C
pmoles	picomoles
RNA	ribonucleic acid
RT	reverse transcriptase
RT-PCR	reverse-transcription polymerase chain reaction
SDS	sodium dodecyl sulphate
SOC	salt optimised broth with carbon
TAE	Tris-acetate-EDTA
TE	Tris-HCl-EDTA
TRIZMA® base	Tris-(hydroxymethyl)-aminomethane
UTP	uridine (5'-)triphosphate
UV	ultraviolet
µg	micrograms
µl	microlitres
µm	micrometers
µM	micromolar
v/v	volume per volume
w/v	weight per volume

Chapter 1

Introduction.

1.1 Introduction.

This Chapter reviews the importance of the G protein-coupled receptor (GPCR) P2Y purinoceptor family. An introduction and overview of the P2Y purinoceptor family is given, followed by a brief review of the literature describing the pharmacological characterisation of the human and canine $P2Y_{11}$ receptors. An overview of GPCR-induced G protein activation and the pathways involved in the formation of intracellular second messengers is also given, followed by the aims and objectives of this thesis.

1.2 The purinoceptor family.

Working on behalf of the Medical Research Council, in 1929, Drury and Szent-Györgyi revealed simple extracts from a minced bullock's heart were able to have a definite and transient effect upon mammalian heart rate, arterial pressure and intestinal movements. A crystalline substance, isolated from the extract, was identified as adenosine 5'-monophosphate (AMP), undoubtedly derived from adenosine 5'-triphosphate (ATP). For some years before these experiments, interest had been stimulated in the adenyl group of compounds, due to the recognition of their importance in the glycolytic process of muscular activity. Drury and Szent-Györgyi's experiments, however, were the first to demonstrate addition of the compounds were able to influence characteristic biological actions.

Since the initial study in 1929, which had itself revealed divergent roles for ATP, extracellular purines, such as adenosine and ADP, and pyrimidines, such as UDP and UTP, have been found to mediate diverse biological responses including regulation of blood flow, mast cell degranulation and smooth muscle relaxation (Burnstock 1972 and 1976; Gordon 1986; Boarder et al., 1994). Regulated pathways or the loss of plasma membrane integrity have been shown as the primary routes for the release of ATP and other nucleotides from cells. Following the initial proposal that purines and pyrimidines could mediate their effects through distinct cell-surface receptors (Burnstock, 1976). The receptors have since been divided into two main classes, the adenosine receptors (P1) and the P2 purinoceptors (Burnstock, 1978). The terms 'purinergic' and 'purinergic receptor' were first used in a study reviewing the evidence of non-adrenergic

and non-cholinergic, purine nucleotide induced responses in the autonomic nervous system (Burnstock, 1972). The 'purinergic receptor' term later evolved to 'purinoceptor' (Burnstock, 1976).

The P1 receptor family consists of the A_1, A_{2A}, A_{2B}, A_3. These receptor subtypes are guanine nucleotide binding protein (G protein) coupled receptors, or G protein-coupled receptors (GPCRs), activated, as highlighted above, by adenosine (Olah and Stiles, 1994). The sub classification of the P1 family has been achieved through both pharmacological and molecular studies. The A_1 and A_2 receptors were initially described in studies that revealed the stimulation (via A_1) and inhibition (via A_2) of adenylyl cyclase following extracellular addition of adenosine to cultured mammalian cells (van Calker et al., 1979). Subdivision of the A_2 subtype was proposed following studies of distinct high and low affinity binding sites for adenosine in the central nervous system (Daly et al., 1983). The subdivision of the P1 family reflects the different molecular and pharmacological characteristics of its members.

Initially divided into six subtypes (P_{2X}, P_{2Y}, P_{2U}, P_{2t}, P_{2z} and P_{2d}) (Burnstock and Kennedy, 1985), the P2 nomenclature was changed to enable the sub classification into ionotropic (P_{2X} and P_{2Z}) and the metabotropic (P_{2Y} P_{2U} and P_{2T}) families (Dubyakand and el-Moatassim, 1993). P2 purinoceptor classification was changed further into more manageable ionotropic, P2X and metabotropic, P2Y families. P2 nomenclature now correctly encompasses the receptors, which may be activated, by purines, pyrimidines, distinct nucleotides and more recently sugar-conjugated nucleotides. The P2 family of receptors are sub-classified into P2X and P2Y receptors, proposed initially by the agonist

potencies of adenine nucleotides on contraction in various tissues (Abbrachio and Burnstock, 1994). The P2X family consists of ionotropic ligand-gated ion channels, whereas the P2Y family are metabotropic GPCRs. There are seven members of the P2X family ($P2X_1$ - $P2X_7$) each composed of intracellular N- and C-terminal domains linked by two transmembrane regions to an extracellular loop. The subunits form homomeric or heteromeric assemblies to produce functional channels. Nucleotide binding and activation of the P2X receptors enable the non-selective passage of cations across the plasma membrane (within as little as 10 ms) (Bean 1992; North 1996). This influx may activate intracellular proteins (via the action of Ca^{2+}) or depolarisation/excitation of the host cells (mediated by the influx of extracellular ions) (Strobaek et al., 1996; Nakamura, 2000). As outlined above the P2Y receptors are nucleotide receptors which couple and signal through G proteins upon agonist stimulation. Expression of multiple P2Y receptors is considered to be canonical for all tissues (Ralevic and Burnstock, 1998). There are currently 8 functional members of the mammalian P2Y receptor family ($hP2Y_1$, $hP2Y_2$, $hP2Y_4$, $hP2Y_6$, $hP2Y_{11}$, $hP2Y_{12}$, $hP2Y_{13}$), unlike the P2X receptors there is evidence to suggest that there may be more P2Y receptor subtypes ($P2Y_{Ap4A}$)(Fredholm et al., 1997). The structure and pharmacology of the P2Y family members is discussed in the following section.

1.3 P2Y receptor subtypes.

The mammalian P2Y purinoceptor family is currently composed of eight members ($P2Y_{1, 2, 4, 6, 11, 12, 13}$ and $P2Y_{14}$) (Table 1.1). The first two P2Y receptors

were cloned in 1993. Heterologous expression of the receptors in oocytes revealed ATP addition could generate a Ca^{2+} response, revealing functional nucleotide receptors were present. These receptors, which activated the phospholipase C (PLC) signalling pathway, were designated $P2Y_1$ and $P2Y_2$. Subsequently isolated P2Y subtypes have been assigned with increasing subscript numbers. $P2Y_1$ and $P2Y_2$, initially isolated from chick brain and murine cells, respectively (Lustig et al., 1993; Webb et al., 1993), have since been isolated from a variety of human tissues, signalling in a similar manner to the chick and murine clones (Janssens et al., 1996; Bowler et al., 1995). The repertoire of valid human P2Y receptors was next added to by the cloning and characterisation of the $hP2Y_4$ receptor, a receptor found to be selective for the pyrimidines UTP and UDP, again activating the PLC pathway (Communi et al., 1995). $hP2Y_6$, a receptor again preferentially stimulated by pyrimidines leading to increased PLC activation, was the next receptor to be designated as a valid human P2Y receptor (Communi et al., 1996).

The $P2Y_{11}$ receptor, initially cloned from a human placenta library was shown to possess the unique ability, upon agonist addition to stimulate the generation of second messengers associated with the stimulation of adenylyl cyclase and PLC (discussed further in section 1.4). Following the isolation of an adenylyl cyclase-linked receptor, three additional hP2Y receptors have been shown to couple to the adenylyl cyclase pathway, ADP activated $hP2Y_{12}$ and $hP2Y_{13}$, and UDP-glucose activated $hP2Y_{14}$ (Chhatriwala et al., 2004; Marteau et al., 2003; Abbracchio et al., 1996). Upon agonist stimulation, $hP2Y_{12}$, $hP2Y_{13}$ and $hP2Y_{14}$ negatively couple to the adenylyl cyclase through inhibitory G proteins. There

are however, some recent data that casts doubt on the ability of the $hP2Y_{14}$ to induce a valid intracellular response (Scrivens and Dickenson, 2005).

Cysteinyl leukotrienes have been shown to regulate numerous cell functions important in inflammatory processes and diseases such as asthma through the activation of cysteinyl leukotriene type 1 and type 2 receptors (CysLT1R & CysLT2R) (Lynch et al., 1999; Heise et al., 2000). The CysLT1R & CysLT2R receptors are included in Table 1.1 because studies have shown UDP can activate these dual specificity receptors, resulting in intracellular calcium mobilisation (Mellor et al., 1998; Mellor et al., 2003).

Many non-human and non-mammalian functional P2Y receptors that are not listed above have been cloned. These, for the most part, share similar rank orders of agonist potency with their human and mammalian orthologues. The exceptions to this rule include the rat $P2Y_4$ and $P2Y_6$ receptors. Although relatively similar in sequence, the pharmacologies differ significantly (Kennedy et al., 2001; Bailey et al., 2001). The dissimilar agonist profiles of the human and canine $P2Y_{11}$ receptor are discussed in section 1.4.

The missing subscript numbers in the P2Y family represent either non-mammalian orthologues or receptors which were initially designated as P2Y receptors due to a degree of sequence identity, but are unresponsive to stimulation by various nucleotides. These proteins are called 'orpharn receptors' to highlight the lack of evidence of functionality. The p2y3 receptor, isolated from chick brain, has been shown to be a functional P2Y receptor activating PLC with an agonist potency order of UDP > UTP > ADP > 2MeSATP > ATP (Webb

et al., 1995 and 1996). It is not designated as a '$P2Y_3$' because the mammalian orthologue has been designated as the $P2Y_6$ receptor. Similarly, $P2Y_8$ is not included in the functional mammalian P2Y subtype list because the *Xenopus* p2y8 has been shown to be a $P2Y_4$ orthologue.

p2y5 is not present as a valid member of the P2Y family, because of the human, turkey and chick orthologues, chick has been shown to indisputably bind nucleotides, no functional responses have been recorded for the subtype. Similarly, p2y10, is, to date, unable to elicit a functional response. The $P2Y_7$ and $P2Y_9$ subtypes are not included in the family because, although initially proposed as nucleotide receptors through pharmacological and sequence identity studies, respectively, both have since been found to be receptors for leukotriene and lysophosphatic acid, respectively. More recently, GPR80 (GPR99) was reported to be 'deorphanised' and renamed as the $P2Y_{15}$ receptor based on the proposed ability of AMP and adenosine to activate the receptor, inducing intracellular responses (Inbe et al., 2004). Studies have since been unable to reproduce this activation, and have revealed the $P2Y_{15}$ receptor is activated by citric acid cycle intermediates. It has been declassified as functional P2Y receptor (Abbrachio et al., 2005). The next new valid member of the P2Y receptor family will therefore be $P2Y_{16}$.

Receptor	*Nucleotide selectivity*	*Signalling pathway(s)*	*Second messengers*
$P2Y_1$	2MeSADP>ADP>2MeSATP	Gq/PLC	Ca^{2+} ↑
$P2Y_2$	ATP≈UTP	Gq/PLC	Ca^{2+} ↑
$P2Y_4$	UTP>>GTP≈ITP [a] (UTP>ATP>GTP>CTP)	Gq/PLC	Ca^{2+} ↑
$P2Y_6$	UDP>>UTP>>ADP [c] (UTP > ADP =2MeSADP)	Gq/PLC	Ca^{2+} ↑
$P2Y_{11}$	2MeSATP≥ATP>2MeSADP>ADP [b] (2MeSADP>2MeSATP>ADP>ATP)	Gq/PLC* Gs/AC	Ca^{2+} ↑* cAMP ↑
$P2Y_{12}$	2MeSADP>ADP	Gi/AC	cAMP ↓
$P2Y_{13}$	2MeSADP	Gi/AC	cAMP ↓
$P2Y_{14}$	UDP-glucose	Gi/AC	cAMP ↓
CysLT1R	UDP	Gq/PLC	Ca^{2+} ↑
CysLT2R	UDP	Gq/PLC	Ca^{2+} ↑

Table 1.1

Pharmacological profiles, signalling pathways and second messenger responses of the mammalian P2Y receptors.

Functional mammalian P2Y rank order of agonist potencies, the signalling pathways activated and the intracellular second messenger response are shown. [a] rat $P2Y_4$, [b]canine $P2Y_{11}$ and [c]rat $P2Y_6$ receptors have been shown to posses different receptor pharmacologies to their hP2Y orthologues [a](Kennedy et al., 2000) [b](Qi et al., 2001[b]) [c](Bailey et al., 2001). * $hP2Y_{11}$ receptor has been shown to mobilise Ca^{2+} in an IP-independent manner (White et al., 2003).

1.4 Pharmacological characterisation of the $hP2Y_{11}$ receptor.

In 1997, Communi *et al.* presented the first paper to document a P2Y receptor, provisionally named $P2Y_{11}$, capable of generating cAMP, IP and Ca^{2+} mobilisation - second messenger responses typical of phosphoinositide and adenylyl cyclase pathway stimulation. Using a $hP2Y_4$ probe, a moderate stringency screen of a human cDNA placenta library uncovered partial sequences of a novel G protein-coupled receptor, which, when screened in a human genomic DNA library, revealed a sequence, interrupted by an intron, of approximately 1113 base pairs - encoding a protein of 371 amino acids. Sequence analysis revealed the open reading frame contained 33 and 28 percent amino acid sequence identity to the $hP2Y_1$ and $hP2Y_2$ receptors, respectively.

Following its isolation the ability of the $hP2Y_{11}$ receptor to signal through the phosphoinositide-signalling pathway, to which the majority of the previously studied P2Y receptors are able to activate, was investigated. The experiments revealed the receptor was able to induce both inositol phosphate (IP) accumulation and Ca^{2+} mobilisation in 1321N1-$hP2Y_{11}$ cells in response to the extracellular addition of ATP. Although the magnitude of the Ca^{2+} response to ATP was not reported and further Ca^{2+} mobilisation studies were not conducted with other agonists, the ligand-screening studies and subsequent concentration-response experiments recording IP accumulation, revealed ATP and 2MeSATP to be the most potent of the nucleotides tested in the study. Whilst similarly efficacious, these two agonists were shown possess a rank order of potency of: ATP > 2MeSATP. A variety of other nucleotides including ADP, 2MeSADP,

AMP, UTP and UDP, were shown to induce minimal IP accumulation in the cells.

In a similar manner to the investigation into IP accumulation, experiments were undertaken to measure the ability of the $hP2Y_{11}$ receptor to induce cAMP accumulation. CHO-$hP2Y_{11}$ cells were used because significant endogenous cAMP production was generated by 1321N1 cells in response to the degradation of the adenine nucleotides into adenosine. The experiments revealed the receptor to be activated by extracellular nucleotides - producing concentration-dependent cAMP responses. The investigation revealed that ATP and 2MeSATP were not only comparably efficacious at the highest concentrations tested, but also possessed the same rank order of potency recorded for the IP accumulation studies undertaken in the 1321N1-$hP2Y_{11}$ cells, namely: ATP > 2MeSATP.

Further pharmacological characterisation, using CHO-$hP2Y_{11}$ and 1321N1-$hP2Y_{11}$ cells for the measurement of cAMP and IP accumulation, respectively (Communi et al., 1999). The agonist-induced responses in both cell lines revealed the potency order of the ligands, for both cAMP and IP accumulation assays, were almost identical ($ATP\gamma S \approx$ BzATP > dATP > ATP > $ADP\beta S$ > 2MeSATP). All of the ligands presented in the study's potency order, except $ADP\beta S$ were able to generate similar maximal IP and cAMP second messenger responses, revealing the agonists to be similarly efficacious at the highest concentrations tested. The study exposed the ATP analogue, AR-C67085, as the most potent agonist, and also revealed $ADP\beta S$ and $AMP\alpha S$ to be partial agonists.

1.4.1 Canine $P2Y_{11}$ receptor produces IP and cAMP responses.

The cloning and characterisation of what was initially labelled a canine '$P2Y_{11}$-like' receptor ($cP2Y_{11}$) from Madin Darby canine kidney (MDCK-D1) cells, revealed the receptor was able to induce both IP and cAMP second messenger responses (Zambon et al., 2001). The investigations into the $cP2Y_{11}$ receptor were undertaken to elucidate $cP2Y_{11}$'s signalling ability and, ultimately, complement previous investigations of MDCK-D1 cells. P2Y agonist treatment of the MDCK-D1 cells had previously been shown to activate phospholipase D (Balboa et al., 1994), phospholipase A_2 (PLA_2)(Xing et al., 1997), and induce IP and cAMP formation (Yang el al., 1997; Post et al., 1996). The pharmacological characterisation of $cP2Y_{11}$ was undertaken in canine thymocyte (CF2Th) cells stably expressing the receptor. P2Y receptor agonists were able to induce Ca^{2+} mobilisation, and the formation of both IP and cAMP (Zambon et al., 2001). The study presented a rank order of potency for IP accumulation (ADPβS = 2MeSADP ~ 2MeSATP >> ADP > ATP), and indicated a similar cAMP potency order, revealing the $cP2Y_{11}$ receptor possesses a markedly different agonist selectivity profile to the $hP2Y_{11}$ receptor.

IP accumulation, Ca^{2+} mobilisation, and cAMP formation, produced by the $hP2Y_{11}$ and $cP2Y_{11}$ receptors in 1321N1 and CHO-K1 cells, was examined in further studies to evaluate the coupling efficiency and agonist potency orders for the two receptors - within the same cell lines (Qi et al., 2001[a]). Results, once again, highlighted the difference in agonist selectivity; whilst $hP2Y_{11}$ was shown to be primarily an adenosine triphosphate nucleotide-preferring receptor, the $cP2Y_{11}$ receptor was confirmed as adenosine diphosphate preferring. The

following agonist potency orders gained from both IP and cAMP accumulation assays in CHO-hP2Y$_{11}$ and CHO-cP2Y$_{11}$ were presented for the two receptors:

hP2Y$_{11}$: ATPγS ≥ 2MeSATP ≥ ATP ≈ ADPβS > 2MeSADP > ADP

cP2Y$_{11}$: 2MeSADP > ADPβS > 2MeSATP > ADP > ATPγS ≥ ATP

Presented in Qi et al. (2001[a])

Apart from the differences observed in the agonist potency order, key differences were found to exist in the maximal agonist induced responses. 2MeSADP, ADPβS and ADP, found to act as partial agonists upon the hP2Y$_{11}$ receptor (Communi et al., 1997; Zambon et al., 2001), were shown to be full agonists of the cP2Y$_{11}$ receptor. EC_{50} values gained from concentration-response experiments revealed both receptors were more efficiently coupled to the IP formation than cAMP production. However, the 7- to 17.3-fold difference in EC_{50}'s recorded in the CHO-hP2Y$_{11}$ cells, and the 1.8- to 3.9-fold difference observed for the CHO-cP2Y$_{11}$ cells, reveals the hP2Y$_{11}$ receptor possesses a markedly larger difference in this efficiency. Antagonist studies of the hP2Y$_{11}$ and cP2Y$_{11}$ receptors, however, have shown there is very little difference between their sensitivity to the nonselective antagonists: Suramin, Reactive Blue and PPADS. Suramin and Reactive Blue are both antagonists of the receptors, whilst PPADS is ineffective (Qi et al., 2001[b]). Despite the different agonist sensitivities, the canine receptor is designated as a P2Y$_{11}$ orthologue because of its ability to induce dual signalling pathways in response to extracellular adenine-nucleotides. The intracellular agonist induced responses of the activated hP2Y$_{11}$ receptor are discussed further in section 1.7.4.

Following the initial pharmacological characterisations, $P2Y_{11}$ signalling has been studied in a variety of different cell types and processes, including pancreatic duct epithelial cells (Nguyen et al., 2001), cardiomyocytes (Balogh et al., 2005), HL-60 cells (Suh et al., 2000) and white cell maturation and differentiation (Van der Weyden et al,. 2000[a] & 2000[b]; Adrian et al., 1999). These studies have extended the pharmacological profile of the receptor and/or implicated a role for $P2Y_{11}$ signalling in the different cell types. Further studies have also shown the $hP2Y_{11}$ receptor can produce Ca^{2+} mobilisation through a pathway independent of IP_3 formation (White et al., 2003). This agonist-specific signalling ability is discussed further in section 1.7.2.

1.5 Structure and activation of GPCRs and G protein heterotrimers.

The basic structure of all GPCRs consists an extracellular N-terminal domain, linked to an intracellular C-terminal domain via seven transmembrane (TM) helices linked in an alternating fashion by. intracellular (i1, i2 and i3) and extracellular loops (o1, o2 and o3) (Figure 1.1). The helices, which can deviate by as much as 25° from a vertical plane, form a tight bundle in a clockwise manner (when viewed from above/extracellular side). The importance of the extracellular N-terminal domain, intracellular loops and, for some GPCRs, the amino acid residues in the upper sections of the TM helices, has been known for some years to be critical in ligand recognition and binding (Schwartz 1994). More recently, studies involving $P2Y_1$, and $P2Y_2$ receptor chimeras have revealed ligand binding is mediated by amino acid residues in the upper regions of the TM domains and the extracellular loops (Gearing et al., 2003).

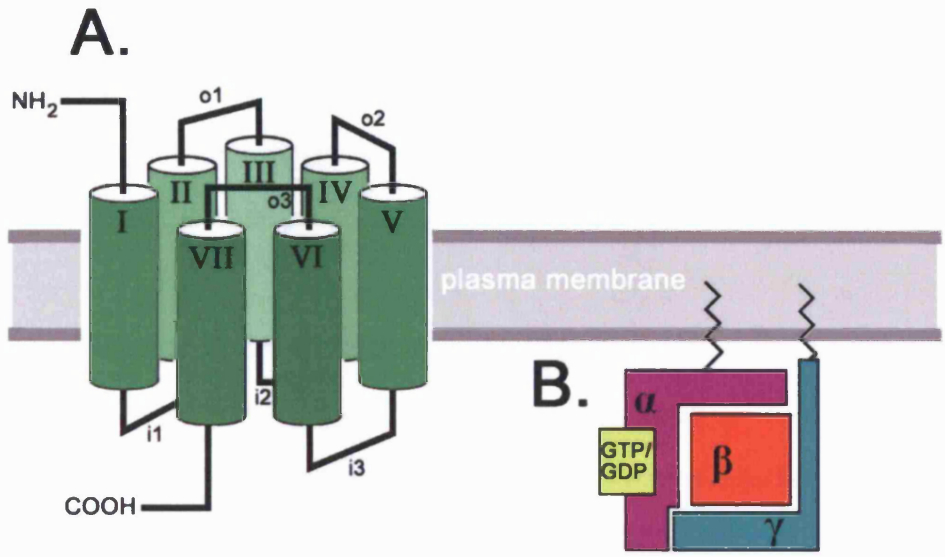

Figure 1.1

Schematic representations of a G protein-coupled receptor and a heterotrimeric G protein.

A, G protein-coupled receptor, showing N-terminal domain, seven tramsmembrane domains (I to VII), three extracellular loops (o1-3) and three intracellular loops (i1-3). **B,** heterotrimeric guanine nucleotide binding protein (G protein) composed of Gα, Gβ and Gγ subunits are shown with the nucleotide-binding site highlighted in yellow.

Ligand binding induces conformational change in GPCRs. The intracellular consequence of this change has been shown using rhodopsin to induce a relatively small outward movement of TMIII and a small change in the conformation of i2 (Farahbakhsh et al., 1995). The movements are accompanied or mediated by a clockwise rotation in the upper segments of the TM helices (Farrens et al., 1996; Dunham and Farrens, 1999). The movement exposes residues, primarily in the i1 and i2 loops, to the cytosol, which may interact with intracellular G proteins (Bourne, 1997). In the absence of bound extracellular agonist, these residues are shielded within the GPCR structure.

Heterotrimeric G proteins are composed of three subunits: a G_α subunit (approximately 40-45 kDa), a G_β subunit (approximately 37 kDa and a G_γ subunit (approximately 8 kDa). The inactive heterotrimer is attached to the cell surface plasma membrane via lipophilic tails on the G_α and G_γ (Figure 1.1). G_β and G_γ are bound strongly through a coiled-coil interaction. G_α and G_β interact through weaker protein and lipophilic interactions. In the inactive state G_α contains a GDP molecule in its nucleotide binding site. Activation of the GPCR enables G_α to directly bind the receptor (Conklin and Bourne 1993). Although the G_α subunit engages in the primary binding between GPCR and heterotrimer, evidence also suggests the G_β and G_γ may also participate in specific contacts with the receptor (Clapham and Neer, 1997). Binding to the activated receptor causes a conformational change within the heterotrimer, resulting in GDP-GTP exchange which dissociates the heterotrimer, releasing free (although still membrane attached) GTP- G_α and $G_{\beta\gamma}$ subunits. The constitutive GTPase ability of the G_α hydrolyses the bound GTP enabling the reformation of the inactive heterotrimer.

There are 18 known G_α subunits, which are divided, based solely on their action upon their effectors, into four main classes: $G_{q\alpha}$,$G_{s\alpha}$, $G_{i\alpha}$, $G_{12/13\alpha}$ (Simon et al., 1991; Downes and Gautam, 1999) (Table 1.2). The G_α subunits differ from each other not only in sequence, but also receptor specificity and effector isoform selectivity (Wong, 2003). G protein heterotrimers are usually shown named after their G_α subunits. The $G_{q\alpha}$ class stimulates phospholipase C, inducing phosphatidyl inositol 4,5-bisphosphate (PIP_2) hydrolysis creating inositol (3,4,5)triphosphate (IP) and 1,2-diacylglycerol (DAG). The $G_{s\alpha}$ and $G_{i\alpha}$ classes stimulate and inhibit adenylyl cyclase, respectively, affecting cAMP production. The $G_{12/13\alpha}$ class acts similarly to $G_{q\alpha}$ class, but possesses a distinct toxin sensitivity and ability to activate the Na^+/H^+ exchanger pathway (Dhanasekaran and Dermott, 1996 and 2002; Kurose 2003). All known G_α subunits undergo post-translational lipid-modifications (Milligan et al., 1995; Casey, 1995). The myristoylation and palmitoylation of various G_α subunits has been shown to be necessary for both receptor binding and effector activation (Wedegaertner et al., 1993). As outlined above the G_β and G_γ subunits may play a role in the activation of GPCR binding. There are currently 5 and 12 known subunits of G_β and G_γ, respectively. Similarly to G_α, following G protein activation the dissociated $G_{\beta\gamma}$ heterodimer may also play a role in activated effector proteins. The members of each G_α, G_β and G_γ class are shown in Table 1.2.

The activation of certain GPCRs , such as members the P2Y family, may also be influenced by the turnover and interconversion of extracellular agonists. ATP-generating and ATP-consuming extracellular pathways in various cell types have been shown to govern the duration and magnitude of intracellular

G protein subunits					
G protein G_α class members				G protein	G protein
$G_{q\alpha}$	$G_{s\alpha}$	$G_{i\alpha}$	$G_{12\alpha}$	G_β subunits	G_γ subunits
$G_{q\alpha}$	$G_{s\alpha}$	$G_{i1\alpha}$	$G_{12\alpha}$	$G_{1\beta}$	$G_{1\gamma}$
$G_{11\alpha}$	$G_{olf\alpha}$	$G_{i2\alpha}$	$G_{13\alpha}$	$G_{2\beta}$	$G_{2\gamma}$
$G_{14\alpha}$		$G_{i3\alpha}$		$G_{3\beta}$	$G_{3\gamma}$
$G_{15\alpha}$		$G_{oa\alpha}$		$G_{4\beta}$	$G_{4\gamma}$
$G_{16\alpha}$		$G_{ob\alpha}$		$G_{5\beta}$	$G_{5\gamma}$
		$G_{t1\alpha}$			$G_{7\gamma}$
		$G_{t2\alpha}$			$G_{8\gamma}$
		$G_{gust\alpha}$			$G_{10\gamma}$
		$G_{z\alpha}$			$G_{11\gamma}$
					$G_{12\gamma}$
					$G_{c\gamma}$

Table 1.2

Members of the mammalian G protein subunit families.

The members of the G protein G_α, G_β and G_γ are shown. The G_α members are subdivided into their corresponding G_α class ($G_{q\alpha}$,$G_{s\alpha}$, $G_{i\alpha}$, $G_{12\alpha}$).

signalling responses (Zimmerman, 1992; Lazarowski et al., 1997). These responses are controlled by the ability of the extracellular pathways to degrade and generate nucleotides in a stepwise manner through the action of various nucleotidases and phosphotransfer reactions - enabling the interconversion of ATP, ADP and AMP. The presence of Ecto-5'-nucleotidase and Adenosine Deaminase may complicate signalling responses further by enabling the sequential degradation of AMP into Adenosine and Inosine.

1.5.1 Production of second messengers following G protein activation.

Following the activation of the G protein heterotrimer, as outlined in section 1.5, the dissociated $G_{\beta\gamma}$ heterodimer and GTP-bound G_{α} subunits may activate many different cellular targets. The activation of target enzymes may produce molecules known as second messengers - effectively acting as intracellular representations of the extracellular signal. Most primary messengers, such as nucleotides, are unable to permeate the plasma membrane; second messenger formation therefore enables the diffusion and amplification of this extracellular signal throughout the cytosol. Following ligand binding, P2Y receptors have been shown, through the activation of G proteins, to act upon adenylyl cyclase and phospholipase C-β. The key signalling components, responses and regulation of these enzymes and their second messengers are presented in the following sections.

1.6 Adenylyl cyclase and cAMP.

One of the first second messengers to be documented was cyclic adenosine 3',5,-monophosphate (cAMP)(Sutherland, 1970). cAMP is synthesised intracellularly by adenylyl cyclase (AC), also known as adenylate cyclase. Molecular cloning has enabled the discovery of multiple genes encoding nine distinct isoforms of membrane-bound mammalian AC, detailed in Table 1.3. Activated adenylyl cyclase catalyses the elimination of a moiety of diphosphate from ATP, creating cAMP and inorganic pyrophosphate (PPi)(reaction shown in Figure 1.2). cAMP is used as a second messenger in many different prokaryotic and eukaryotic organisms (Danchin, 1993).

As previously outlined in section 1.5.1 and Table 1.3 GPCRs that can, upon activation, couple to and stimulate the G_s or G_i heterotrimeric G-proteins are able to stimulate and inhibit adenylyl cyclase activity, respectively. The basic regulatory pathways involved in adenylyl cyclase stimulation and inhibition are shown in Figure 1.3. Some of the downstream targets, which may be activated as a consequence of raised cAMP levels, namely PKA (Protein Kinase A), ion channels and GEP (GTP exchange proteins), are also shown in Figure 1.3, and are discussed further in Sections 1.6.5 and 1.6.6. The multiple isoforms of the components are not shown to simplify the schematic representation.

1.6.1 Structural topology of adenylyl cyclase.

All nine different isoforms of adenylyl cyclase share the same predicted basic structure. They are composed of two membrane-anchoring domains (M1 and

Adenylate cyclase isoform	Regulatory Signals				
	$G_{s\alpha}$	$G_{i\alpha}$	$G_{\beta\gamma}$	Protein Kinase	Ca^{2+}/CaM
I	⇑	⇓	⇓	⇑ (PKC)	⇑
II	⇑		⇑	⇑ (PKC)	
III	⇑	⇓		⇑ (PKC)	⇑
IV	⇑		⇑	⇓ (PKC)	
V	⇑	⇓		⇑ (PKC) ⇓ (PKA)	
VI	⇑	⇓		⇓ (PKA)	
VII	⇑		⇑	⇑ (PKC)	
VIII	⇑				⇑
IX	⇑				

Table 1.3

Summary of the regulatory inputs affecting adenylyl cyclase isoforms.

The stimulatory (⇑) and inhibitory (⇓)effect of $G_{s\alpha}$, $G_{i\alpha}$, $G_{\beta\gamma}$, protein kinases (A and C), and Ca^{2+}/CaM, upon the nine mammalian membrane-bound adenylyl cyclase isoforms (AC I to IX) are presented in the above table.

M2), each containing six transmembrane helices, and two structurally related intracellular domains (C1 and C2). The C1 domain connects the M1 and M2 domains, whereas the C2 domain is present at the C-terminus of the M2 domain. The M2 domain in each of the AC isoforms contains one or more sites that may be glycosylated. Crystal structure determination of adenylyl cyclase undertaken in the presence and absence of GTPγS-$G_{s\alpha}$ has enabled the visualisation of the spatial arrangement of these domains and the configuration of the catalytic site (Zhang et al., 1997; Tesmer et al., 1997 & 2002). The basic topology of these different domains is shown in a diagrammatic representation of a generic adenylyl cyclase isoforms in Figure 1.2.

1.6.2 G protein activation of adenylyl cyclase.

The heterotrimeric G protein Gs is able to activate AC through the interaction of the dissociated GTP-bound $G_{\alpha s}$ subunit with the intracellular C2 domain. (Whisnant et al., 1996). $G_{s\alpha}$ binding initiates a conformational change in the AC, altering the interaction between the C1 and C2 domains. Upon activation, amino acid residues from both C1 and C2 domains create a substrate binding site which can catalyse the formation of cAMP (Sunahara et al., 1997). Adenylyl cyclase remains in an active state whilst the GTP-$G_{s\alpha}$ subunit is bound to the C2 domain. The inherent GTPase activity of the $G_{\alpha s}$ subunit hydrolyses the bound GTP permitting the dissociation of the AC and $G_{s\alpha}$. Following GTP hydrolysis, the GDP-$G_{s\alpha}$ subunit may reassociate with the $G_{\beta\gamma}$ heterodimer.

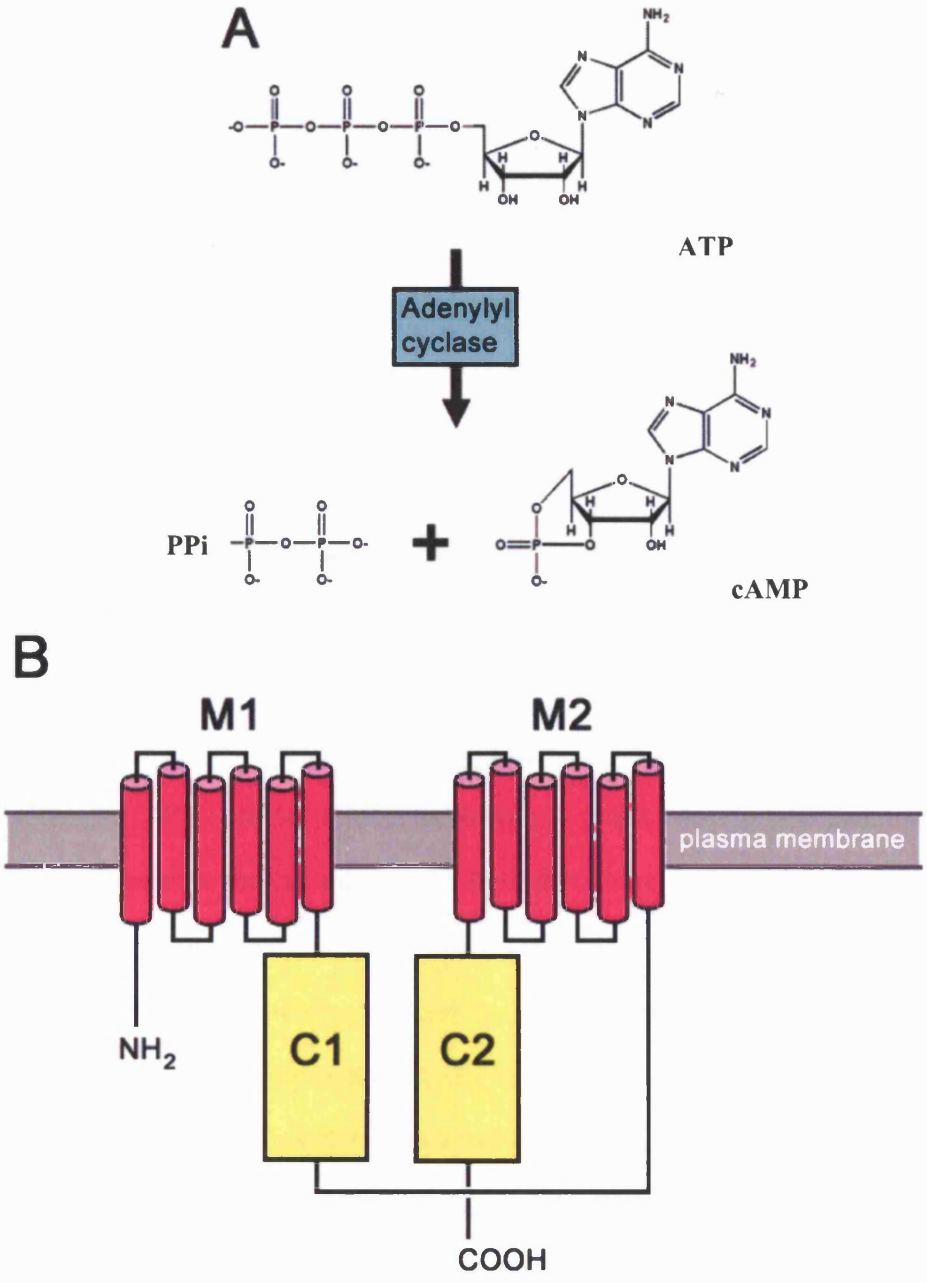

Figure 1.2

Adenylyl cyclase: Reaction catalysed and structural topology.

A. Adenylyl cyclase catalyses the elimination of a diphosphate moiety (inorganic pyrophosphate, PPi) from adenosine 5'-triphosphate (ATP) to create adenosine 3',5'-phosphate (cAMP). **B.** Schematic representation of the structural topology of the membrane anchoring (M1 and M2) and catalytic (C1 and C2) domains of adenylyl cyclase.

In addition to the stimulatory effect of the $G_{s\alpha}$ subunits, the dissociated $G_{\beta\gamma}$ heterodimer may also stimulate adenylyl cyclase. As outlined in Table 1.3, $G_{\beta\gamma}$ is able to influence the ability of certain AC isoforms to produce cAMP. It must be noted however, that ability of the $G_{\beta\gamma}$ heterodimer to activate certain AC isoforms in only achieved in the presence of GTP-$G_{s\alpha}$ (Feinstein et al., 1991; Gao & Gilman, 1991).

1.6.3 Adenylyl cyclase inhibition through G protein interaction.

As outlined in Figure 1.3 and Table 1.3, GTP-$G_{i\alpha}$ can inhibit various AC isoforms (Chen and Iyengar, 1993). Following appropriate GPCR activation, the direct binding of GTP-$G_{i\alpha}$ to AC reduces its ability to catalyse cAMP production. In a similar manner to the $G_{s\alpha}$ subunit, the intrinsic GTPase activity of $G_{i\alpha}$ subunit induces conformational change of the G_{α} subunit through GTP hydrolysis, reducing the binding affinity between $G_{i\alpha}$ and AC. The resulting dissociation terminates the inhibitory action of $G_{i\alpha}$. Contrary to its ability to stimulate various AC isoforms, Table 1.3 reveals the $G_{\beta\gamma}$ heterodimer has also been shown to inhibit the AC I isoform (Tang & Gilman, 1991). The ability of the different G protein subunits to stimulate and inhibit the various AC isoforms stems from their ability to bind different regions of the catalytic domain (Taussig et al., 1994), inducing distinct conformational changes.

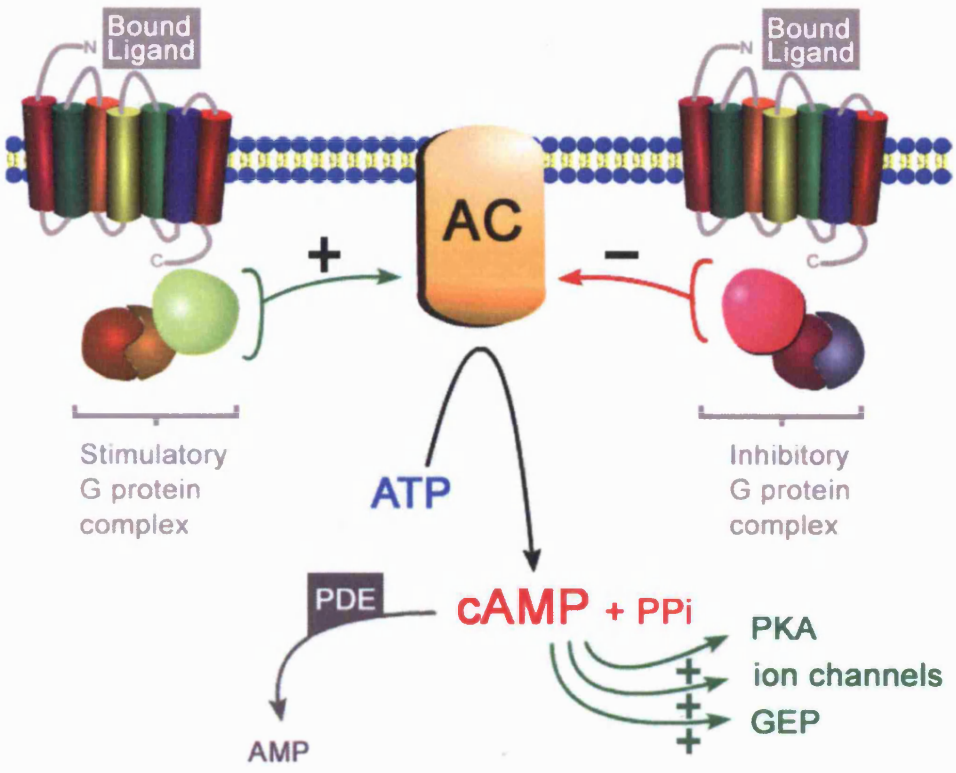

Figure 1.3

Activation and inhibition of adenylyl cyclase mediated by stimulatory and inhibitory G protein complexes.

Following ligand binding to the appropriate GPCR, stimulation and inhibition of adenylyl cyclase (AC) is primarily mediated by the $G_{s\alpha}$ (stimulatory) and $G_{i\alpha}$ (inhibitory) subunits, released from the activated G protein complexes. In addition, various isoforms of AC may also be regulated by the dissociated $G_{\beta\gamma}$ heterodimer. cAMP formation, through AC activation, and degradation by cyclic nucleotide phosphodiesterases (PDE), is shown, along with some of the cellular targets of cAMP.

1.6.4 Other regulatory inputs affecting adenylyl cyclase activity.

A variety of other regulatory factors that also influence the activity of AC are also presented in Table 1.3. The table reveals Ca^{2+}, which can stimulate AC activity, through the action of Calmodulin (as is the case with ACI and ACVIII)(Cooper et al., 1998; Lee et al., 1999), has also been found to inhibit AC activity via direct binding (ACV and ACVI)(Cooper et al., 1998). In addition Ca^{2+} may inhibit AC indirectly through the activation of Calcineurin (affecting ACIX)(Paterson et al., 1998) and calmodulin-dependent protein kinase II (CaM Kinase II)(inhibiting ACIII)(Wayman et al., 1995). The ability of Ca^{2+} or Ca^{2+}-calmodulin (CaM) to regulate AC activity is presented in Table 1.3. In addition to the regulatory action induced by G protein subunits and Ca^{2+} on AC activation, the level of cAMP may also be regulated by protein kinases. As outlined in Table 1.3 various AC isoforms are stimulated and inhibited by protein kinase C (Jacobowitz et al., 1993; Lusitg et al., 1993; Hellevuo, 1995) and protein kinase A (Chen et al., 1997; Iwami et al,. 1995).

1.6.5 cAMP activation of Protein kinase A.

cAMP-Dependent Protein Kinase A (PKA) is an ubiquitous serine/threonine protein kinase present in many different varieties of tissues. PKA is composed of two regulatory subunits (R) and two catalytic subunits (C), creating an R_2C_2 holoenzyme ([1]Taylor et al., 1992; [2]Taylor et al 1992). Intracellular cAMP regulates the activation of PKA by binding to the regulatory subunits, causing the inactive tetramer to dissociate. Two cAMP molecules bind to each regulatory

subunit; binding and subsequent dissociation creates R_2-$cAMP_4$ and two active catalytic subunits. The free catalytic subunits of PKA can phosphorylate a wide range of intracellular target proteins, including, as outlined above, AC. The inhibitory phosphorylation of certain AC isoforms, performed by the cAMP-activated PKA may therefore act as a negative feedback mechanism, ultimately reducing the ability of AC to produce cAMP.

1.6.6 Activation of GTP exchange proteins and ion channels by cAMP.

cAMP has also been found to play a pivotal role in the stimulation of exchange proteins activated by cAMP (EPAC)(de Rooij et al., 1998 and 2000). The cAMP bound EPAC are GTP exchange proteins (GEP), which control the turnover of GTP bound to the Rap1 (Ras-related protein-1) GTPase. The GTPase superfamily consists of various GTP-binding switch proteins (including the G_α subunits and Ras protein), which alternate between active and inactive states depending on the presence of a bound GTP molecule. GEPs in partnership with GTPase activating proteins (GAPs) play an essential role in the regulation of GTPases activity, through their control of GTP turnover and hydrolysis (Hall, 1992). The ability of cAMP to activate Rap1, through the activation of EPAC, enables cAMP to modulate the mitogen-activated protein-kinase (MAP-kinase) pathway. Activated Rap1 influences the MAP-kinase pathway by binding to and activating BRaf and/or inhibiting the Ras-Raf pathway (Fimia and Sassone-Corsi, 2001).

The MAPK proteins form a superfamily of enzymes which play a critical role in transducing a large array of signals generated by a variety of extracellular and intracellular mediators. These signals include, and are in no way limited to, those generated by the activated P2Y receptors. There are, of course many signalling pathways that operate independently of Ca^{2+} and cAMP activation that are not detailed in this thesis, examples of which include the MAPK and PI3K pathways.

As indicated in Figure 1.3 cAMP may also bind and activate cyclic nucleotide gated ion channels (Yau, 1994), which, apart from their ability to conduct various ions including Na^{+} and K^{+}, may also influence the activity of AC through their ability to conduct Ca^{2+} (Wei et al,. 1998). The ability of cAMP to control ion channel conductance (in addition to PKA and GEP activation), enables cAMP to indirectly regulate various metabolic, cytochemical and transcriptional events.

1.6.7 Regulation of cAMP concentration by phosphodiesterases.

The indefinite presence of cAMP in cells would result in the continual activation of various target proteins listed above. cAMP breakdown into AMP is achieved by cyclic nucleotide phosphodiesterases (PDEs)(Houslay, 1998). Similar to AC, multiple subtypes of PDEs exist (PDE I to VIII), which respond (in terms of stimulation and/or inhibition) in various degrees, to the regulatory control of Ca^{2+} and protein phosphorylation (Beltman et al., 1993). The activities of PDEs

are therefore an important mechanism in regulating the concentration of intracellular cAMP.

1.7 IP and Ca^{2+} responses.

Although the ability of Ca^{2+} to function as a second messenger was well established through investigations of muscle and secretory cells (Douglas et al., 1963), and agonist induced PI hydrolysis was known to occur (Hokin & Hokin, 1953), these early studies did not investigate the interaction between the two signalling responses. The mechanism by which cell surface receptors elicit intracellular calcium mobilisation was initially proposed following the observation that activated receptors that generate PI turnover are also responsible for Ca^{2+} signalling (Michell, 1975). Subsequent investigations revealed IP_3 was the molecule responsible for Ca^{2+} mobilisation (Streb et al., 1983). Inositol (3,4,5-)triphosphate ($Ins P_3$), referred to (as with many other P2Y studies) as 'IP' throughout this thesis, is produced following receptor-triggered hydrolysis of phosphatidyl inositol 4,5-bisphosphate (PIP_2). The reaction results in the creation of IP and 1,2-diacylglycerol (DAG) (Figure 1.4). The following sections describe the processes involved in the creation, targeting and regulation of the IP, DAG and Ca^{2+} responses.

1.7.1 Phospholipase activation through G protein interaction.

Phospholipase C (PLC) proteins are soluble membrane anchored cytosolic proteins, belonging to a family of lipase enzymes that catalyse the hydrolysis of glycerophospholipids (other members include PLA_1, PLA_2, PLB, and PLD). To date, 10 isoforms of PLC have been cloned in mammals. All ten of these PLC isoforms share the same predicted topology; composed of catalytic X, Y and C2 (complement component 2) domains. The ten PLC proteins are further classified, by their structure and function, into four classes: PLC-β(1-4), PLC-γ(1-4) and PLC-δ (1-2). As outlined previously, following appropriate GPCR stimulation, PLC proteins are activated by the activated G_q G protein heterotrimer. PLC-β-1 and PLC-β-2 are activated by the GTP bound $G_{q\alpha}$ subunit,

1.7.2 Cellular targets of IP, DAG and Ca^{2+}.

As outlined in Figure 1.4, GPCR activation of PLC-β results in the creation of IP and DAG. Following activation, IP, which is now free of its membrane anchor may diffuse freely within the cytosol. IP may bind IP-sensitive Ca^{2+} channels present on the endoplasmic reticulum (Bosnac et al., 2004). These channels are composed of four subunits, which may each bind an IP molecule (Bosnac et al., 2002). IP binding activates the channel, releasing sequestered Ca^{2+} into the cytosol (increasing cytosolic Ca^{2+} levels from nM to μM concentrations) (Evenas et al., 1998[a]).

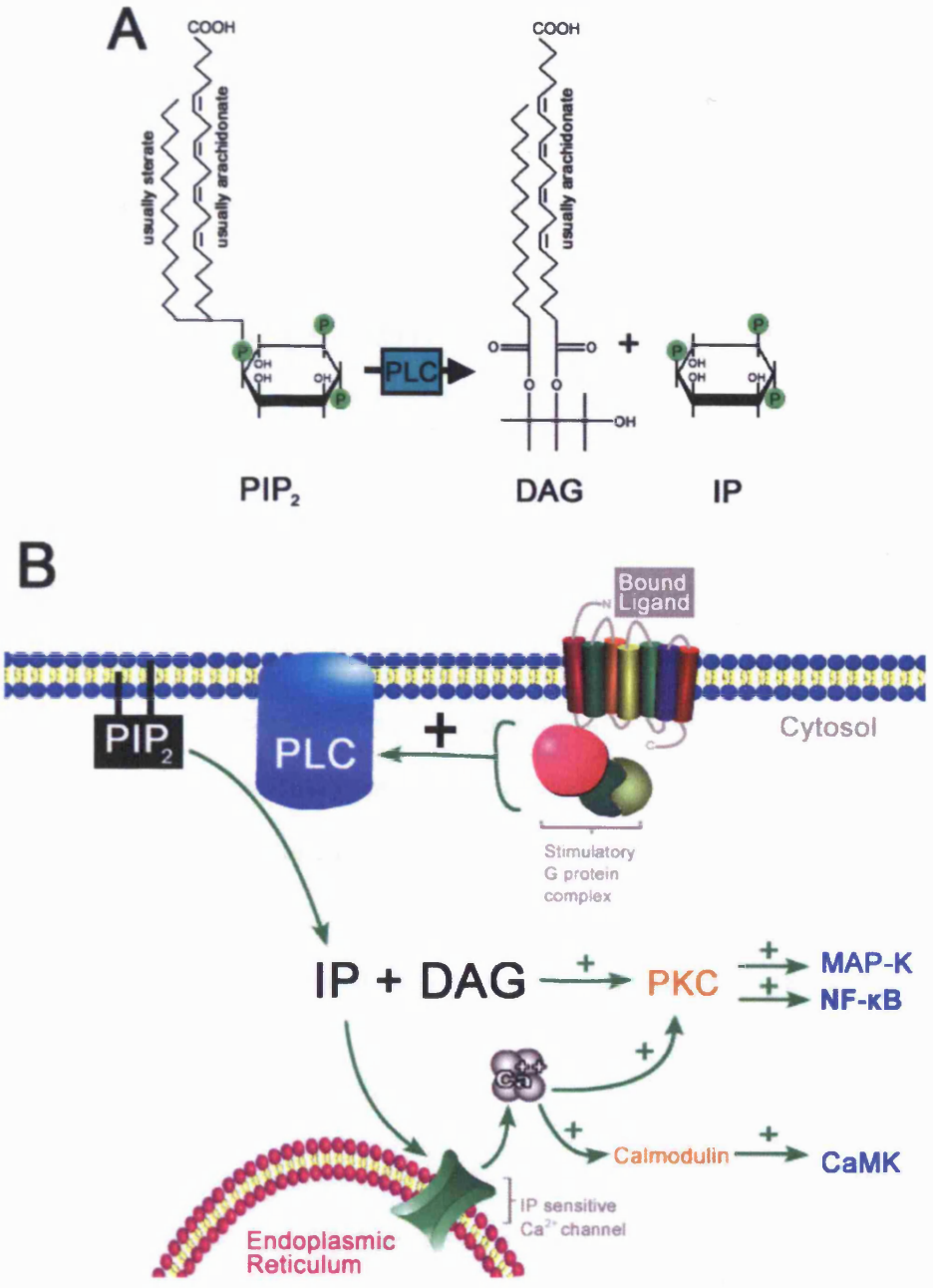

Figure 1.4

Reaction and pathways catalysed by stimulated mammalian PLC-β.

A. PLC-β catalyses the hydrolysis of phosphatidyl inositol 4,5-bisphosphate (PIP_2), creating inositol (3,4,5-)triphosphate (IP) and 1,2-diacylglycerol (DAG). **B.** Schematic representation of the pathways activated following ligand binding to the appropriate GPCR, stimulation of PLC-β is mediated by the $G_{\beta\gamma}$ and GTP bound $G_{q\alpha}$ subunits (depending on PLC-β isoform) released from the activated G protein heterotrimer.

whilst PLC-β-3 is activated by the dissociated $G_{\beta\gamma}$ heterodimer. Appropriate GPCR activation therefore stimulates IP and DAG formation.

The released cytosolic Ca^{2+} may serve as a second messenger, regulating almost every aspect of cellular activity (Berridge et al. 2000), ranging from exocytosis to contraction (Bruzzone, 1990; Harnett, 2003). Ca^{2+} produces these effects through binding and activating various intracellular protein targets. Ca^{2+} may bind (in a cooperative manner) to the ubiquitous protein, calmodulin (Evenas et al., 1998[a]). Calmodulin, which binds three or four Ca^{2+} ions via four separate EF-hand binding motifs, may activate a variety of different targets either on its own (including: Ca^{2+},Mg^{2+} ATPases, AC and myosin light chain kinase) or as part of a protein, such as calmodulin-dependent protein kinase (CaM-kinase). Ca^{2+} may also stimulate the two major families of intracellular Ca^{2+} channels, the IP_3-sensitive channel and the ryanodine receptor. The activation and subsequent release of Ca^{2+}, is known as Ca^{2+}induced Ca^{2+}release (CICR). The process enables amplification and oscillations in the concentration of free intracellular Ca^{2+}.

As previously outlined in section 1.4.1, the $hP2Y_{11}$ receptor has been shown to produce, in response to UTP, Ca^{2+} mobilisations using a pathway independent of IP formation (White et al,. 2003). This work concurs with previous studies, which have shown nucleotides may stimulate Ca^{2+} mobilisation in an IP-independent manner following receptor activation (Frelin et al., 1992). The signalling ability of the $hP2Y_{11}$ receptor is therefore not limited to the stimulation of AC and PLC-β. The $hP2Y_{11}$ receptor may produce Ca^{2+} mobilisation through a similar pathway to that described for a novel

temperature-sensitive Ca^{2+} release mechanism (Wissing et al., 2002), or, as previously stated (White et al., 2001), through the action of NAADP (Gallione et al., 2000; Churchill and Galione, 2001). The mobilisation may, however, be produced by an, as yet, unknown second messenger and/or signalling pathway. The intracellular signalling responses of P2Y receptors (including the typical IP-induced Ca^{2+} response pathway of the $P2Y_{11}$ responses), are discussed and shown in section 1.7.4, and Figures 1.5 and 1.6.

In addition to Ca^{2+} mobilisation, the DAG released by PIP_2 hydrolysis may activate (in conjunction with Ca^{2+}) PKC (Hannun et al., 1985; Bell et al., 1986). DAG may therefore stimulate a wide variety of proteins and signalling cascades through the ability of PKC to activate various target proteins such as AC, Ras-MAPK (Zheng et al., 2005) and Nuclear Factor Kappa -B (NF-κB) (Arenzana-Seisdedos et al., 1993).

1.7.3 Regulation of Ca^{2+}, IP and DAG.

Ca^{2+} release from the endoplasmic reticulum is quickly removed from the cytosol by ATPases present in the endoplasmic reticulum and plasma membranes (Guerini et al,. 2005). Because of the rapid removal of free Ca^{2+} from the cytosol, Ca^{2+} must rapidly bind to proteins such as calmodulin (outlined above) in order to transduce its activity. The effect induced by free IP is negated by its hydrolysis to an inactive 1,4-bisphosphate conformation, which is unable to bind IP-sensitive Ca^{2+} channels. DAG is also rapidly metabolised, either through hydrolysis (generating glycerol and a fatty acid) or phosphorylation

(creating diacylglycerol 3-phosphate, also known as phophatidate). The initial creation of IP and DAG may also be regulated by the phosphorylation of PLC itself by PKA (Liu et al., 1996).

Rapid Ca^{2+} release into the cytosol, inducing CICR, and its equally rapid removal enables Ca^{2+} oscillations to occur- often visualised in studies as spikes of free intracellular Ca^{2+} concentrations. These oscillations enable the amplification and regenerative propagation of the intracellular Ca^{2+} response. The range of calcium oscillations, with varying amplitudes, frequencies and number of Ca^{2+} rises, allows a large degree of control over many cellular processes such as parental and zygotic gene expression and (Dean et al., 2003; Malcuit et al., 2005).

1.7.4 P2Y Activation of adenylyl cyclase and phospholipase C-β.

Following the examination of cAMP , IP and Ca^{2+} production (sections 1.6 to 1.7.3), the following sections examine the cellular mechanisms involved in second messenger production activated by the P2Y receptors. As outlined previously, pharmacological characterisations of the P2Y receptors have often examined their ability to produce Ca^{2+}, IP and cAMP responses. A schematic representation of the activation of the AC and PLC-β second messenger signalling pathways induced by activated P2Y receptors is shown in Figure 1.5. The activation and inhibition of the pathways, produced by the subunits of activated membrane-bound G proteins are shown following appropriate extracellular ligand binding to the receptors. In order to simplify the schematic

representation, stimulation and inhibition of AC and PLC isoforms induced by $G_{\beta\gamma}$ heterodimers are not shown. The IP, Ca^{2+} and cAMP second messengers, are shown in red.

As described previously, multiple components and targets of the stimulated AC and PLC-β pathways may interact with upstream components of the cascades, effectively acting as negative and /or positive feedback loops. In order to visualise some of the key feedback mechanisms influencing AC and PLC, Figure 1.6 highlights the positive and negative effects of these downstream components (shown with green and red arrows, respectively). Where the isoforms of AC or PLC direct whether the feedback is positive or negative, the arrows are shown in blue. Figure 1.6 reveals the intricacies of the interaction occurring between the AC and PLC signalling pathways following stimulation of the P2Y receptors. In the same way as Figures 1.3 and 1.4, Figures 1.5 and 1.6 are first-level representations, where the multiple isoforms of the components are not shown. The various isoforms of and PKA, PKC, PDE, AC, PLC and subtypes of G_{α}, G_{β} and G_{γ}, reveal multiple responses can be produced by the P2Y receptors depending on the expression pattern of these proteins. The cross talk between the pathways is therefore also complicated further by the various sensitivities exhibited by these isoforms in response to their effectors.

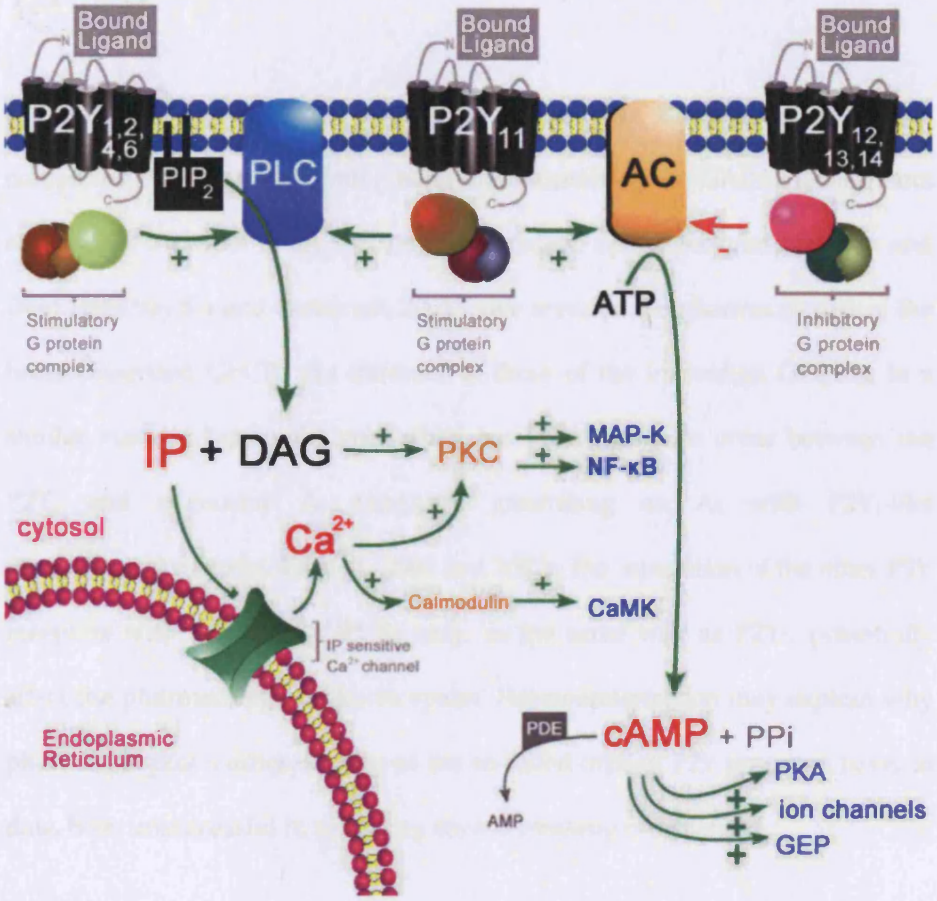

Figure 1.5

Second messenger production following P2Y receptor activation.

Schematic representation of the pathways activated following appropriate agonist binding to the P2Y receptors. Stimulation of PLC-β and the stimulation and inhibition of adenylyl cyclase (AC) and the subsequent signalling cascades produced by the P2Y receptors are shown. Second messengers, which have been used extensively to pharmacologically characterise the P2Y receptors are shown in red.

1.7.5 Factors influencing the second messenger production of the P2Y receptors.

Certain GPCRs have been shown to function as dimeric or oligomeric complexes. Studies investigating heterodimerisation of the $GABA_B$ (Kaupmann et al., 1998; Marshall et al., 1999) and, separately, opioid receptors (Jordan and Devi 1999; Snyder and Pasternak, 2003) have revealed the pharmacologies of the heterodimerised GPCRs are different to those of the individual GPCR's. In a similar manner, hetero-oligomerisation has been shown to occur between the $P2Y_1$ and adenosine A_1 receptors, generating an A_1 with $P2Y_1$-like pharamacology (Yoshioka et al., 2001 and 2002). The interaction of the other P2Y receptors with additional GPCRs may, in the same way as $P2Y_1$, potentially affect the pharmacology of the receptors. Heterodimerisation may explain why pharmacological studies of some of the so-called orphan P2Y receptors have, to date, been unsuccessful in recording second messenger responses.

As highlighted previously, the second messenger responses produced by the P2Y receptors are subject to negative feedback from downstream elements of the activated signalling cascades. This control is sometimes referred to as heterologous desensitisation, because the phosphorylation by PKA or PKC may occur independently of the receptor's activation, as is shown in Figure 1.6. Homologous desensitisation may also occur, where activated GPCRs interact with arrestins, following phosphorylation by G protein-coupled receptor kinases (GRKs), thus reducing the ability of the receptor to bind G proteins (Simon, 2003). Down-regulation of plasma membrane bound GPCRs through endocytosis may also occur, resulting in the internalisation of the receptor,

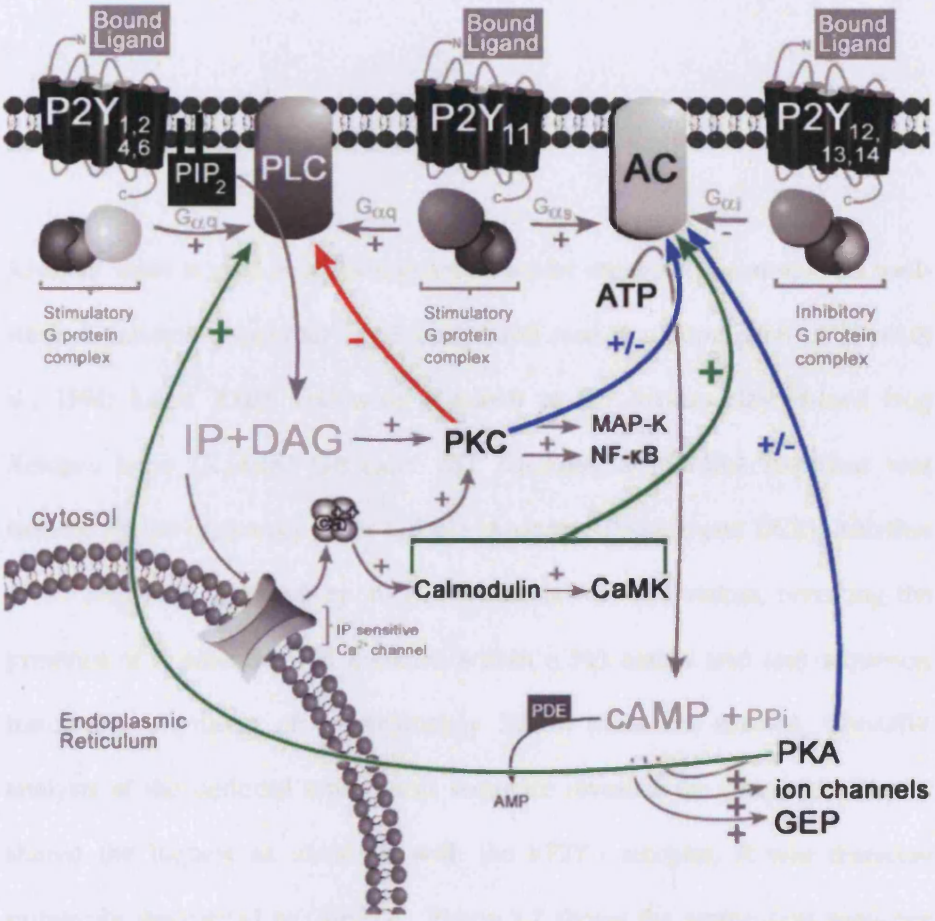

Figure 1.6

Interaction of downstream effectors with PLC-β and AC following P2Y receptor activation.

Schematic representation of the pathways activated following agonist binding to the P2Y receptors, highlighting the interaction of downstream effectors with PLC-β and AC. Stimulation and inhibition of PLC-β and AC are denoted with green and red arrows, respectively. Where the stimulation or inhibition is subject to the isoforms of AC or PLC-β, the arrows are shown in blue.

which may either be recycled back to the plasma membrane or subjected to proteolytic degradation in lysosomes (Tulapurkar et al., 2005; Jacob et al., 2005).

1.8 Introduction to the XlP2Y$_{11}$ receptor.

Xenopus laevis is used as a developmental model organism because of its well-studied patterns of external development and ease of manipulation (Vignali et al., 1994; Jones, 2005). Following a search of the African clawed-toed frog *Xenopus laevis* (*X.laevis*) GenBank EST database, a P2Y-like sequence was isolated by the laboratory of Dr L. Dale (Anatomy Department, UCL). Isolation of the sequence, followed by mRNA synthesis was undertaken; revealing the presence of 7 potential TM domains within a 313 amino acid (aa) sequence, translating a protein of approximately 35kDa (data not shown). ClustalW analysis of the deduced amino acid sequence revealed the potential receptor shared the highest aa identities with the hP2Y$_{11}$ receptor, it was therefore putatively designated as 'XlP2Y$_{11}$'. Figure 1.7 shows the amino acid sequence comparison of the hP2Y$_{11}$, cP2Y$_{11}$ and the novel XlP2Y$_{11}$ sequence. The comparison reveals the XlP2Y$_{11}$ sequence shares approximately 40 percent identity with the hP2Y$_{11}$ amino acid sequence (NP_002557), and approximately 32 percent identity with published cP2Y$_{11}$ amino acid sequence (Zambon et al., 2001). The hP2Y$_{11}$ and cP2Y$_{11}$ sequences share approximately 65 percent identity. The alignment reveals XlP2Y$_{11}$ possesses the least aa's of the three sequences analysed (hP2Y$_{11}$, 374aa; cP2Y$_{11}$, 370; XlP2Y$_{11}$, 313). Figure 1.7 also shows the putative transmembrane domains of all three sequences.

Figure 1.7

Multiple Sequence alignment of XlP2Y$_{11}$'s deduced amino acid sequence with human and canine P2Y$_{11}$ orthologue (hP2Y$_{11}$ and cP2Y$_{11}$) amino acid sequences.

ClustalW was used to align the deuced amino acid sequence of the XlP2Y11 receptor, the hP2Y$_{11}$ amino acid sequence (NP_002557) and the published cP2Y$_{11}$ amino acid sequence (Zaqmbon et al., 2001). Shaded residues indicate sequence identities and similarities. The putative positions of the 7 transmembrane domains are underscored in red.

Currently, there are two P2Y receptors that have been cloned and characterised from *X.laevis*. These have been shown to possess $P2Y_1$ (Cheng et al., 1993) and $P2Y_4$-like pharmacologies (Bogdanov et al., 1997). When compared to $hP2Y_1$ receptor, the $XlP2Y_1$ receptor shares approximately 85 percent sequence identity. Because of the relatively low identity shared between the $XlP2Y_{11}$ sequence, and the known P2Y receptors, the translated $XlP2Y_{11}$ sequence does not therefore necessarily encode a functional receptor. Only pharmacological analysis enables the identification of $XlP2Y_{11}$ protein as a functional P2Y receptor.

1.9 Aims and outline of this study.

The aim of this work was to pharmacologically investigate the human $P2Y_{11}$ receptor ($hP2Y_{11}$) and the *Xenopus laevis* $P2Y_{11}$ ($XlP2Y_{11}$) receptor. As outlined previously, the ability of the $hP2Y_{11}$ and $cP2Y_{11}$ receptor orthologues to couple to two different stimulatory signal transduction pathways is unique amongst the P2Y family. Investigating the $hP2Y_{11}$ receptor was undertaken to, first, use the receptor's unique ability to induce $G_{q\alpha}$ and $G_{s\alpha}$ pathways to establish appropriate assay conditions required for determining Ca^{2+} and cAMP responses, and secondly, to obtain a pharmacological profile with which to compare the second messenger responses of the $XlP2Y_{11}$ receptor. Using a range of P2Y agonists and antagonists, the work presented in this thesis extends the current pharmacological profile of the $hP2Y_{11}$ receptor and identifies the $XlP2Y_{11}$ receptor as a functional P2Y receptor, capable, upon nucleotide stimulation of producing cAMP and Ca^{2+} second messengers.

Chapter 2

Materials and Methods.

2.1 Molecular Biology Techniques.

The molecular biology techniques presented in the following sections were used upon pcDNA3.1-XlP2Y_{11} (supplied by the laboratory of Dr L. Dale - Anatomy Department, UCL) and pcDNA3.1-hP2Y_{11} in order to create and use pcDNA3.1G418-hP2Y_{11} and pcDNA3.1G418-XlP2Y_{11} constructs in pharmacological studies (described in Section 2.3). These constructs were created by the sequential digestion and isolation of the XlP2Y_{11} and hP2Y_{11} (a gift from Dr Jean-Marie Boeynaems, Genbank accession number AF030335) coding sequences from pcDNA3.1 followed by their ligation into pcDNA3.1G418. Small and large scale preparations of plasmid DNA were undertaken in order to produce a large quantity of the constructs.

2.1.1 Restriction endonuclease digestion of DNA.

Where digestion of plasmid DNA or PCR products was required, specific restriction endonuclease(s) (Promega and New England Biolabs), at a concentration of approximately 1/10th of the total reaction volume were used. Digests were incubated for a minimum of one hour at a suitable temperature (typically 37°C) and in the appropriate 1x buffer - as specified by the manufacturers. BSA was added where required.

2.1.2 Ligation of DNA fragments.

50-100ng of cut plasmid DNA was incubated with approximately three times the concentration of insert DNA (from restriction digest or PCR), 1 µL of T4 DNA Ligase and 1µL of T4 DNA Ligase Buffer (10x concentration, containing 10mM ATP) (New England Biolabs M0202S and B0202S, respectively). Total reaction volume was increased to 10µL with distilled water where necessary. Reactions were incubated at either room temperature for 1-2 hour or overnight at 14°C or 4°C. The whole ligation reaction mixture was then used to transform competent *E.coli* cells.

2.1.3 Transformation of *E.coli* cells.

Plasmid DNA or recombinant plasmid DNA produced as a result of ligation reactions was added to approximately 50µL of competent One Shot ® TOP10F' chemically competent *E.coli* cells (Invitrogen, C3030-03), melted on ice. The reaction was incubated on ice for a further 30-minutes, before undergoing heat-

shock treatment at 42°C for 90-seconds. The mixture could then be stored on ice before the addition of warmed SOC media to increase the total volume to approximately 200µL. The mixture was then incubated at 37°C for 10- to 30-minutes to enable the activation of the antibiotic resistance gene (encoded for in the plasmid DNA). The transformed Bacteria were then plated onto LB-agar plates containing 100µg/ml Ampicillin (Boehringer Mannheim) and incubated overnight at 37°C.

2.1.4 Creating LB stocks and plates for bacterial growth.

LB Broth Base (Lennox L Broth Base, Invitrogen) and LB Agar (Lennox L Agar, Invitrogen) were used, according to the manufacturer's instructions, to create bacterial LB culture media and LB-agar plates. All media stocks and glassware used in the growth of bacterial cultures was autoclaved at 121°C for 15-minutes. Where required, the antibiotic Ampicillin was added, after autoclaving, to a final concentration of 100µg/ml.

2.1.5 Small scale preparation of plasmid DNA (Miniprep).

Using a sterile pipette tip or loop, 2.5mL of LB containing 100µg/ml Ampicillin in a 14mL round-bottom Falcon 2059 tube was inoculated with a single plasmid-containing bacterial colony grown overnight on LB-agar plates. The inoculated LB-medium was grown overnight at 37°C in a shaking incubator.

Following overnight growth, 1mL of the saturated bacterial culture was placed in a 1.5mL Eppendorf tube. The bacteria were pelleted by centrifugation at a

relative centrifugal field (xg) of 13,000. Following aspiration of the supernatant, the pellet was resuspended in 100µL of Solution I (50mM glucose, 25mM Tris-HCl (pH8), 10mM EDTA (pH8)) containing 50mg/mL lysozyme (Roche), and incubated at room temperature for five minutes. 200µL of Solution II (0.2N NaOH, 1 percent SDS) was then added and mixed. After a 5-minute incubation at room temperature, 150µL of ice-cold Solution III (11.5 percent v/v glacial acetic acid, 3M KAc) was added and mixed before undergoing a further incubation, this time on ice, for 15-minutes. The mixture was then pelleted by centrifugation (13,000g for 5-minutes) and the supernatant transferred to a new 1.5mL Eppendorf tube containing a 0.5 to 1 volume of phenol:chloroform. Phenol chloroform extraction was then performed; whereupon the upper aqueous phase was removed and transferred to a new 1.5mL tube.

Ethanol precipitation was then undertaken on the contents of the new tube. 1mL of ethanol (EtOH) was added and the mixture was shaken thoroughly before incubation at room temperature for 2-minutes. The tube was then spun at 13,000g for 10-minutes before aspiration of the EtOH. The same ethanol precipitation procedure was then repeated with 70% EtOH. The final pellet, following centrifugation and aspiration of the EtOH, was then resuspended in TE buffer (with or without 10µg/ml RNaseA - depending on future use) following a brief period of air-drying. The plasmid DNA product suspended in the TE was then quantified using the protocol outlined in section 2.1.7 and /or verified using restriction enzyme digestion and agarose gel analysis also described in this chapter (section 2.1.18). The unused saturated bacterial culture could be used to either create a glycerol stock (typically 500µL culture to approximately 500µL sterile glycerol) (stored at -80°C) or used to directly

inoculate a larger volume of LB for the large scale isolation of plasmid DNA (Maxiprep).

2.1.6 Large scale preparation of plasmid DNA (Maxiprep).

The inoculation of a flask containing 500mL of LB containing 100μg/ml of the antibiotic Ampicillin was undertaken with the product of a previous inoculation and overnight growth of bacteria in 2.5mL of LB containing Ampicillin (as described in section 2.1.5). The flask was placed in a 37°C shaking incubator and left overnight to produce a saturated bacterial culture. 1mL of this overnight culture was used to create a glycerol stock as previously described in section 2.1.5, whilst the remainder of the culture was centrifuged (either in separate, balanced centrifuge bottles or undertaken sequentially within the same bottle) for 25-minutes at approximately 5,000g. Following aspiration of the supernatant and pellet resuspension in the centrifuge bottle with 18mL of Solution I (50mM glucose, 25mM Tris-HCl (pH8), 10mM EDTA (pH8)), a further 2mL of Solution I with 10mg/mL of lysozyme (1mg/mL final concentration) was added to the mixture and left to sit at room temperature for 10-minutes. 40mL of Solution II (0.2N NaOH, 1 percent SDS) was then added before further incubation at room temperature for a 5-minutes. 20mL of cold Solution III (11.5 percent v/v glacial acetic acid, 3M KAc) was then added to the centrifuge bottle, gently mixed, and left on ice for 15-minutes. 5mL of distilled water was added to the mixture before being spun at approximately 5,000g for 15-minutes.

Following the centrifugation, the supernatant was poured through double layered gauze into smaller centrifugation bottles, to which 45mL of isopropanol

was added whilst gently shaking. The bottle was then spun for 15 minutes at approximately 7,000g, before aspiration and pellet resuspension in 6.5mL of TE. 150µL of 0.5M EDTA and approximately 90µL of 2M TRIZMA®base (Sigma)(or enough to achieve a pH level of approximately 7.5) was added before adjusting the final volume to 10mL with TE. This entirety of the 10mL was then added to 12g of accurately weighed CsCl powder in a 14mL falcon tube. After shaking the tube to fully dissolve the CsCl, ethidium bromide was added to a final concentration of 0.5mg/mL. The content of the falcon tube was then carefully placed into a 10ml Beckman Quick-seal centrifuge tube, which, before heat-sealing using the Beckman tube-sealer (Beckman, Palo Alto, California), was balanced precisely against a second centrifuge tube.

The balanced tubes were spun in a Beckman Coulter OPTIMA L-100 XP centrifuge at 60,000rpm for 24 hours. The gradient, produced by the centrifugation, typically concentrates two distinct bands of DNA towards the top of the tube. These correspond to 'nicked' plasmid DNA (higher band) and a covalently closed circular super-coiled plasmid DNA species (lower band). After piercing the top of the centrifuge tube, the lower band was removed using a syringe with an 18-gauge needle and placed in a 14mL falcon tube. 2 to 3mL of butanol were then added to the falcon tube, and, after shaking, the top organic phase was removed using a Pasteur pipette. Further butanol was added and the process was repeated until the lower phase was clear and the CsCl was bordering on falling out of the solution. The lower phase was then removed from the tube and placed into dialysis bags (created from 15.9mm dialysis tubing from Medicell) and dialysed for 2 to 3 hours in 2L of 1xTE (or until the CsCl stopped falling out of the dialysis membrane). The contents of the

membrane was then placed in a new 14mL falcon tube and RNase A added to final concentration of 10µg/mL. The tube was then incubated for one hour at 65°C. The tube was then incubated for a further hour at 37°C, after the addition of proteinase K and SDS (added to final concentrations 100µg/mL and 0.2 percent, respectively). Following the incubation, phenol-chloroform extraction was performed and the aqueous phase was placed in 30mL glass Corex tubes. 3 to 5 volumes of ethanol was added to the tubes with NaCl at a final concentration of 250nM present. The tube was spun for 30-minutes at approximately 15,000g. Following aspiration of the EtOH, the precipitate formed was resuspended in 500µL of TE after a brief air-drying period.

The resuspended DNA could then undergo quantification (using the spectrophotometer) and verification (using restriction enzyme analysis).

2.1.7 Quantitation of DNA.

DNA quantities were assayed on a single-beam Pharmacia Biotech Gene Quant II spectrophotometer (Amersham Pharmacia Biotech, Piscataway, NJ). DNA was diluted with distilled water and placed in Hellma Precision Far-UV quartz cells (Hellma cells, Plainview, NY) and read against a distilled water blank. Readings were taken at 260 nm wavelengths (OD_{260}). DNA quantity could be calculated in mg/mL and pmol/µL using the following equations:

Equation 1

$[\ OD_{\text{read at } 260} \times \text{dilution factor} \times K^1\ ] \ / \ 1000 = \mu g \text{ of oligonucleotide per } \mu L$

Equation 2

$[\ \mu g \ / \ \mu L\ ] \ / \ [\ \text{length of oligo in kb} \times 0.330\ ] = \text{picomoles (pmol) oligo per } \mu L$

Where ^{1}K is the specific absorption coefficient (double-stranded DNA: 50; single-stranded RNA: 40; single-stranded DNA: 37).

The ratio of absorbance at 260nm to absorbance at 280nm (OD_{260}/OD_{280}) was used as an indicator of nucleic acid purity. Ratios of approximately 1.8 and 2.0 reveal pure samples of DNA and RNA, respectively.

2.1.8 Analysis using agarose gels.

Plasmid DNA, PCR products and DNA products from restriction digests were separated by electrophoresis on 1% agarose gels. The gels, made with 1X TAE buffer (0.4M Tris-acetate, 1mM EDTA) containing 0.5μg/ml ethidium bromide (added from a 10mg/mL stock created with ethidium bromide tablets, E-2515) and agarose (A9539), were microwave-heated and briefly cooled prior to pouring into gel trays with appropriately sized combs. Following further cooling and solidification of the gel, the DNA samples were mixed with 5xDNA BlueRun™ loading dye (IH0023e, Hybaid), and loaded into the wells. 0.5μg to 1.5μg of 1Kb DNA ladder (GIBCO BRL 1kb PLUS, 10787-018), used as a distance marker, was also loaded into wells alongside the samples.

The gels were electrophoresed at for approximately 20 to 80 minutes at 110 to 140 volts (or until the DNA samples had undergone sufficient progression) in a gel tank containing 1xTAE buffer. A short-wave UV transilluminator was used to visualise the displacement of the fragments, and used in conjunction with a digital camera to record the result. If required, DNA fragments were excised from the gel.

2.1.9 Purification of DNA from agarose gel.

DNA fragments were excised from agarose gel using a scalpel and purified using the Wizard ® PCR Preps DNA Purification System (Promega, A7170)(undertaken according to the manufacturer's instructions).

2.1.10 Oligonucleotide primers for use in PCR.

Oligonucleotide primer sequences, designed using MacVector (Accelrys) and created by ThermoHybaid, were received by the laboratory in a dried state. The oligonucleotides were resuspended in a volume of dH_2O as directed by the quality certificate supplied by Thermo Hybaid. The resuspended DNA oligonucleotides were then quantified using the protocol outlined in section 2.1.7, and the volume of dH_2O was adjusted in order to create 100pmol/µL (100 µM) stocks.

2.1.12 Amplification of DNA sequences using Polymerase Chain Reaction (PCR).

Where PCR was used for the amplification of DNA fragments, two methods were employed:

Method 1: Using Biomix Red polymerase (Bioline, Boston, MA).

1 µL of template DNA (at concentrations ranging from 0.1 to 0.5 µg/µL) and 1µL of each appropriate oligonucleotide primer (at 10pmol/µL) were added to

Biomix Red ready-to-go format (Bioline, BIO-25005), a 2x reaction mix containing BIOTAQ Red DNA polymerase, 1.5mM $MgCl_2$ and ultra-pure dNTPs. The reaction total volume was increased with distilled water to 25µL to achieve a 1x concentration of the Biomix Red. Where 50 µL total volume reactions were used, 2µL of each primer and additional distilled water were added to 25µL of Biomix Red.

Method 2: Using AGS gold DNA polymerase (Hybaid, Ashford, UK).

The following reactions were created:

0.5 to 2 µL..... Template DNA (0.1 to 0.5 µg/µL)

2.5 µL..... 10x buffer

1 µL..... Primer 1 (10pmol/µL)

1 µL..... Primer 2 (10pmol/µL)

1 µL..... dNTPs (**)

0.5 µL..... AGS Gold taq DNA polymerase (5 units per µL)

17 to 18.5 µL... dH_2O

25µL final volume

PCR reactions were performed in a Hybaid PCR Express ® Thermocycler under standard conditions. Typical cycles consisted of:

1st stage:

1 cycle of 95°C for 5 minute

2nd stage (repeated 20-30 times):

1 cycle of 95°C for 1 minute.

1 cycle of optimal annealing temperature of primer pair, for 1 minute.

1 cycle of 72°C for 1 minute.

3rd stage:

1 cycle of 72°C for 4 minutes.

Temperature, time and repetition of second stage was altered to accommodate the various differences in optimal annealing temperature (appropriate for oligonucleotide primer pairs) and size of both template DNA and primer pair product. PCR fragments, where indicated, were cleaned using the Wizard ® PCR Preps DNA purification system (Promega, A7170).

2.1.13 Direct PCR amplification of plasmid DNA from bacterial colonies.

Lyse-N-Go™ PCR reagent (Pierce) was used as outlined in the manufacturer's instructions to lyse cells picked from a single plasmid-containing bacterial colony grown overnight on LB-agar plates. PCR amplification was performed after the addition of the appropriate primers and amplification mixture (as outlined in section 2.1.12) made up to 9 times the volume of lysate. The PCR product was then run out on an agarose gel for analysis.

2.1.14 Preparing samples for Sequencing DNA.

ABI PRISM® BigDye™ Terminator Cycle Sequencing Kits (version 3.1) were used as described below to amplify specific regions of plasmid DNA that required sequencing.

PCR reaction content:

2.0 µL..... BigDye Dilution Buffer

2.0 µL..... BigDye 3.1

0.5 - 3.5 µL..... Template DNA (500ng)

2.0 µL..... Primer (2 µM)

0.5 µL..... DMSO

0 – 3.0 µL..... dH_2O

10 µL final volume

PCR Thermocycler protocol:

1st stage:

1 cycle of 95°C for 5 minute

2nd stage (repeated 25 times):

1 cycle of 95°C for 30-seconds.

1 cycle of 50°C for 30-seconds.

1 cycle of 60°C for 4-minutes.

3rd stage:

1 cycle 65°C for 4 minutes.

Following the PCR amplification of the sequence of interest The reaction was placed in a new 1.5mL Eppendorf tube and 10µL of dH_2O was added before the

addition of 2µL of 3M Sodium Acetate and 50µL of EtOH. The mixture was then incubated on ice for 10-minutes. Following the incubation, ethanol precipitation was undertaken on the contents of the new tube; whereby the tube was spun at 13,000g for 20-minutes before aspiration of the EtOH. The procedure was then repeated with 70% EtOH. The pellet was left to air-dry before being resuspended in 10µL of Formamide. The resulting suspension of DNA was then sequenced as outlined in section 2.1.14.

2.1.11 Oligonucleotides used in the polymerase chain reaction (PCR).

Target receptor and primer name	Oligonucleotide sequence (5'-3')	Primer-pair annealing temperature (°C)	Product size (bp)
$hP2Y_1$			
hP2Y1-F	CAATGACAGGGTTTATGCCACG		
hP2Y1-B	AGGTGTTTGGAGATTCTTGTGCC	**55.0**	**253**
$hP2Y_2$			
hP2Y2-F	ATCAATGGCACCTGGGATGG		
hP2Y2-B	CGGCACAAGAAGATGTAGAGCG	**57.9**	**149**
$hP2Y_4$			
hP2Y4-F	CAAGTTCATCCTGCTGCCTGTG		
hP2Y4-B	TCCCTTTGTTGCTGGTTGTGAC	**59.3**	**443**
$hP2Y_5$			
hP2Y5-F	CATCTGCGTCCTCAAAGTCC		
hP2Y5-B	ACTGAACAAAAACGGCGG	**52.0**	**341**
$hP2Y_6$			
hP2Y6-F	TTTCCTCATCTGCTGCCTCTCC		
hP2Y6-B	TGAACTCCGCCTTCCAAAGC	**57.2**	**200**
$hP2Y_{11}$			
hP2Y11-F	TGCCGACGACAAACTCAGTGG		
hP2Y11-B	GATGAAGATGACGCTGCCAG	**61.4**	**307**
$hP2Y_{12}$			
hP2Y12-F	GATTCTCTCTGTTGTCATCTGGGC		
hP2Y12-B	GGGCACTTCAGCATACTTATCAAGG	**54.2**	**522**
Xlp2y11			
XlP2Y11-F	TGCTACCAGGAGAGCCAAGATG		
XlP2Y11-B	TGGGTTCAAGAGGATGCTTCC	**55.3**	**410**

2.1.15 Dideoxy sequencing.

DNA was sequenced on an ABI PRISM® 3100-AVANT automated DNA capillary sequencer (ABI Applied Biosystems, Lingley House, 120, Birchwood Boulevard, Warrington) using BigDye™ Terminator Cycle Sequencing chemistry (ABI PRISM® BigDye™ Terminator Cycle Sequencing Kits, version 3.1). Sequencing reactions were both assembled and precipitated as described in section 2.1.13.

Sequences were resolved on a 50 cm standard sequencing capillary, running optimal ABI PRISM® 3100 POP6™ polymer. Sequence data was extracted and analyzed using ABI PRISM® Data Collection Software v2.0 and DNA Sequencing Analysis Software v5.1.1 respectively.

Sequence data was exported in the ABI format (.abi) to the sequence analysis program Trace Viewer®. The fluorescence traces were manually verified against the automated sequence data. Verified sequences were converted to FASTA format for further use and analysis using the MacVector® sequence analysis program (Accelrys).

2.1.16 Isolation of RNA from cultured cells.

TRIZOL® Reagent (Invitrogen, cat#: 15596-026), was used to facilitate the purification of RNA from cultured 1321N1 human astrocytoma cells. TRIZOL® enables the isolation of total RNA by an acid guanidinium thyocyanate-phenol-

chloroform single extraction method. RNA isolation and extraction was performed according to the manufacturer's instructions.

2.1.17 Reverse Transcription Polymerase Chain Reaction (RT-PCR).

A two-tube RT-PCR method was used in order to allow multiple PCR experiments to be undertaken, using the cDNA product of the reverse-transcription reaction.

2.1.17.1 Making template cDNA.

Following the manufacturer's instructions, Omniscript ® RT Kit (Qiagen, cat#: 205110) was employed for first-strand cDNA synthesis. Oligo(dT) and random hexamer (dN_6) primers were used (separately) in conjunction with the Omniscript ® RT Kit, and 50ng to 2µg of template RNA, isolated from cultured plasmid-transfected and untransfected 1321N1 human astrocytoma cells.

2.1.17.2 Performing PCR on the cDNA.

PCR was performed with specific oligonucleotide primers (as outlined in section 2.1.12) using the cDNA, synthesised in the reverse-transcription reaction, as the template DNA. Appropriate negative controls were created for each set of reactions (-RT; reactions undertaken without template cDNA).

2.2 Cell culture Techniques.

The following sections describe the cell culture techniques used in order to create 1321N1-hP2Y_{11} and XlP2Y_{11} cells, and the method required for the isolation of RNA from transfected and untransfected 1321N1 cells - for use in RT-PCR experiments (previously described in Section 2.1.17).

2.2.1 Cell lines and culture conditions.

Adherent 1321N1 human astrocytoma cells acquired from the European Collection of Cell Cultures (Porton Down, Salisbury) were cultured in Dulbecco's Modified Eagle's Medium (DMEM) (Sigma) supplemented with 10% fetal calf serum (FCS) and L-glut (where required, added to a final concentration of 2mM). Cells were grown at 5% CO_2 in a 37°C humidified incubator and were manipulated in a Class II laminar flow safety cabinet.

2.2.2 Passaging, splitting and counting.

To passage, cells were washed with Hanks' Balanced Salt Solution (Sigma) before incubation in an appropriate volume of PBS-EDTA at 37°C in the cell-culture incubator for 5 minutes. Volume of PBS-EDTA was adjusted depending on the size of the plate or flask used. The resuspended cells could then be used to either seed further flasks, used to create freezer amplues for long term storage of cell lines, or used for calculating the number of cells present in the solution (shown below).

Cells were counted after PBS-washing and incubation/lifting in PBS-EDTA. 200μL of the resuspended cells were added to 200μL of 0.4% trypan blue solution (Sigma). Two to three drops of the mixture were then placed under a glass coverslip on a bright light counting chamber (Hausser Scientific Company). The number of viable cells (not dyed blue by the tryptan blue) was then counted in each of the five $1mm^2$ sections of the counting chamber. The following equation could then be used to calculate the number of cells resuspended in the PBS-EDTA.

equation 3

cells per square mm x dilution factor (typically 2) x 10,000 = cells per 1μL

Transfected stable cell lines used in the experiments presented in this thesis were used between passage numbers 5 and 20.

2.2.3 Transfection of cells with plasmid DNA.

Transfection of cells in 10cm Petri plates was undertaken using the Lipofectamine™2000 (Invitrogen) and calcium phosphate methods. Lipofectamine™ 2000 was used as in accordance with the manufacturer's instructions.

2.2.3.1 Calcium phosphate transfections (modified from Chen and Okayama, 1987).

20µg of plasmid DNA mixed with 50µL of 2.5M $CaCl_2$ and 450µL dH_2O was gently vortexed whilst 500µL of 2xBBS was added drop-wise. Following 30-minutes of incubation at room temperature, the entire mixture was added to untransfected 1321N1 cells, grown for one day in 10cm Petri plates (at initial concentrations of approximately 20,000 to 25,000 cell/cm^2). The plates were gently swirled to allow the uniform dilution of the mixture in the DMEM. The plates were then placed in a container, filled with an air mixture containing 3% CO_2, and incubated at within the 37°C incubator for 24 hours. The plates were then removed from the container with 3% CO_2 and replaced in the 5% CO_2 incubator. Antibiotic selection was initiated following 24 hours of incubation. Method was modified from Chen and Okayama,1987.

2.2.4 Generation of stable cells lines.

Antibiotic selection of cells was undertaken following transfection of 1321N1 cells as outlined in section 2.2.3. After a PBS-wash, the antibiotic neomycin (Geneticin®, Gibco) was added at a final concentration of 400µg/mL to the 10cm plates with new DMEM. The process of washing the cells with PBS and replacing the media with fresh DMEM containing the antibiotic was repeated once every 2 to 3 days for approximately three weeks. Within this period, cell death of untransfected cells, and the expansion of cell foci containing Geneticin® resistant cells, was observed. Previous studies undertaken in the

laboratory have found the replenishment of selective media in this way, containing 400μg/mL of Geneticin, prevents the growth of untransfected cells within two to three weeks.

2.2.4.1 Isolation of cell pellet from cultured cells for isolating RNA.

Following one to two weeks of cell growth after the antibiotic selection, a proportion of the cultured cells were isolated after washing with PBS and lifting with PBS-EDTA as described in section 2.2.2. The cells were then spun in a 15mL screw-top tube for 2 minutes at 1000rpm in an Eppendorf 5804R centrifuge (approximately 500g). After removal of the supernatant, the pellet of cells could then either be stored (at -80°C or -20°C for long or short-term storage, respectively) or treated directly with TRIZOL ® Reagent to isolate the total RNA. This was then used in RT-PCR experiments to examine the presence or absence of transfected DNA (undertaken as described in sections 2.1.16 and 2.1.17).

2.2.5 Freezing stocks of stable cell lines.

Multiple freezer ampules were created for the long term storage of transfected cell lines. Following a PBS-wash and lifting of the cells in 10mL of PBS-EDTA from a T_{150} flask, 5 to 8 mL of the PBS-EDTA containing the cells was placed in a 15mL screw top tube, centrifuged for 2 minutes at 500g before aspiration of the supernatant. At the same time, 9mL of thawed FBS was added to 1mL of DMSO, this mixture was then used to fully resuspend the cell pellet (avoiding any

clumping of cells). The resuspended cells were then aliquotted into multiple NUNC™ Cryotube™ 2mL vials.

2.3 Pharmacology Techniques.

The following techniques were used in order to pharmacologically characterise the cAMP and Ca^{2+} second messenger responses of the 1321N1-$hP2Y_{11}$ and 1321N1-$XlP2Y_{11}$ cells.

2.3.1 The cAMP accumulation assay:

The assay is a modification of the techniques described by White and Zenser, 1970; Salomon et al,. 1973 and Johnson and Salomon (1991).

2.3.1.1 cAMP assay: Tissue culture preparation.

After performing a PBS-wash on a confluent monolayer of cells in a T_{150} flask. The cells were incubated and suspended in 20mL of PBS-EDTA after a 10-minutes incubation. 2mL of the PBS-EDTA containing the cells was then added to 48mL of DMEM. 1mL of this final dilution was then added to each well of a Costar® Tissue Culture Treated 24 well plate (Corning), the cells were plated at approximately 20,000 cells/cm^2. In this way 2 plates could be created. Where required, different quantities of a similar dilution could be created to produce a larger number of plates. The plates were incubated in the cell culture incubator for 2 to 3 days (or until approaching 100 percent confluency).

2.3.1.2 cAMP assay: ^{3}H adenine loading.

50μL of 8-^{3}H Adenine ([8-^{3}H] Adenine in aqueous solution containing 2%ethanol; 27.0 Ci/mmol)(Amersham Biosciences) was added to 25mL of Hanks' Balanced Salt Solution (Sigma) in a 50mL falcon tube and mixed. After aspiration of the media present on the 24 well plates, 1mL of the ^{3}H-Hanks media was added to each well of the plate (2μCi/well). The plates were then returned to the incubator. Following 2 hours of incubation the media was aspirated and each well was washed with 1.5mL of Hanks buffer, this washing procedure was repeated 3 times to remove unloaded ^{3}H. Following the final wash an appropriate volume* of Hanks containing phosphodiesterase inhibitor (Ro20-1724, a type 4 phosphodiesterase inhibitor; added to a final concentration of 1μM) and adenosine deaminase (ADA, type VI inhibitor; added to a final concentration of 1 unit/mL).

If an antagonist experiment was conducted, the appropriate concentrations of antagonists were added at this point to allow the compound to reach a binding equilibrium with the receptors. Following 30-minutes of incubation in the cell culture incubator, the appropriate concentration of compounds required for the stimulation or inhibition of cAMP response was added to each well. A vehicle control (10μL of PBS) and control response to isoproterenol (added to a final concentration of 10μM), was undertaken for each plate in triplicate. The incubation with the compounds was terminated after exactly ten-minutes with the addition of 50μL of concentrated HCl (11.91M), inactivating the metabolism

of the cells in each well of the plate. The plate could either be stored at -20°C or used directly in the quantification of *de novo* cAMP (described below).

*(Total volume in each well after the addition of agonists (or agonists and antagonists) was exactly 1000μL. Depending on the individual experiments conducted, the volume of Hanks containing Ro20-1724 and ADA was therefore adjusted appropriately).

2.3.1.3 cAMP assay: Column preparation for chromatography.

Dowex columns were prepared after the creation and addition of 2.4mL of a 50:50 slurry of AG®50W-X4 cation exchange resin (Bio-Rad) and distilled water. Addition of the mixture to 9cm poly-prep columns (Bio-Rad) resulted in the accumulation of approximately 1.2mL of Dowex resin in the columns. 10mL of dH_2O was added to the top of the columns before the addition of 5mL of 1M HCl, which was followed by a further 20mL of dH_2O (added in 2x10mL aliquots). Alumina columns were also created in 9cm poly-prep columns; whereby 0.6g of neutral alumina was placed in the columns before the addition of 20mL of 0.1M imidazole (added in 2x10mL aliquots). Each addition of liquid to both sets of columns was allowed to drain fully through the columns before further additions of liquid.

2.3.1.4 Sample preparation and chromatography.

The entire 1mL was removed from each of the 24 wells and placed into new 1.5mL Eppendorf tubes and centrifuged for 10-minutes at 13,000g to pellet the

cell debris. If stored at -20°C, the plates were given enough time to thoroughly defrost. The supernatant was then removed and placed into new 1.5mL tubes. 50μL was taken from each of the new tubes and placed into numbered 20mL scintillation vials (Packard) containing 5mL of Optiphase 'HiSafe'3 scintillation fluid (Perkin Elmer). 50μL of a prediluted stock of ^{14}C-cAMP ([adenine-U-^{14}C]cyclicAMP)(256 mCi/mmol) was added to the remainder of the supernatant in the new 1.5mL tubes. The tubes were then carefully sealed and briefly vortexed to mix.

The contents of the vortexed tubes were then added to individual Dowex columns (prepared as outlined in section 2.3.1.3). 2mL of dH_2O, added to each column, was left to drip through the columns, permitting the size-elution of the non-cyclic nucleotides. The columns were then placed on top of the Alumina columns (prepared as outlined in section 2.3.1.3) before the addition of a further 4mL of dH_2O. The eluate, containing the ^{3}H-labelled cAMP, was therefore collected within the alumina columns. The cAMP was then eluted from the alumina columns, after the addition of 4mL of 0.1M imidazole, into 20mL scintillation vials - to which 15mL of 'HiSafe'3 scintillation fluid was then added. 15mL of the scintillation fluid was also added to three vials containing 50μL of ^{14}C-cAMP only, these vials were created in order to gauge the efficiency of the columns.

2.3.1.4 cAMP assay: Column regeneration and Scintillation counting.

Following the chromatography stages, the dowex and alumina colums were regenerated for future use. Dowex columns were washed with 7.5mL 1M HCl and 20mL of H_2O, whilst the alumina columns were subjected to 20mL of imidazole. Further regeneration was performed once every 10 uses in order to strip the columns of any bound nucleotides, with the addition of 5mL of 1N NaOH. The columns were then subjected to a typical regeneration procedure (outlined above).

The vials containing 5mL and 15mL scintillation produced before, and as a result of, the chromatography procedure, outlined above, were placed in the a liquid scintillation analyser (Tri-CARB 2900TR, Packard). The vials containing 5mL of scintillant were subjected to a 1-minute ^{3}H count, whilst the 15mL scintillant vials underwent a five-minute ^{3}H and ^{14}C count. The interaction between the ^{3}H and ^{14}C isotopes (both possessing beta-emission) and the solute-solvent cocktail allowed the counts per minute to be recorded and outputted via the Quanta smart V.1.31 program (Packard). Results were inputted and manipulated using Excel and GraphPad Prism © V.3.0.

The use and disposal (by either: sink, scintillation and solid waste) of radioactive material in the assay was logged during and after the assay.

2.3.2 The Ca^{2+} mobilisation assay.

2.3.2.1 Tissue culture preparation.

After performing a PBS-wash and resuspending a confluent monolayer of cells from a T_{150} flask in PBS-EDTA. An appropriate portion of the PBS-EDTA was added to Ca^{2+} free DMEM and 100µL of the mixture was used to seed each well of a 96-well poly-D-Lysine black plastic plate with clear bottoms in each well (BD BioCoat™, BD Biosciences) (final concentration approximately 10,000 cells per well). The cells were then incubated overnight at 37°C in the cell-culture incubator or until a confluent monolayer of approximately 80,000 cells was observed per well.

2.3.2.2 Dye loading.

A 1x stock of Reagent B (10xHanks' BBS with 20mM HEPES at pH 6.0) from the Calcium Plus assay kit (cat.#: R-8051)(Molecular Devices) was initially created; whereby 5mL of 10x Reagent B and 600µL of 1N NaOH was added to 45mL of H_2O in a 50mL falcon tube. This was then added to the Calcium Plus Component A bottle and left to incubate at room temperature for 5-minutes.

Approximately 30mg of probenecid was added to a 1.5mL Eppendorf tube before the addition of 210µL of 1N NaOH and 210µL of 1xDPBS (vortexing thoroughly in-between each addition). 105µL of this probenecid mixture was then added to the component A bottle. The mixture was pipetted up and down to ensure thorough mixing of the components. 10.5mL of the solution was placed into a plastic reservoir before 100µL of the solution was dispensed using

a multipipette, into each of the 96 wells of the plate. The plate was then covered with foil and left for 30-minutes for the dye to load. Using the Calcium Plus assay kit in conjunction with the FLIPR machine avoids any wash steps, which may damage the cells and thus the assay precision.

2.3.2.3 Creating the ligand plates.

Following the calculation of the correct volumes and concentrations of the appropriate drugs to be pharmacologically tested, the drugs dilutions were created in PBS and placed into clear V-bottom 96-well plates. The antagonist dilutions, created in the same way with PBS as the diluent, where required, were then added to the incubating cells within the first 5-minutes of the 30-minute incubation in order to allow a minimum of 25 minutes for antagonist-receptor binding equilibrium to occur.

2.3.2.2 Using the FLIPR machine to measure Ca^{2+} mobilisation.

A FLIPR (fluorometric imaging plate reader) machine (Molecular Devices, Sunnyvale, California) was used in conjunction with Coherent™ Innova 90C argon LASER, producing a 1.5mm diameter beam at a wavelength of 488nm. Data collection was undertaken with a CCD camera within the FLIPR machine coupled to a computer running software supplied by Molecular Devices. The FLIPR machine allows the real-time recording of fluorescence change emitted by the dye (dye content not named by Molecular Devices) loaded into the 1321N1 cells in the presence of Ca^{2+} released from intracellular Ca^{2+} stores.

After the 30-minute incubation, the 96 well plate was placed in the FLIPR machine. Before the addition of any agonists using the robotic delivery system, an initial reading, in arbitrary fluorescence units, was undertaken in order to measure the fluorescence emission for each well. Following dye excitation with 488nm wavelength light, the FLIPR machine collects emission data through a standard 510-570 nm emission filter (the dye emits at a wavelength of 515nm). This was done in order to adjust the exposure length, shutter speed (of the camera) and/or power of the LASER. Saturation of the CCD occurs at approximately 64,000 arbitrary fluorescence units. Therefore, if initial readings are too high, the software cannot successfully resolve the change in fluorescence induced by the addition of agonists.

The internal robotic system of the FLIPR machine could be programmed to add a specified volume of agonist or antagonists from the V-bottom to the 96-well plate to the 96-well plate containing the cells loaded with fluorescent dye. A typical volume of 22μL of agonist dilution was added, to increase the total volume of each well 220μL. This volume was added at the slowest dispensing speed to avoid unnecessary disruption of the cells. Agonists were typically added at the 10-second time-point in order to visualise a basal fluorescence level. Following agonist addition the fluorescence change as a result of Ca^{2+} mobilisation from intracellular stores was recorded for 3 minutes. The initial fluorescence reading and the real-time fluorescence change was recorded and available for transfer between computers in Excel format. These files were then analysed to calculate the intracellular Ca^{2+} response.

2.4 Data handling and figure creation.

All data handling and statistical analysis was carried out using Excel and GraphPad Prism © V.3.0. T-testing (Student's two-tailed paired *t*-test, using 95 and 99 percent confidence intervals) and one-way analysis of variance (ANOVA) (using confidence intervals of 95 percent), were undertaken where required using Graphpad.

Each data set was comprised of a 3 or more replicates for each time point and / or concentration level. All concentration-response curves in figures showing the pharmacological concentration-responses were chosen for presentation because they represent the curve with the closest EC/IC_{50} value to the mean EC/IC_{50} value calculated for the ligand. All concentration-response curves were analysed using the non-linear regression sigmoidal dose response equation (variable and non-variable). None of the data analysed preferred the non-variable sigmoidal dose response equation. Where Kd is displayed the following equations were used:

equation 4

$$\text{dose ratio} = \frac{EC_{50} \text{ of agonist in presence of antagonist}}{EC_{50} \text{ of agonist without antagonist}}$$

equation 5

$$Kd = [\text{antagonist}]/\text{dose ratio} - 1$$

Figures showing second messenger responses were created using GraphPad Prism © V.3.0. Figures showing response pathways were created using Pathway Builder V1.0. Chemical reactions were drawn using the MDL ISIS™/DRAW V2.5 chemical drawing program.

Chapter 3

Pharmacological characterisation of the hP2Y$_{11}$ receptor.

3.1 Introduction

As described in Chapter 1, the conformational change of P2Y purinoceptors following the binding of specific extracellular ligands conveys a signal to intracellular G proteins which, in turn, transduce the signal further downstream. This signal transmission leads to the creation of second messenger molecules, able to transduce and amplify the signal generated by extracellular receptor-ligand interaction. The pharmacological characterisation of P2Y receptors, therefore, is achieved using assays that are able to record these changes in intracellular second messenger responses generated following receptor activation.

The transfection, and subsequent generation of cell lines stably expressing a receptor of interest, from a parent cell line shown to be devoid of endogenous

P2Y receptor expression, simplifies the process of second messenger pharmacological characterisation by negating the possibility of unwanted ligand-P2Y receptor interactions. In this way, second messenger responses generated by a single receptor subtype may be examined without the generation of multiple or overlapping second messenger responses.

This chapter endeavours first to confirm the absence of any endogenous P2Y receptor subtypes from the reportedly P2Y-null 1321N1 human astrocytoma cell line, using the RT-PCR technique described in Chapter 2, and, subsequently, to establish the appropriate assay conditions for determining Ca^{2+} and cAMP responses in the cell line. These assays will be established using pharmacological ligands shown to act as agonists upon receptors endogenous to 1321N1 cells. These control responses will subsequently be used in the evaluation of second messenger responses from the transfected receptor of interest, allowing the normalisation of the experimental recordings to a known endogenous response. This transformation of data will allow the results to be expressed in percentage terms and making it possible to directly compare data from different experiments.

Following the initial examination of second messenger responses induced by endogenous receptors in untransfected 1321N1 cells; this chapter also presents a pharmacological characterisation of the human $P2Y_{11}$ receptor, a G_s and G_q-coupled receptor (stably expressing in 1321N1 cells) able to produce Ca^{2+} and cAMP second messengers in response to agonist stimulation. As outlined in Chapter 1, previous studies of the $P2Y_{11}$ receptor orthologues, both human ($hP2Y_{11}$) and canine ($cP2Y_{11}$), have shown this subtype, upon activation, is able

to promote both *de novo* inositol phosphate and cyclic AMP production, and increase Ca^{2+} mobilisation (Communi et al. 1997; Zambon et al., 2001). The hP2Y$_{11}$ receptor's unique ability amongst the known P2Y subtypes to promote dual signalling pathway responses, allows the study of both functional responses within a single cell line.

In addition to establishing the conditions for both cAMP and Ca^{2+} second messenger assays, the characterisation of the human P2Y$_{11}$ receptor was undertaken in preparation for the pharmacological characterisation of the XlP2Y$_{11}$ receptor. Using a variety of agonists and antagonists, including ligands previously untested on the hP2Y$_{11}$ receptor, this chapter endeavours to use the cAMP and Ca^{2+} assays to extend the pharmacological profile of the hP2Y$_{11}$ receptor.

3.2 RT-PCR analysis of untransfected and transfected 1321N1-cells.

Using the molecular biology methods described in Chapter 2, large scale preparations of plasmid DNA constructs (pcDNA3.1G418) containing hP2Y$_{11}$ and XlP2Y$_{11}$ coding sequences were created. BBS transfection of the constructs into 1321N1 human astrocytoma cells followed by antibiotic selection was used to create stable 1321N1-hP2Y11 and 1321N1-XlP2Y$_{11}$ cell lines. RT-PCR analyses were performed on the untransfected 1321N1, 1321N1-hP2Y$_{11}$ and 1321N1-XlP2Y$_{11}$ cell lines to determine whether any P2Y receptor subtypes were expressed. The analyses were undertaken in order to complement previous studies, which have stated the 1321N1 cells possess no detectable Ca^{2+}

mobilisation or IP responses when tested with a variety of P2Y receptor agonists (Filtz et al., 1994; Patel et al., 2001). Figure 3.1 presents agarose gel analyses of PCR and RT-PCR products. Panels **A** to **F** examine the presence, in untransfected 1321N1 cells, of RNA encoding $hP2Y_1$ (**A**), $hP2Y_2$ (**B**), $hP2Y_4$ (**C**), $hP2Y_6$ (**D**), $hP2Y_{11}$ (**E**), $hP2Y_{12}$ (**F**). The figure reveals that none of these receptors were detected in the untransfected 1321N1-cells. Panels **G** and **H** reveal the presence of RNA encoding the $hP2Y_{11}$ and Xlp2y11 receptors in 1321N1-$hP2Y_{11}$ and 1321N1-Xlp2y11 cells, respectively.

The expected PCR primer-pair products sizes for each panel are as follows: $hP2Y_1$ (**A**) 253 bp, $hP2Y_2$ (**B**) 149 bp, $hP2Y_4$ (**C**) 443 bp, $hP2Y_6$ (**D**) 200 bp, $hP2Y_{11}$ (**E**) 307 bp, $hP2Y_{12}$ (**F**) 522 bp, $hP2Y_{11}$ (**G**) 307 bp, $XlP2Y_{11}$ (**H**) 410 bp. RNA extraction, RT-PCR, PCR and agarose gel analyses were performed as described in Chapter 2. The cultured untransfected 1321N1 cells and 1321N1-$hP2Y_{11}$ cells were used in the experiments presented in this chapter. The experiments undertaken on the 1321N1-$XlP2Y_{11}$ cells are shown in subsequent results chapters.

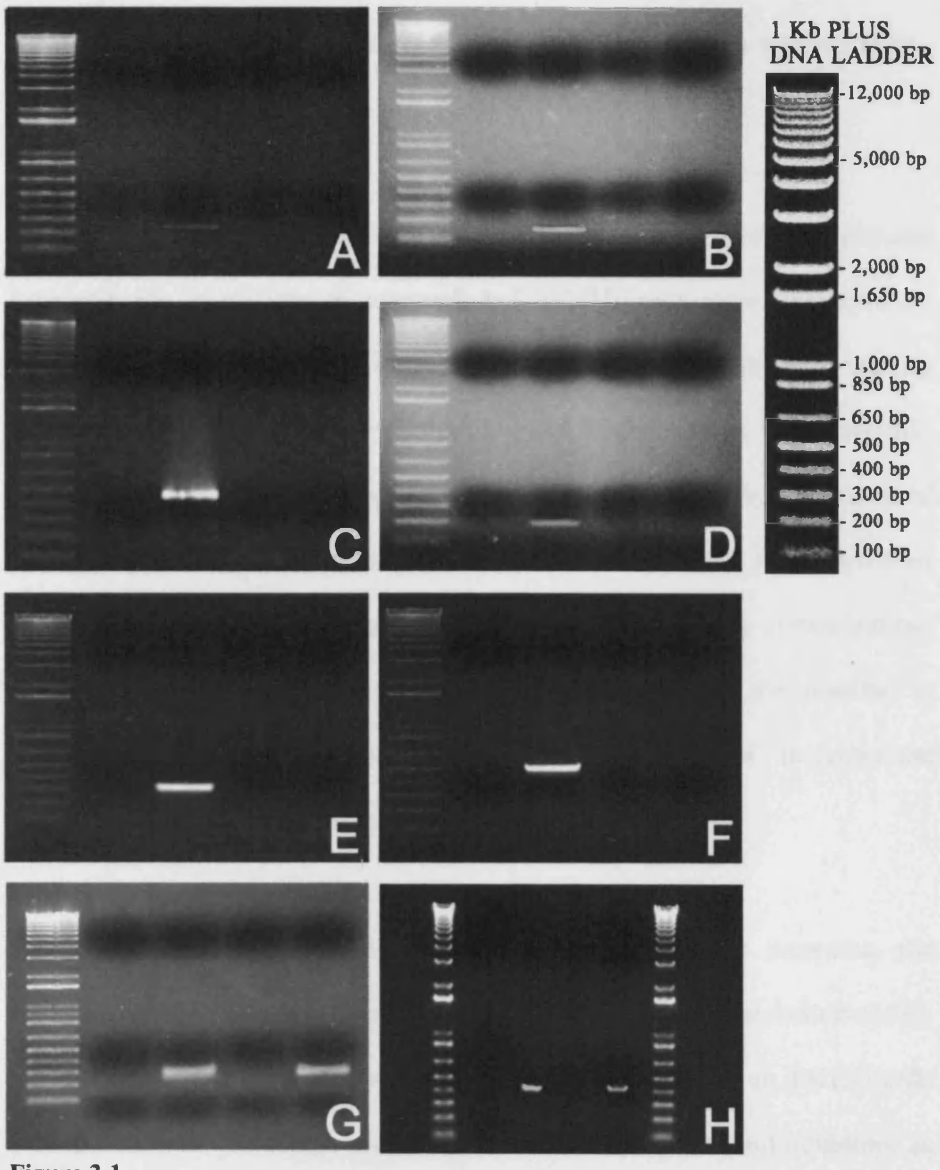

Figure 3.1

RT-PCR analysis of untransfected and transfected 1321N1 cells.

For each panel 1st lane: DNA Marker, 2nd lane: negative control (no template DNA), 3rd lane: positive control, 4th lane: negative control (no RT used), 5th lane: RT-PCR undertaken with oligo d(T) primers followed by P2Y-primer specific PCR. P2Y primer pair used in each experiment: hP2Y$_1$ (**A**), hP2Y$_2$ (**B**), hP2Y$_4$ (**C**), hP2Y$_6$ (**D**), hP2Y$_{11}$ (**E**), hP2Y$_{12}$ (**F**), hP2Y$_{11}$ (**G**) XlP2Y$_{11}$ (**H**). RT-PCR in panels **A** to **F** undertaken with RNA from untransfected 1321N1-cells. Panels **G** and **H** show products of the RT-PCR experiments undertaken with 1321N1-hP2Y$_{11}$ and 1321N1-XlP2Y$_{11}$ cell RNA, respectively.

3.3 cAMP production in untransfected 1321N1 cells and 1321N1-$hP2Y_{11}$ cells.

The initial part of this study focuses on recording *de novo* cAMP synthesis following the incubation of untransfected 1321N1 cells with isoproterenol. Isoproterenol activates the β_2-adrenoceptor endogenous to 1321N1 cells, causing synthesis of intracellular cAMP (Haragughi and Rodbell, 1991). Isoproterenol-induced cAMP response will be of use as a control in further investigations of transfected 1321N1 cells, enabling the normalisation of various ligand-induced exogenous receptor cAMP responses. By determining the concentration-dependent cAMP responses of the β_2-adrenoceptor, it will be possible to determine the appropriate supramaximal concentration of isoproterenol required for its use as an endogenous cAMP response standard.

The measurement of the cAMP response is achieved by recording the accumulation of, over a set period of time, intracellular radiolabelled-cAMP, which has been created following adenylyl cyclase activation in 1321N1-cells loaded with [8-^{3}H] Adenine. Using the appropriate conditions and inhibitors, as described in Chapter 2, prevents radiolabelled-cAMP production, causing an intracellular accumulation of *de novo* cAMP production. Because total *de novo* cAMP production is recorded over a fixed period of time, the cAMP assay will also be used to quantify the time-dependency of the cAMP accumulation in 1321N1-$hP2Y_{11}$ cells. The second part of this study examines the *de novo* cAMP production of 1321N1 cells stably expressing the $hP2Y_{11}$ receptor in responses to a variety of P2Y agonists and antagonists.

3.3.1 Isoproterenol produces concentration-dependent cAMP accumulation in 1321N1 human astrocytoma cells.

Untransfected 1321N1-cells are able, in response to treatment with isoproterenol, to produce concentration-dependent cAMP accumulation. Figure 3.2 presents the cAMP responses (expressed in disintegrations per minute of the accumulated radiolabelled-cAMP) of untransfected 1321N1 cells following incubation with PBS (■) and isoproterenol (▼)(added to final concentrations ranging from 0.1nM to 10μM; log values: -10 to -5). Ten minute ligand incubations were undertaken, in accordance with previous cAMP pharmacological studies presented for the P2Y$_{11}$ receptor (Qi et al., 2001[a]; Zambon et al., 2001). The data in Figure 3.2 represent one experiment of the three identical independent experiments performed.

Figure 3.2 reveals that *de novo* cAMP was produced in a concentration-dependent manner in untransfected 1321N1-cells following the addition of increasing concentrations of isoproterenol. The mean EC_{50} value (61.4nM, log EC_{50} = - 7.21 $\pm$ 0.05) was determined following non-linear regression analysis of each of the three independent isoproterenol concentration-response experiments. The addition of the PBS vehicle-control not only confirms the purity of the PBS (also used to dilute the isoproterenol), but also reveals the mechanical pressure exerted on the 1321N1 cells during ligand addition is unable to release sufficient ATP to produce an intracellular cAMP response.

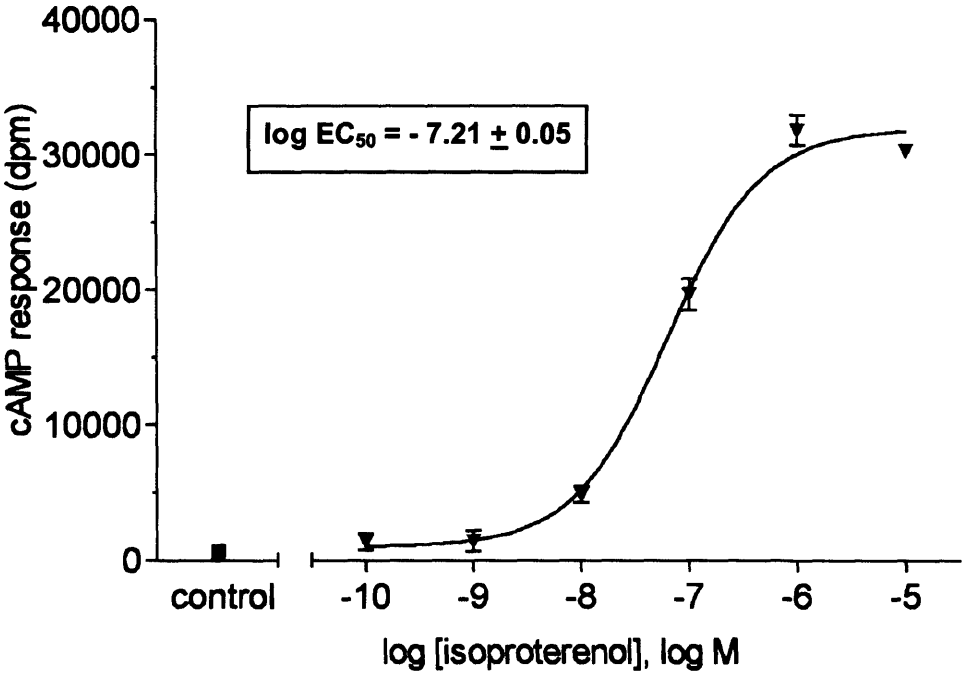

Figure 3.2

Concentration-response curve of isoproterenol on cAMP accumulation in untransfected 1321N1 human astrocytoma cells.

The cAMP response to PBS (■) and increasing concentrations of isoproterenol (▼) was measured in cultured cells as described in the Materials and Methods. Results are expressed as disintegrations per minute. The data are the mean ± s.e.m. of one representative experiment of 3 performed.

The PBS-induced cAMP response also reveals that the cAMP produced by the incubation of the 1321N1 cells at the lower concentrations of isoproterenol (0.1nM and 1nM; log values: -10 and -9) are at a basal level. The figure reveals a 10μM final concentration of isoproterenol is sufficient to produce a supramaximal cAMP response. Further experiments investigating the cAMP response of exogenous receptors will be normalised to the cAMP response generated by the 10μM isoproterenol control included in each experimental data set, thus negating any fluctuations in the magnitude of the cAMP responses which may be produced by a direct comparison of different experiments.

3.3.2 1321N1-hP2Y$_{11}$ cells express a functioning hP2Y$_{11}$ receptor.

The ability of untransfected 1321N1 human astrocytoma cells to produce cAMP in response to ATP was examined. Figure 3.3 shows the percentage cAMP response generated in 1321N1- hP2Y$_{11}$ cells and untransfected 1321N1-cells following ten-minute incubations with PBS and ATP (added to a final concentration of 100μM). ATP, able to induce a sizeable cAMP response (34.6 $\pm$ 1.4 percent) in the 1321N1-hP2Y$_{11}$ cells, was unable to elicit similar cAMP accumulations in the untransfected cell line. Statistical analysis shows a significant difference between the PBS and ATP responses recorded in the transfected 1321N1 cells (p value < 0.01 by Student's two-tailed paired *t*-test), revealing functional expression of hP2Y$_{11}$ in the 1321N1-hP2Y$_{11}$ cells.

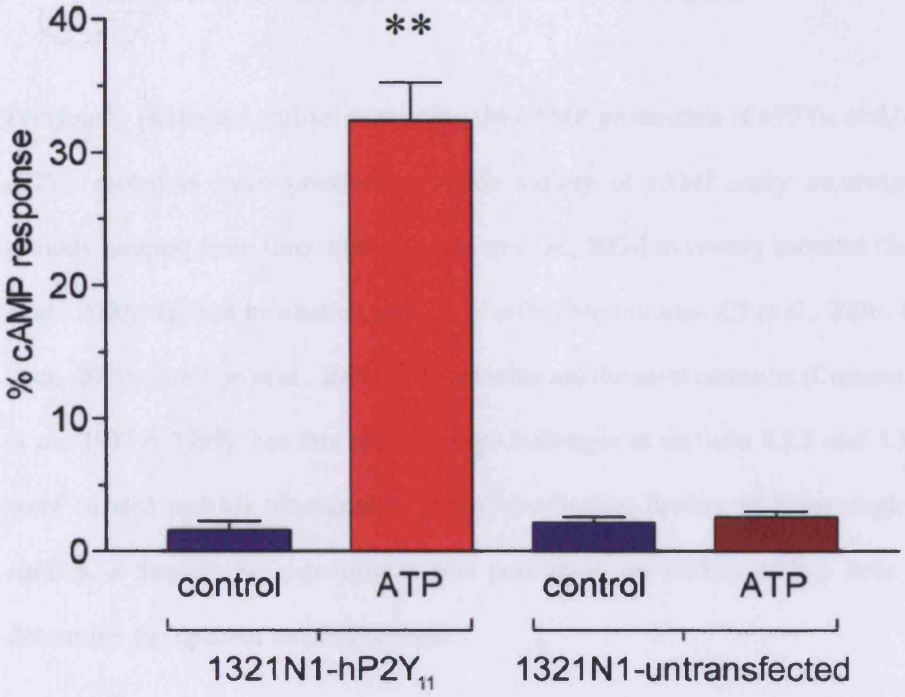

Figure 3.3

1321N1-hP2Y$_{11}$ cells express a functioning hP2Y$_{11}$ receptor.

Untransfected 1321N1 human astrocytoma cells and 1321N1 cells stably expressing hP2Y$_{11}$ were screened for their ability to produce a cAMP second messenger signal in response to ATP. *De novo* cAMP production was measured after a ten-minute incubation with ATP at a final concentration of 100μM. Results are expressed as a percentage of the cAMP response to a supramaximal concentration of isoproterenol (10μM). The data displayed are the mean ± s.e.m. of three experiments, each performed in triplicate. **, $p < 0.01$, compared with control, Student's t-test.

3.3.3 ATP elicits a time-dependent cAMP response in 1321N1 human astrocytoma cells stably expressing the $hP2Y_{11}$ receptor.

Previously published studies examining the cAMP production of $hP2Y_{11}$ and/or $cP2Y_{11}$ receptors have presented a wide variety of cAMP-assay incubation periods ranging from three minutes (Dixon et al., 2004) to twenty minutes (Suh et al., 2000). Typical incubation periods of either ten minutes (Qi et al., 2001[a]; Qi et al., 2001[b]; Zambon et al., 2001) or 15 minutes are the most common (Communi et al., 1997 & 1999). For this reason drug challenges in sections 3.3.1 and 3.3.2 were carried out for ten-minutes. Before conducting further pharmacological studies, a time-course experiments was performed on 1321N1-$hP2Y_{11}$ cells to determine the optimal incubation time.

Figure 3.4 shows the cAMP response of 1321N1 human astrocytoma cells stably expressing $hP2Y_{11}$. *De novo* cAMP production, generated by ATP added to final concentrations of either 0.1mM (■) or 10μM (▲)(log values: -4 and -5), was measured across six different incubation periods (1, 5, 7.5, 10, 15 and 20 minutes). The results are expressed as a percentage cAMP response, normalised to the control isoproterenol. The data shown are from one representative experiment of three identical independent experiments performed for each concentration of ATP. The curves plotted to the data were generated following non-linear regression analysis using the one-site binding hyperbola.

The cAMP accumulation generated by ATP is incubation-time dependent at early time points, leading to a plateau in the response at later time points. The half-maximal value was achieved at approximately 2 to 3 minutes for both ATP

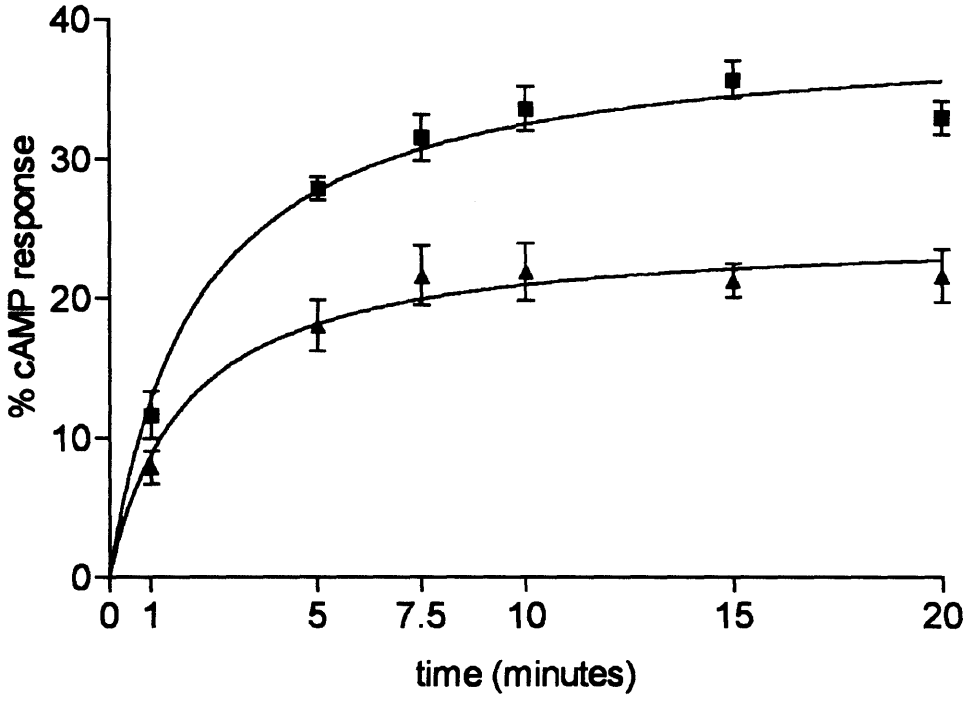

Figure 3.4

Time-dependent cAMP response generated by ATP in 1321N1 human astrocytoma cells stably expressing the human P2Y$_{11}$ receptor.

The cAMP response to 100μM (■) and 10μM (▲) concentrations of ATP were measured in cultured cells (as described in the Materials and Methods) following a range of different incubation periods. Results are expressed as a percentage of the cAMP response to a supramaximal concentration of isoproterenol (10μM). The data are the mean ± s.e.m.

concentrations. Statistical analysis reveals no significant difference exists between the percentage cAMP response recorded for the ten- and twenty-minute incubation periods (where p value > 0.05 by Student's two-tailed paired *t*-test) for all three experiments undertaken at both concentrations of ATP, illustrating that no substantial increase in cAMP accumulation is generated beyond the initial ten minutes for either concentration of ATP. These data confirm that the maximal response to the agonist is reached within the ten-minute incubation period. This incubation period was used in all subsequent studies.

3.3.4 1321N1- $hP2Y_{11}$ cells are activated by nucleotides, producing a cAMP response.

Figure 3.5 shows the percentage cAMP response generated in 1321N1-$hP2Y_{11}$ cells following ten-minute incubations with 100μM of: UTP, ADP, BzATP, ATP, β,γ-meATP and α,β-meATP. The figure reveals the 1321N1-$hP2Y_{11}$ cell line was able to successfully generate a cAMP second messenger response following activation by extracellular nucleotides and nucleotide analogues, further confirming successful expression of the $hP2Y_{11}$ receptor and coupling to the cAMP transduction pathway. UTP and ADP elicited a minimal cAMP response (2.9 ± 1.9 and 5.4 ± 0.3 percent, respectively) when compared to BzATP (31.6 ± 0.2 %) or ATP (35.7 ± 1.1 %). Interestingly, the two methylenephosphonate compounds produced the greatest cAMP responses: β,γ-meATP (41.0 ± 0.3 %) and α,β-meATP (47.4 ± 3.3 %).

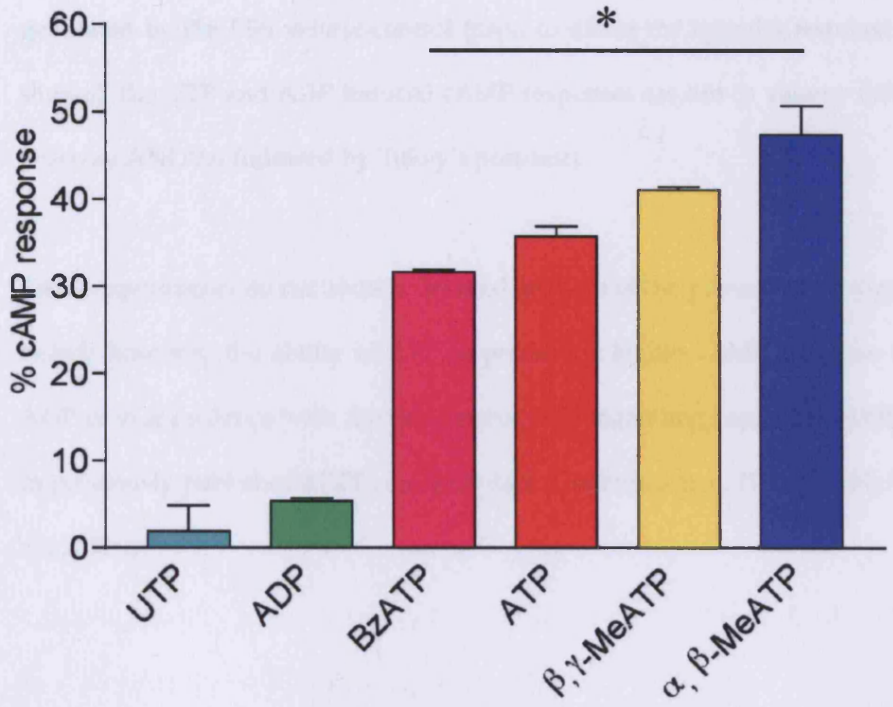

Figure 3.5

hP2Y$_{11}$ is activated by nucleotides, producing a cAMP response.

Nucleotides and nucleotide analogues were screened for their ability to induce a cAMP response in 1321N1 human astrocytoma cells stably expressing the hP2Y$_{11}$ receptor. *De novo* cAMP production was determined after incubation with: UTP, ADP, BzATP, ATP, β,γ-MeATP and α,β-MeATP (each added to final concentration of 100μM). Results are expressed as a percentage of the cAMP response to a supramaximal concentration of isoproterenol (10μM), and represent the mean ± s.e.m. of three different experiments, each performed in triplicate. *, $p < 0.05$, by ANOVA with Tukey's post-test, comparing each with the control response. The data shown are control response deducted.

Statistical analysis has shown, that whilst the cAMP responses generated by BzATP, ATP, β,γ-meATP and α,β-meATP are significantly different to that generated by the PBS vehicle-control (used to dilute the ligands)(response not shown), the UTP and ADP induced cAMP responses are not (p value > 0.05 by one-way ANOVA followed by Tukey's post-test).

These experiments do not allow a detailed analysis of the potency of the ligands tested; however, the ability of ATP to produce a higher cAMP response than ADP is in accordance with the preferential ATP signalling capability exhibited in previously published hP2Y$_{11}$ receptor data (Communi et al. 1997 & 2001; Qi et al., 2001[b]).

3.3.5 Concentration-response curves of nucleotides on cAMP accumulation in 1321N1-hP2Y$_{11}$ cells.

Having shown, in section 3.3.4, that the hP2Y$_{11}$ receptor is able to induce cAMP production in the 1321N1-hP2Y$_{11}$ cells in response to various nucleotide analogues, the concentration-responses of these agonists on cAMP production was examined. Figure 3.6 shows the percentage cAMP response of 1321N1-hP2Y$_{11}$ cells following ten minute incubations (with: UTP, ADP, BzATP, ATP, β,γ-meATP or α,β-meATP). These agonists were applied at varying concentrations (ranging from 0.01μM to 100μM; log values: -8 to –4). Figure 3.6 reveals that most of the agonists were able to successfully increase the cAMP production in the 1321N1-hP2Y$_{11}$ cells in a concentration-dependent manner.

Non-linear regression analysis was performed on each of the three to five sets of data for each ligand. The representative experiments presented in Figure 3.6 show curves fitted to ADP (△), BzATP (▼) ATP (◆) β,γ-meATP (■) and α,β-meATP (▲). The analysis was unable to fit a curve to the cAMP responses produced throughout the range of UTP concentrations. The UTP (□) data is shown with a dotted connecting line. The regression analysis has enabled the calculation of the EC_{50} value for: BzATP (0.9μM, log EC_{50} = -6.05 ± 0.06), ATP (5.7μM, log EC_{50} = -5.24 ± 0.07), α,β-MeATP (23.0μM, log EC_{50} = -4.64 ± 0.07) and β,γ-MeATP (24.4μM, log EC_{50} = -4.61 ± 0.14)(also shown in Table 3.1). Consistent with previous pharmacological characterisations (Communi et al., 1997, White et al., 2003), Figure 3.6 reveals maximal cAMP responses are achieved for the agonists within approximately 2 to 2.5 log units of the agonist concentration required to produce a minimal/basal cAMP level.

Although a 'curve' has been plotted to the ADP data in Figure 3.6, the minimal responses recorded, and the fact that this clearly does not reach a maximal response within the range of ADP concentrations tested here, does not allow an EC_{50} value to be calculated accurately for this ligand. The minimal cAMP concentration-responses produced by UTP and ADP conform to the data recorded in the single-concentration ligand screen undertaken in section 3.3.2.

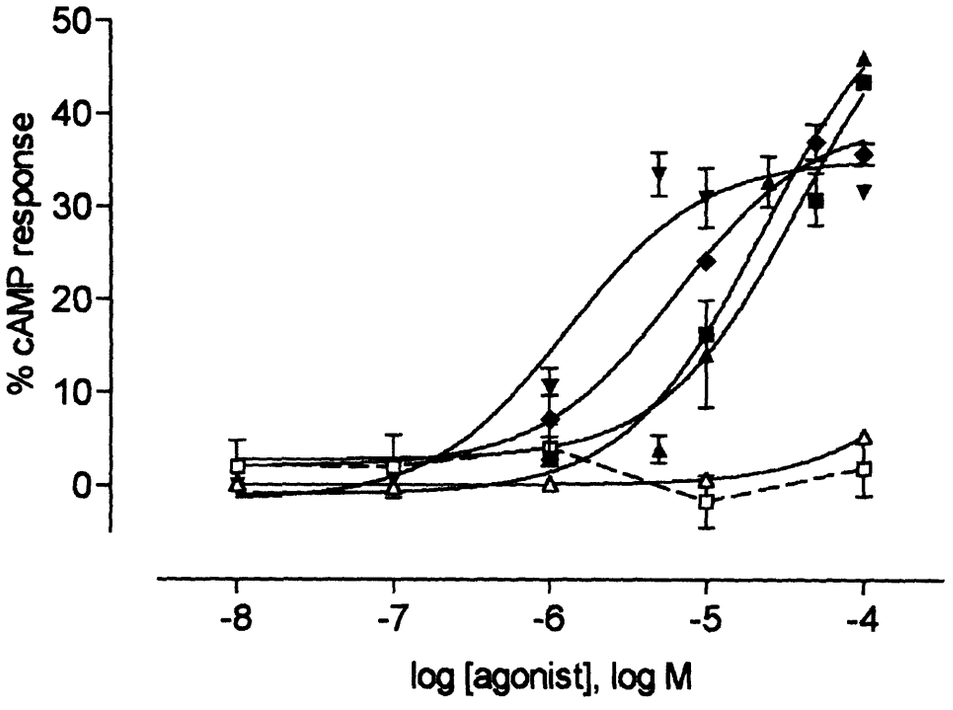

Figure 3.6

Concentration-response curves of nucleotides on cAMP accumulation in 1321N1 human astrocytoma cells stably expressing the hP2Y$_{11}$ receptor.

The cAMP response was measured following the incubation of 1321N1-hP2Y$_{11}$ cells with increasing concentrations of: UTP (□), ADP (△), BzATP (▼), ATP (◆), β,γ-meATP (■) and α,β-meATP (▲). Results are expressed as a percentage of the cAMP response to a supramaximal concentration of isoproterenol (10μM). The data are the mean ± s.e.m. of one representative experiment of three to five performed for each ligand.

Calculation of the EC_{50} values enables the relative effectiveness of the agonists to be compared and the rank order of potency of these in producing a cAMP response at the hP2Y$_{11}$ receptor is:

BzATP > ATP > α,β-meATP = β,γ-meATP

3.3.6 Reactive Red is an antagonist of the cAMP response induced by the activated hP2Y$_{11}$ receptor.

In order to expand the current pharmacological profile of the hP2Y$_{11}$ receptor, the ability of Reactive Red (a P2Y-receptor antagonist)(Bültmann et al., 1995) to inhibit hP2Y$_{11}$-mediated cAMP responses was investigated. The percentage cAMP response generated by BzATP (used at a final concentration of 10μM) when added alone, and the response induced by 10μM BzATP in the presence of Reactive Red, added at a final concentration of 1mM is shown in Figure 3.7. BzATP was chosen for this experiment because of its potency and high efficacy at a final concentration of 10μM (previously presented in sections 3.3.4 and 3.3.5). Consistent with the agonist characterisations of the hP2Y$_{11}$ receptor shown in these previous sections, the cAMP responses are presented normalised to the control isoproterenol response. As Figure 3.7 shows, Reactive Red (1mM) is able to fully inhibit BzATP-induced cAMP production in the 1321N1-hP2Y$_{11}$ cell line, decreasing the BzATP-induced cAMP BzATP-induced cAMP response to a minimal value shown by statistical analysis to be indistinguishable from the PBS control response (p value < 0.05 by Student's two-tailed paired *t*-test).

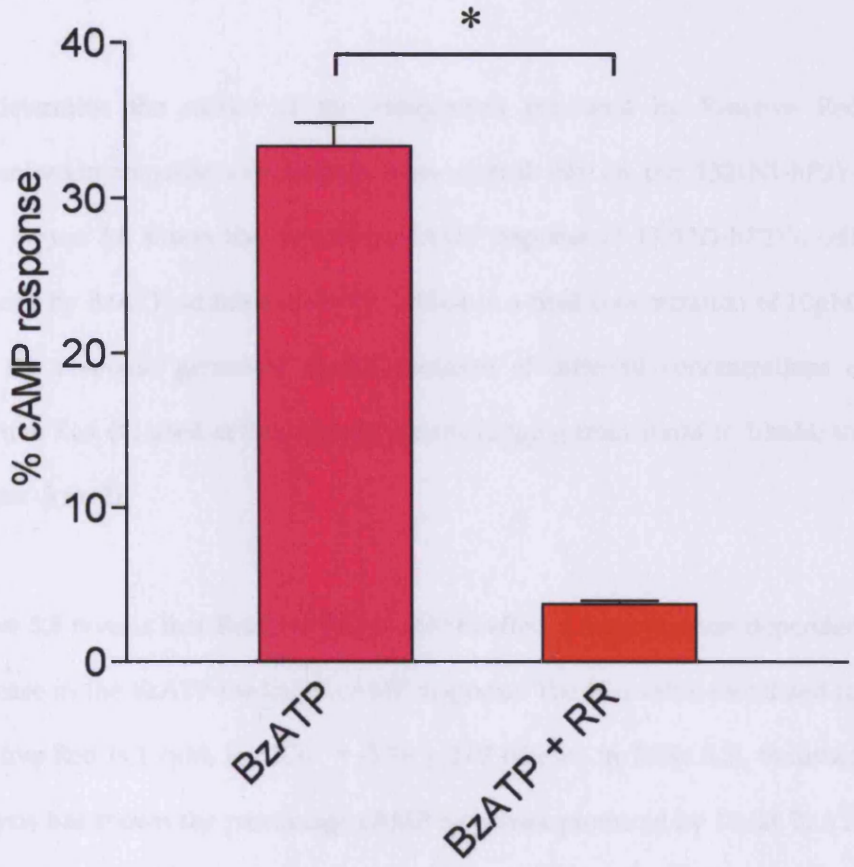

Figure 3.7

Reactive Red inhibits cAMP accumulation produced by BzATP activation of $hP2Y_{11}$.

Reactive Red's ability to inhibit cAMP accumulation produced by BzATP activation of $hP2Y_{11}$. Following pre-incubation with Reactive Red (added to a final concentration of 1mM), *de novo* cAMP production was measured after incubation with 10μM of BzATP. Results are expressed as a percentage of the cAMP response to a supramaximal concentration of isoproterenol (10μM). The data represent the mean ± s.e.m. of three different experiments each performed in triplicate. *, $p < 0.05$, Student's t-test. The results shown are control response deducted.

3.3.7 Reactive Red reduces agonist-induced cAMP responses of the hP2Y$_{11}$ receptor in a concentration-dependent manner.

To determine the nature of the antagonism produced by Reactive Red, concentration-response experiments were carried out on the 1321N1-hP2Y$_{11}$ cells. Figure 3.8 shows the percentage cAMP response of 1321N1-hP2Y$_{11}$ cells induced by BzATP addition alone (▼; added to a final concentration of 10μM), and the response generated in the presence of different concentrations of Reactive Red (▽; used at final concentrations ranging from 10nM to 10mM; log values: -8 to -2).

Figure 3.8 reveals that Reactive Red is able to affect a concentration-dependent decrease in the BzATP-mediated cAMP response. The IC_{50} value calculated for Reactive Red is 1.7μM, log IC_{50} = -5.76 ± 0.07 (shown in Table 3.2). Statistical analysis has shown the percentage cAMP responses produced by 10μM BzATP in the presence of higher concentrations of Reactive Red (above 5μM; log value -5.3) are indistinguishable from the PBS-induced negative control responses (p value < 0.05 by Student's paired *t*-test). The ability of Reactive Red to reduce the agonist-induced response to a basal level over approximately 2 log units of concentration change is characteristic of previously studied P2Y antagonists (Qi et al., 2001[b]) and reveal the novel finding that Reactive Red is able to fully inhibit the cAMP responses of the hP2Y$_{11}$ receptor.

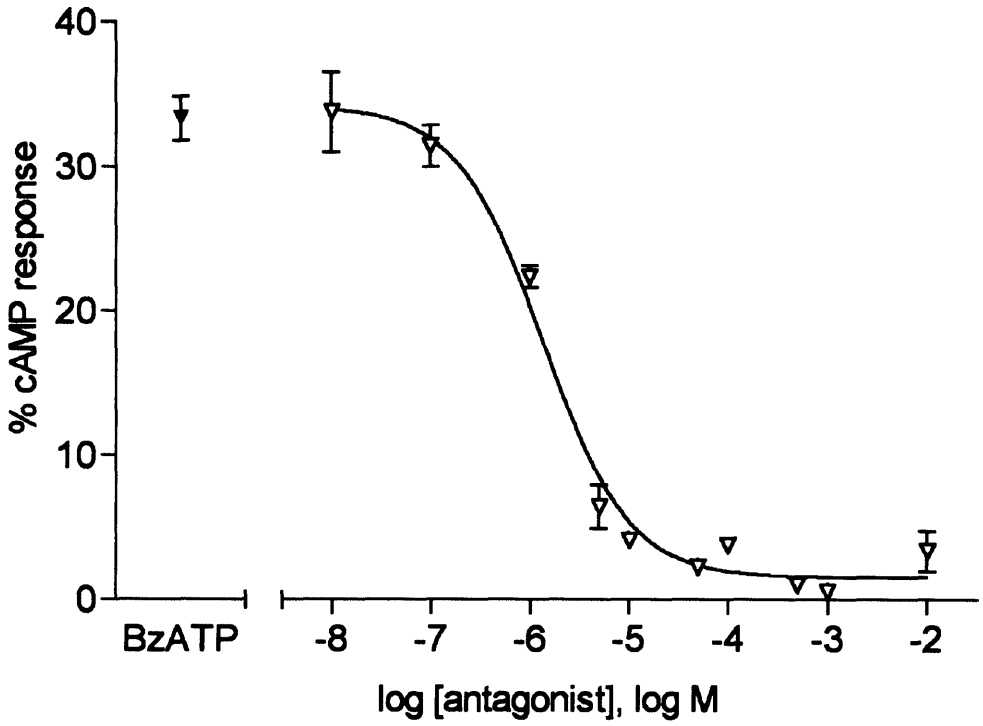

Figure 3.8

Concentration-inhibition curves of Reactive Red on cAMP accumulation generated by BzATP, in 1321N1 human astrocytoma cells stably expressing the hP2Y$_{11}$ receptor.

The cAMP response to 10μM BzATP was measured in 1321N1-hP2Y$_{11}$ cells, alone (▼) and following pre-incubation with increasing concentrations of Reactive Red (▽). Results are expressed as a percentage of the cAMP response to a supramaximal concentration of isoproterenol (10μM). The data are the mean ± s.e.m. of a representative experiment of three independent experiments performed.

3.4 Ca^{2+} mobilisation in untransfected 1321N1 cells and 1321N1-$hP2Y_{11}$ cells.

Whilst I was developing the cAMP assay, the Ca^{2+} assay was also being established in the laboratory. The results of the Ca^{2+} assays, performed by Dr Townsend-Nicholson and analysed by myself, are presented in the following sections of this chapter.

Similar to the methodology applied to the establishment of the cAMP accumulation assay, the appropriate assay conditions were established for the determination, upon receptor stimulation, of intracellular Ca^{2+} mobilisation in 1321N1-cells. The first part of this investigation was performed in order to examine the ability of carbachol to stimulate a Ca^{2+} second messenger response in untransfected 1321N1 cells. Carbachol, an agonist of the muscarinic receptor (M3), endogenous to 1321N1 cells (Stephan and Sastry, 1992), has been shown to stimulate inositol phosphate (IP) accumulation in a concentration-dependent manner. Similarly to the use of isoproterenol as a control response in the cAMP assay (Section 3.3.1), the concentration-dependence of carbachol-induced Ca^{2+} mobilisation was undertaken to determine the supramaximal concentration of carbachol for use as an endogenous control responses in 1321N1 cells. The use of an endogenous standard allows the normalisation of intracellular responses produced by exogenous receptors. The second part of the study examines the intracellular Ca^{2+} responses induced by the activated $hP2Y_{11}$ receptor, beginning with the characterisation of the Ca^{2+} response of the 1321N1-$hP2Y_{11}$ cells to ligands previously shown to act at the $hP2Y_{11}$ receptor.

As described in Chapter 2, the Ca^{2+} assay utilises a fluorescent dye, which fluoresces at a specific wavelength in the presence of free Ca^{2+}, i.e. Ca^{2+}, released from intracellular stores following receptor activation. This fluorescence change is measured by the fluorometric imaging plate reader (FLIPR). Unlike the cAMP assay, which can only be used to record total *de novo* cAMP production over a set period of time, quantification of the Ca^{2+} response is achieved by recording the increase in fluorescence at any given time point, as opposed to the accumulated fluorescence over the total time point, following the addition of ligand. The fluorescence difference between basal levels and the peak of an agonist induced fluorescence change is used to quantify the Ca^{2+} response.

3.4.1 Carbachol produces concentration-dependent Ca^{2+} mobilisation in 1321N1 human astrocytoma cells.

The addition of carbachol to the 1321N1 cells is able to successfully mobilise Ca^{2+} from intracellular stores (Figure 3.9). The fluorescence responses (expressed in relative fluorescence units) of untransfected 1321N1 cells, generated by intracellular Ca^{2+} mobilisation in response to the addition of PBS (■) and various concentrations of carbachol (▼) ranging from 1nM to 1mM (log values: -9 to -3) are shown in the figure. The data are the means ± s.e.m. of one representative experiment taken from one of the three independent experiments performed.

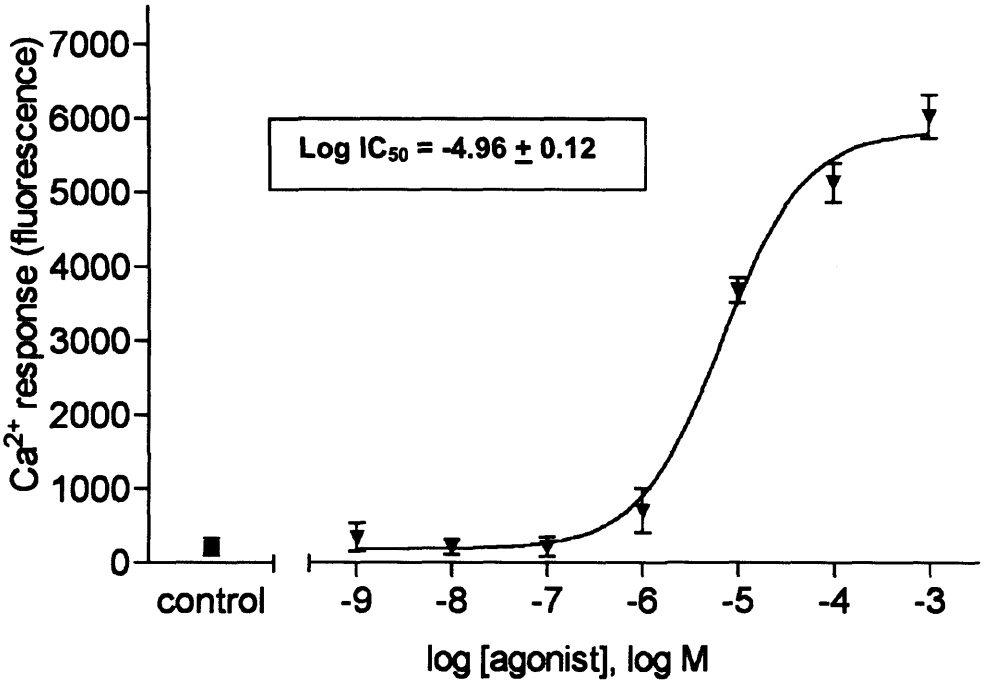

Figure 3.9

Concentration-response curve of carbachol on Ca^{2+} mobilisation in untransfected 1321N1 human astrocytoma cells.

The Ca^{2+} response to PBS (■) and increasing concentrations of carbachol (▼) was measured in cultured cells as described in the Materials and Methods. Results are expressed as fluorescence units. The data are the mean ± s.e.m. of one representative experiment of 3 performed.

The carbachol-induced response, presented in Figure 3.9, is shown to be concentration-dependent, with increasing concentrations of carbachol able to mobilise increasing amounts of intracellular Ca^{2+}. Non-linear regression analysis was performed on each carbachol response data set (as described in Chapter 2). From these analyses, concentration-response curves were plotted, and the EC_{50} values for each of the three independent experiments were calculated - enabling the mean EC_{50} value ($\pm$ s.e.m.) of 11.0μM (log EC_{50} = -4.96 $\pm$ 0.12) to be determined. Figure 3.9 also reveals that the addition of the PBS vehicle-control is unable to elicit any substantial Ca^{2+} mobilisation. The minimal Ca^{2+} response exhibited by the addition of the PBS control confirms that the response levels achieved by the addition of the lower concentrations of carbachol (1nM, 10nM and 0.1μM; log values: -9 to -7) are at basal levels. The maximal Ca^{2+} response recorded is induced by carbachol at 1mM final concentration and this concentration was used in subsequent experiments to normalise the Ca^{2+} responses of exogenous receptors.

3.4.2 $hP2Y_{11}$ is activated by nucleotides, producing a Ca^{2+} response.

ATP and BzATP, previously presented in sections 3.3.2 and 3.3.5 as agonists of the $hP2Y_{11}$ cAMP response, are also able to induce Ca^{2+} mobilisation in 1321N1 cells stably expressing the $hP2Y_{11}$ receptor. Figure 3.10 shows the Ca^{2+} response of 1321N1-$hP2Y_{11}$ cells following the addition of BzATP and ATP (each added to a final concentration of 0.1mM). This single high-concentration ligand-screen reveals that FLIPR is a suitable means of quantifying Ca^{2+} mobilisation in response to P2Y receptor activation.

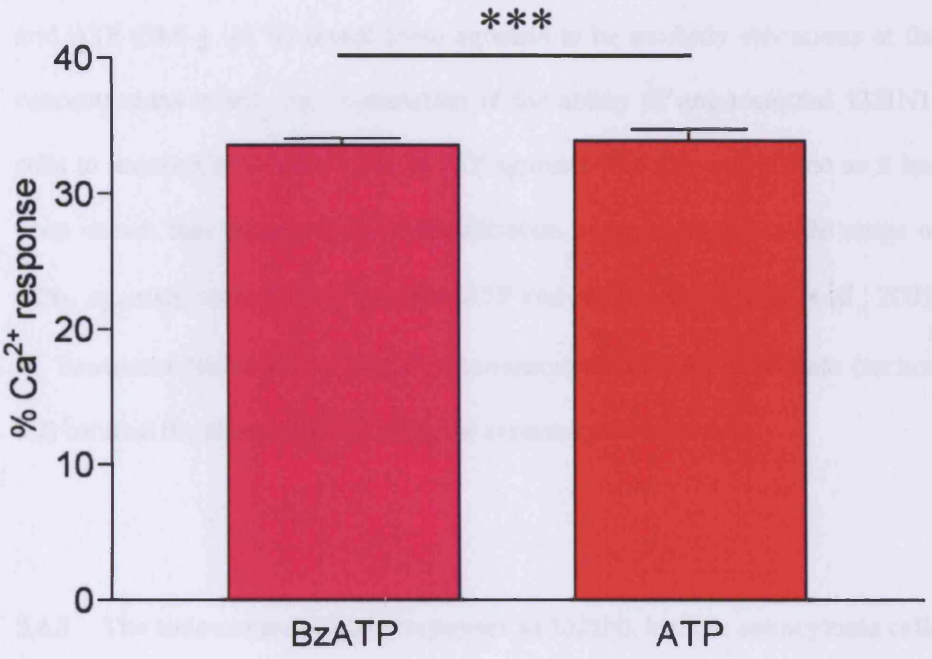

Figure 3.10

hP2Y$_{11}$ is activated by nucleotides, producing a Ca^{2+} response.

BzATP and ATP were screened for their ability to induce a Ca^{2+} response in 1321N1 human astrocytoma cells stably expressing hP2Y$_{11}$. Ca^{2+} mobilisation was measured after the addition of BzATP and ATP (each at 100 μM). Results are expressed as a percentage of the Ca^{2+} response to a supramaximal concentration of carbachol (1mM) and represent the mean ± s.e.m. of at least three different experiments, each performed in triplicate. ***, $p < 0.005$, compared with the control response, Student's t-test. The data shown are control response deducted.

Similarly to the ligand-screening experiments undertaken with the cAMP assay (section 3.3.2), the results of these experiments offer no insight into the potencies of each ligand. However, the Ca^{2+} responses produced by BzATP (33.6 $\pm$ 0.5 %) and ATP (33.9 $\pm$ 0.8 %) reveal these agonists to be similarly efficacious at the concentrations tested. An examination of the ability of untransfected 1321N1-cells to induce Ca^{2+} mobilisation to P2Y agonists was not undertaken as it has been shown that there is no Ca^{2+} mobilisation in response to a wide range of P2Y$_{11}$ agonists, including ATP, β,γ-MeATP and α,β-MeATP (Patel et al., 2001, A. Townsend-Nicholson, personal communication) and my own data (section 3.2) confirm the absence of P2Y receptor expression in these cells.

3.4.3 The time-course of Ca^{2+} responses in 1321N1 human astrocytoma cells stably expressing the hP2Y$_{11}$ receptor.

In order to better understand the profile of intracellular Ca^{2+} mobilisation in 1321N1-hP2Y$_{11}$ cells, the changes in fluorescence (expressed in fluorescence units) produced by concentrations of carbachol, BzATP and PBS were investigated. Figure 3.11 shows the Ca^{2+} responses produced by 1321N1-hP2Y$_{11}$ cells before and after the addition of the ligands. Carbachol and BzATP, previously shown to be agonists of the muscarinic receptor (M3) (Stephan and Sastry, 1992) and hP2Y$_{11}$ receptor (section 3.3.2 and 3.4.2) respectively, were added to a final concentration of 1mM (carbachol) and 10µM (BzATP). An equal volume of PBS was added into the control wells.

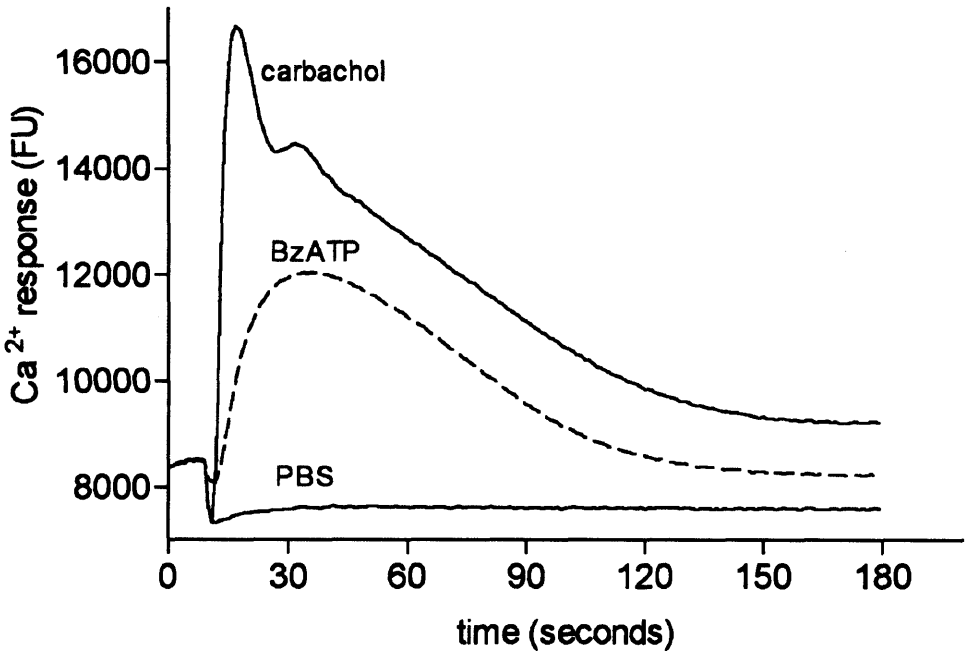

Figure 3.11

Fluorescence response over time generated following the addition of PBS, BzATP and carbachol to 1321N1 human astrocytoma cells stably expressing the human P2Y$_{11}$ receptor.

The Ca^{2+} response to carbachol (1mM final concentration), BzATP (10μM final concentration) and PBS was measured over time in cultured cells as described in the Materials and Methods. Ligands, or the PBS control, were added at t=10 seconds. Results are expressed as fluorescence units. The data are the mean from a single representative experiment. Error bars have been omitted to more clearly visualise the shape of the curves.

The assay was run for 180 seconds with fluorescence measured once a second. For this reason the resulting 180 data points are shown with a connecting line only (large data point symbols and s.e.m. error bars are excluded to ease the visualisation of the connecting line). All of the ligands were added at the 10 second time point in the assay. The real-time fluorescence response of the 1321N1-$hP2Y_{11}$ cells shown in Figure 3.11 is a representative experiment (undertaken in triplicate) taken from one of three independent experiments performed. It is the peak height of the response that is used to determine the magnitude of the Ca^{2+} response, and represents Ca^{2+} entry and Ca^{2+} mobilisation from intracellular stores.

Figure 3.11 demonstrates that intracellular Ca^{2+} is released following addition of both carbachol, which acts at the endogenous muscarinic receptor, and BzATP, which acts upon the transfected $hP2Y_{11}$ receptor. The maximum response generated by each of these agonists is achieved within the 180 second time course of the experiment. Carbachol, added at the supramaximal concentration of 1mM, has created the largest fluorescence change of the two agonists tested, representing the largest Ca^{2+} release from intracellular stores. Following the rapid increase in the recorded fluorescence there is an equally rapid decrease, representing the release and subsequent use / chelation of Ca^{2+} by intracellular proteins and reabsorbtion of Ca^{2+} into intracellular stores. This initial rapid decreasing gradient becomes less steep from approximately 40 seconds onwards, with a decrease of approximately 800FU (fluorescence units) observed every 10 seconds. This gradient eventually levels at approximately 150 seconds. The dual fluorescence peaks created following the addition of carbachol was seen in each of the three independent experiments performed and is typical of

the carbachol response. This fluorescence pattern may represent the result of different downstream effector proteins activated by the muscarinic receptor (M3), or the release of Ca^{2+} from a more rapidly deployable store.

BzATP, an agonist of the $hP2Y_{11}$ receptor, is also able to generate a fluorescence response in the 1321N1 cells stably expressing $hP2Y_{11}$. The response rapidly increases following agonists addition before degrading at a gradient comparable to that of carbachol. A similar decrease of approximately 800FU every ten seconds was observed, ultimately reaching a basal level at approximately 150 seconds.

The low fluorescence response of PBS shown in Figure 3.11 confirms that the vehicle control is unable to produce any sizeable fluorescence response. It also shows that the flow rate and pressure of drug addition do not cause mechanosensory release of ATP in quantities sufficient for $P2Y_{11}$ receptor activation. The initial decrease in fluorescence shown in Figure 3.11 (at approximately 10 seconds), exhibited by all three of the ligands tested is likely a result of the addition of the ligand itself, which may dilute the fluorescent dye in the surrounding media loaded onto each well of the 96-well plate, causing a reduction in the background fluorescence. This drop in fluorescence is also seen in the PBS control.

3.4.4 Concentration-response of nucleotides on Ca^{2+} mobilisation in 1321N1 human astrocytoma cells stably expressing the $hP2Y_{11}$ receptor.

Following the identification of Ca^{2+} mobilisation in the 1321N1-$hP2Y_{11}$ cell line in response to several nucleotide analogues, the potency of each of these ligands was investigated. Figure 3.12 shows the percentage Ca^{2+} response of 1321N1-$hP2Y_{11}$ cells following the addition of BzATP (▼) and ATP (◆). These agonists were applied at varying concentrations (ranging from 1nM to 1mM; log values: -8 to -4). These agonists are able to successfully induce Ca^{2+} mobilisation in a concentration-dependent manner.

The concentration-response curves shown in Figure 3.12 were calculated and plotted following non-linear regression analysis of the data. Similar to the cAMP concentration-response experiments, Figure 3.12 shows that a maximal response is achieved for the ligands over approximately 2 log units of agonist concentration. The non-linear regression analysis enables the calculation of EC_{50} values for each of the agonists (BzATP: 5.5μM, log EC_{50} = -5.26 ± 0.10; ATP: 8.5μM, log EC_{50} = -5.07 ± 0.03), revealing the agonists to be similarly potent:

ATP ≈ BzATP

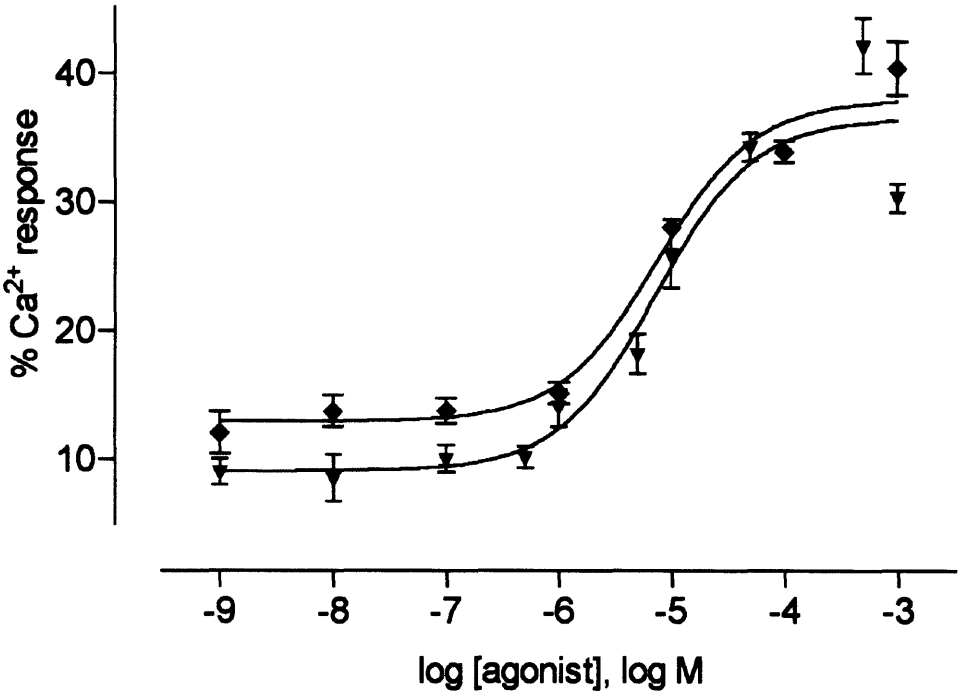

Figure 3.12

Concentration-response curves of Ca^{2+} mobilisation following nucleotide activation of 1321N1 human astrocytoma cells stably expressing the hP2Y$_{11}$ receptor.

The Ca^{2+} response to increasing concentrations of ATP (◆) and BzATP (▼) was measured in 1321N1-hP2Y$_{11}$. Results are expressed as a percentage of the Ca^{2+} response to a supramaximal concentration of carbachol (1mM). The data are the mean ± s.e.m. of one representative experiment of three performed.

3.4.5 Various antagonists inhibit Ca^{2+} mobilisation induced by the activated $hP2Y_{11}$ receptor.

Following the identification of Reactive Red as a novel antagonist of $hP2Y_{11}$-mediated cAMP responses in section 3.3.6, the ability of the Reactive Red and other P2Y antagonists to inhibit Ca^{2+} responses induced by the agonist-activated $hP2Y_{11}$ receptor was investigated. In addition to data analysis, I was also involved in the set-up of the antagonist experiments presented in the following sections and created the antagonist drug plates for use in the FLIPR machine.

The ability of Acid Blue, Phenol Red, Reactive Red and Suramin to reduce BzATP-induced Ca^{2+} mobilisation in the 1321N1-$hP2Y_{11}$ cells was examined. BzATP was used as a reference agonist in these experiments due to its ability to induce Ca^{2+} mobilisation in the 1321N1-$hP2Y_{11}$ cells, and its previous use in the cAMP antagonists experiments (presented in sections 3.3.6 and 3.3.7). Figure 3.13 shows the percentage inhibition of the Ca^{2+} response generated by BzATP (added to a final concentration of 10μM) in 1321N1-$hP2Y_{11}$ cells, following pre-incubation with Acid Blue, Phenol Red, Reactive Red and Suramin. Owing to the solubility of Acid Blue, the compound was used at a final concentration of 10μM, whereas Phenol Red, Reactive Red and Suramin were all added to final concentration of 0.1mM.

Several of the compounds were able to inhibit the $hP2Y_{11}$ functional response. Suramin (78.1 $\pm$ 1.2 % inhibition) was found to give the greatest inhibition followed by Reactive Red (42.8 $\pm$ 3.9%). Statistical analysis has shown the antagonist-induced percentage Ca^{2+} inhibition generated by Phenol Red and

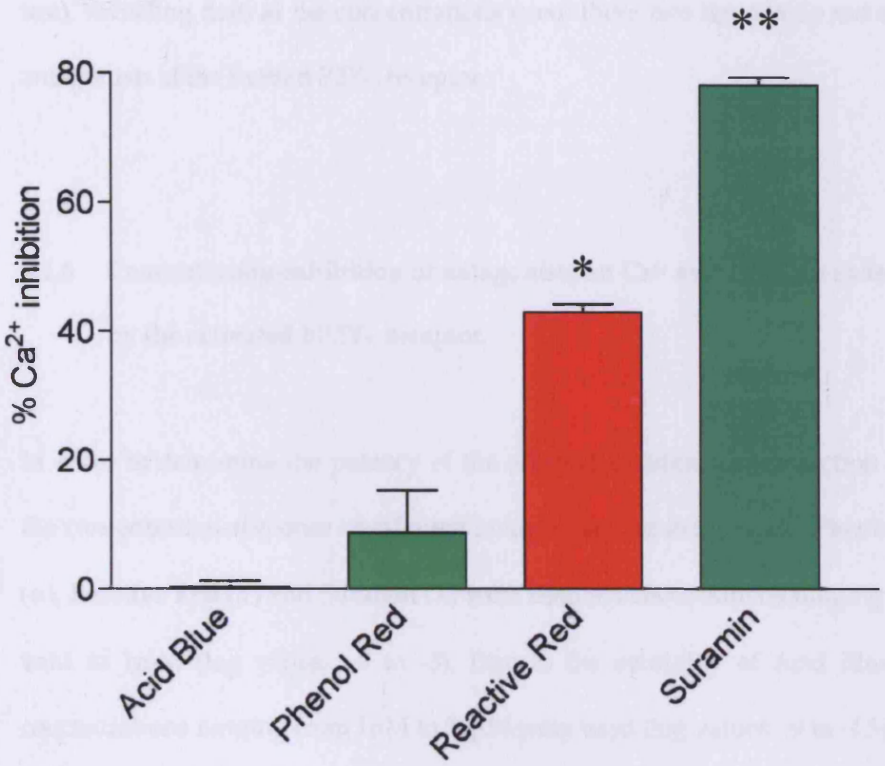

Figure 3.13

Antagonists inhibit Ca^{2+} mobilisation produced by BzATP activation of $hP2Y_{11}$.

Several ligands were screened for their ability to inhibit Ca^{2+} mobilisation generated by BzATP (10μM) activation of $hP2Y_{11}$. Ca^{2+} mobilisation was measured after the addition of BzATP, following pre-incubation of 1321N1-$hP2Y_{11}$ cells with: Phenol Red, Reactive Red, Suramin (each at 0.1mM final concentration) and Acid Blue (added to 10μM final concentration). Results are expressed as a percentage inhibition of the Ca^{2+} mobilisation produced by the addition of the BzATP. Results are the mean ± s.e.m. of three different experiments each performed in triplicate. **, $p < 0.01$; *, $p < 0.05$; when compared with control, by ANOVA with Tukey's post test.

Acid Blue to be indistinguishable from control responses used in the experiments (p value > 0.05 by one-way ANOVA followed by Tukey's post-test), revealing that, at the concentrations used, these two ligands do not act as antagonists at the human P2Y$_{11}$ receptor.

3.4.6 Concentration-inhibition of antagonists on Ca^{2+} mobilisation induced by the activated hP2Y$_{11}$ receptor.

In order to determine the potency of the antagonists identified in section 3.4.5, the concentration-response of different antagonists was determined. Phenol Red (●), Reactive Red (▽) and Suramin (△) were used at concentrations ranging from 1nM to 1mM (log values: -9 to -3). Due to the solubility of Acid Blue (○), concentrations ranging from 1nM to 50μM were used (log values: -9 to -4.3). The Ca^{2+} response of the BzATP-activated hP2Y$_{11}$ receptor (BzATP, ✳; used at a final concentration of 10μM) in the presence and absence of the different concentrations of antagonists was examined.

Suramin and Reactive Red were able to affect the BzATP-mediated hP2Y$_{11}$ Ca^{2+} response in a concentration-dependent manner (Figure 3.14). Suramin (△) was the most potent antagonist of the ligands tested, followed by Reactive Red (▽). The figure also shows Phenol Red (●) and Acid Blue (○) do not antagonise the BzATP induced Ca^{2+} response within the range of concentrations tested. Non-linear regression analysis was performed for each concentration-response experiment. The curves generated by the analysis are shown fitted to Suramin

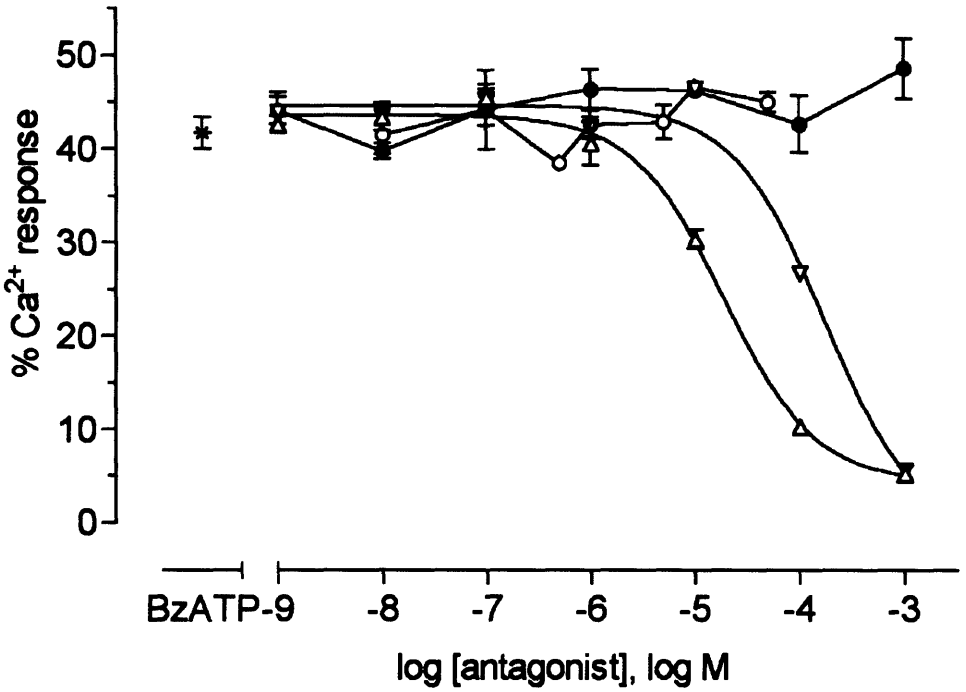

Figure 3.14

Inhibition curves for antagonists on Ca^{2+} mobilisation produced by BzATP, in 1321N1 human astrocytoma cells stably expressing the hP2Y$_{11}$ receptor.

The Ca^{2+} response to 10μM BzATP in 1321N1-hP2Y$_{11}$ cells was measured, following pre-incubation with increasing concentrations of Suramin (△), Reactive Red (▽), Phenol Red (•) and Acid Blue (○). Results are expressed as a percentage of the Ca^{2+} response to a supramaximal concentration of carbachol (1mM). The data are the mean ± s.e.m. of a representative experiment.

and Reactive Red, which gave IC_{50} values of 28.3 $\pm$ 9.43 μM (Suramin) and 270 $\pm$ 98.4 μM (Reactive Red). Phenol Red and Acid Blue were unable to act as antagonists and these data are, therefore, shown with connecting lines drawn between the data points.

	Cyclic AMP accumulation		*Ca^{2+} mobilisation*	
Nucleotide	*EC_{50} (μM)*	*Log EC_{50}*	*EC_{50} (μM)*	*Log EC_{50}*
BzATP	0.9	-6.05 ± 0.06	5.5	-5.26 ± 0.10
ATP	5.7	-5.24 ± 0.07	8.5	-5.07 ± 0.03
α,β-MeATP	23.0	-4.64 ± 0.07		
β,γ-MeATP	24.4	-4.61 ± 0.14		
ADP		ND[a] ± ND		
UTP		ND ± ND		

Table 3.1

EC_{50} values of nucleotides and nucleotide analogues recorded with the cAMP accumulation and Ca^{2+} mobilisation assays in 1321N1-hP2Y$_{11}$ cells.

EC_{50} values were calculated after non-linear regression analysis of the agonist concentration-response experiments. Results are expressed as the mean EC_{50} value (in μM), and log EC_{50} ± s.e.m., of three to five independent experiments - each performed in triplicate. [a]ND, not determined, indicates that the responses generated could not be used to calculate an EC_{50} value.

	Ca^{2+} mobilisation		*Cyclic AMP accumulation*	
antagonist	*IC_{50} (μM)*	*Log IC_{50}*	*IC_{50} (μM)*	*Log IC_{50}*
Suramin	28.3	-4.55 ± 0.15		
Reactive Red	270.0	-3.57 ± 0.17	1.7	-5.76 ± 0.07
Phenol Red		ND[a] ± ND		
Acid Blue		ND ± ND		

Table 3.2

Antagonists IC_{50} values recorded with the cAMP accumulation and Ca^{2+} mobilisation assays in 1321N1-hP2Y$_{11}$ cells.

IC_{50} values were calculated after non-linear regression analysis of the antagonist concentration-response experiments. Results are expressed as the mean IC_{50} value (in μM), and log IC_{50} ± s.e.m., of three independent experiments, each performed in triplicate. [a]ND, not determined, indicates that the responses generated could not be used to calculate an IC_{50} value.

3.5 Summary

RT-PCR analysis on the cell lines used throughout the experiments presented in this chapter revealed the absence of RNA encoding various P2Y receptors ($hP2Y_1$, $hP2Y_2$, $hP2Y_4$, $hP2Y_6$, $hP2Y_{11}$, $hP2Y_{12}$) in the untransfected 1321N1 cells, and the presence of RNA encoding the $hP2Y_{11}$ receptor in the 1321N1-$hP2Y_{11}$ cells.

Following the creation of the stable cell lines the ability of the β_2-adrenoceptor, endogenous to 1321N1 cells, to produce cAMP following incubation with isoproterenol was examined. Concentration-response experiments were undertaken with untransfected 1321N1 cells to investigate the conditions required for the use of the β_2-adrenoceptor as a cAMP-producing endogenous standard. The mean EC_{50} value, obtained for isoproterenol (61.4nM, log EC_{50} = -7.21 $\pm$ 0.05), revealed the cAMP assay could accurately record *de novo* cAMP production in the 1321N1 cells and that cAMP response induced by 10μM isoproterenol was appropriate for use as the endogenous standard to which all exogenous receptor cAMP responses would be normalised.

The development of the use of an endogenous response was followed by an investigation into the ability of 1321N1-$hP2Y_{11}$ cells to produce a cAMP response upon ligand activation. The time-course experiments confirmed maximal cAMP accumulation was achieved within the first ten minutes of incubation with ligand and this incubation period was used in all subsequent experiments. The ability of the agonist stimulated 1321N1-$hP2Y_{11}$ cells to

promote cAMP accumulation (and the inability of the untransfected cells to induce a similar response) revealed that functional $hP2Y_{11}$ receptors were expressed in the cell line.

High-concentration agonist-screening experiments on 1321N1-$hP2Y_{11}$ cells confirmed the ability of the $hP2Y_{11}$ to act as a nucleotide receptor capable of inducing intracellular cAMP accumulation in response to BzATP, ATP, βγ-MeATP and αβ-MeATP. The activation of adenylyl cyclase by ATP in the initial agonist screening experiments, and the absence of any cAMP response in the PBS control or UTP and ADP experiments conforms to previous pharmacological studies undertaken on the $hP2Y_{11}$ receptor (Communi et al. 1997), where preferential activation by 100μM ATP and minimal responses at 100μM ADP or 100μM UTP are reported. The subsequent concentration-response experiments, undertaken with the 1321N1-$hP2Y_{11}$ cells, revealed *de novo* cAMP accumulation to be agonist-concentration dependent, with the following cAMP-response agonist rank order of potency for the $hP2Y_{11}$ receptor:

BzATP > ATP > α,β-meATP = β,γ-meATP

The antagonist study, which investigated the inhibition of agonist-induced cAMP production in the 1321N1-$hP2Y_{11}$ cells, revealed that Reactive Red, a previously unknown $hP2Y_{11}$ receptor antagonist, was able to inhibit cAMP accumulation in a concentration-dependent manner.

Ca^{2+} mobilisation was examined in the 1321N1 cells and the ability of the endogenous muscarinic M3 receptor to generate an intracellular Ca^{2+} response upon stimulation with carbachol was investigated. Carbachol was found to produce a maximal Ca^{2+} response at a final concentration of 1mM (log value -3) and was used at this concentration as the endogenous standard in all subsequent experiments. The EC_{50} value calculated for carbachol (11.0μM, log EC_{50} = -4.96 ± 0.12), is similar to that obtained previously in 1321N1 cells (Stephan and Sastry, 1992), however, these EC_{50} values are not directly comparable, as the previous study investigated IP accumulation and not Ca^{2+} mobilisation. The present experiments therefore represent a novel investigation into carbachol-induced Ca^{2+} mobilisation in 1321N1 cells.

Following the development of the endogenous standard for Ca^{2+} responses, the ability of the 1321N1-hP2Y$_{11}$ cells to induce Ca^{2+} mobilisation in response to known P2Y agonists was examined. The high-concentration agonist screening experiments and subsequent concentration-response experiments revealed ATP and BzATP to be similarly efficacious and potent. BzATP-evoked Ca^{2+} responses have not been described previously and represent a novel characterisation of the human P2Y$_{11}$ receptor. EC_{50} values for the P2Y$_{11}$-mediated Ca^{2+}-response give the following rank order of potency: **BzATP = ATP.** In a similar manner to the time-course investigations undertaken with the cAMP assay, an examination of Ca^{2+} mobilisation over time, using carbachol, BzATP and PBS revealed the maximum fluorescence response was generated within the assay's time frame.

Following the investigation of agonist-induced Ca^{2+} responses, the ability of various ligands to antagonise hP2Y$_{11}$-mediated Ca^{2+} mobilisation was examined.

In addition to Suramin, a previously known non-selective antagonist of $hP2Y_{11}$ receptor, Reactive Red was found to inhibit Ca^{2+} mobilisation in a concentration-dependent manner. This antagonist had not previously been characterised at $P2Y_{11}$ receptors and this is a novel finding.

This chapter has shown that the 1321N1-$hP2Y_{11}$ cells express functional $hP2Y_{11}$ receptors, confirmed by the activation of the dual signalling pathways previously reported for the receptor. The similarities and differences between the agonist and antagonist responses presented in this chapter with previously published $hP2Y_{11}$ and $cP2Y_{11}$ receptor data are explored further in Chapter 6.

Chapter 4

Agonist responses of the XlP2Y$_{11}$ receptor.

4.1 Introduction

As described in Chapter 1, when stably expressed in 1321N1 human astrocytoma and CHO-K1 cells, the human P2Y$_{11}$ receptor has been shown to be a selective purinoceptor, activated by various nucleotides and nucleotide analogues (Communi et al., 1997 & 2001; Qi et al., 2001[a]). As outlined in Chapter 1, a large proportion of the receptors termed valid members of the P2Y receptor family have been shown to stimulate PKC and generate an intracellular Ca^{2+} second messenger response. A smaller group of P2Y receptors has been shown to inhibit adenylyl cyclase, decreasing cAMP production.

Previous studies on the P2Y$_{11}$ receptor orthologues, both human (hP2Y$_{11}$) and canine (cP2Y$_{11}$), have shown this receptor subtype to hold a unique position within the P2Y purinoceptor family, as it possesses the capacity, upon

activation, to generate second messenger responses typical of phospholipase C and adenylyl cyclase activation, resulting in an increase in *de novo* cyclic AMP production and intracellular Ca^{2+} mobilisation (Communi et al., 1997; Zambon et al., 2001). The work presented in this chapter endeavours to identify whether the *Xenopus* orthologue of the human $P2Y_{11}$ receptor, $XlP2Y_{11}$, can be justifiably termed a valid member of the P2Y purinoceptor family. That is, can it generate a second messenger response to extracellular nucleotides. This chapter also examines whether $XlP2Y_{11}$, like the previously characterised $hP2Y_{11}$ and $cP2Y_{11}$ orthologues, possesses the unique ability within the P2Y receptor family of stimulating phospholipase C (PLC) and adenylyl cyclase (AC) responses upon receptor activation. In order to investigate the dual-pathway signalling capacity of $XlP2Y_{11}$, the cAMP accumulation and Ca^{2+} mobilisation assays (as seen in Chapter 3) have been employed to evaluate the second messenger production of the novel *Xenopus laevis* receptor in response to various nucleotide ligands. Responses typical of PLC activation will be assessed through the measurement of intracellular Ca^{2+} mobilisation, whilst the activity of AC will be assessed through the measurement of *de novo* cAMP production.

As outlined above, to date, only human and canine orthologues of the $P2Y_{11}$ receptor have been cloned and characterised. Consequently, these experiments represent the first characterisation of a non-mammalian orthologue of the $P2Y_{11}$ receptor. This study provides a unique opportunity to learn more about the pharmacological profile of this particular P2Y receptor subtype.

4.2 Ca^{2+} mobilisation in 1321N1 human astrocytoma cells stably expressing the $XlP2Y_{11}$ receptor.

In order to examine the ability of $XlP2Y_{11}$ to generate a second messenger response, the Ca^{2+} assay was employed to quantify intracellular calcium release from 1321N1 cells stably expressing the $XlP2Y_{11}$ receptor. The 1321N1-$XlP2Y_{11}$ cells were incubated with nucleotide analogues shown to have activity at mammalian $P2Y_{11}$ receptors and the calcium response was determined, as described in Chapter 2. The ligands selected for this characterisation were tested previously in pharmacological characterisations of the human and canine $P2Y_{11}$ orthologues (Communi et al., 1999; Qi et al., 2001[a]; Zambon et al., 2001). These studies, and my own pharmacological characterisation of the $hP2Y_{11}$ receptor, shown in Chapter 3, reveal that the most potent agonists are able to generate substantial second messenger responses at a final concentration of 100µM, with responses able to be elicited by partial agonists at 1mM. Therefore, UTP, ATP, 2MeSATP, 2MeSADP and BzATP were used in these initial high-concentration ligand screening experiments at a final concentration of 100µM. As outlined in Chapter 1, these previous pharmacological characterisations of the human $P2Y_{11}$ receptor have shown ADP to be a weak agonist, generating small second messenger responses in both PLC and AC activated pathways, in response to high concentrations of ligand. Given this, and given the sequence similarity between the human and *Xenopus* $P2Y_{11}$ receptors, ADP was used in these initial high-concentration ligand screening experiments at a final concentration of 1mM.

4.2.1 $XlP2Y_{11}$ is activated by nucleotides, producing a Ca^{2+} response.

Figure 4.1 shows the percentage Ca^{2+} response of 1321N1 human astrocytoma cells stably expressing $XlP2Y_{11}$ following addition of: UTP, ATP, 2MeSATP, 2MeSADP, BzATP (all added to a final concentration of 10μM) and ADP (added to a final concentration of 1mM). The results are normalised to the Ca^{2+} response produced after the addition of 1mM carbachol, and are expressed as a percentage of this value.

The 1321N1-$XlP2Y_{11}$ cell line was able to produce a second messenger signal in response to extracellular nucleotides and nucleotide analogues (Figure 4.1), thus identifying $XlP2Y_{11}$ as a nucleotide receptor capable of causing intracellular Ca^{2+} mobilisation upon the addition of extracellular ligands. The normalised Ca^{2+} responses produced by ATP (7.9 $\pm$ 0.71 %), 2MeSADP (17.2 $\pm$ 1.13 %), 2MeSATP (12.2 $\pm$ 4.88 %) and BzATP (20.4 $\pm$ 2.94 %) are all significantly different from the Ca^{2+} mobilisation produced by the PBS vehicle control (p value < 0.05 by Student's two-tailed paired *t*-test), whereas the Ca^{2+} responses generated by incubation with UTP (1.3 $\pm$ 1.03 %) and ADP (3.21 $\pm$ 0.65%) are not significantly statistically different from the negative control.

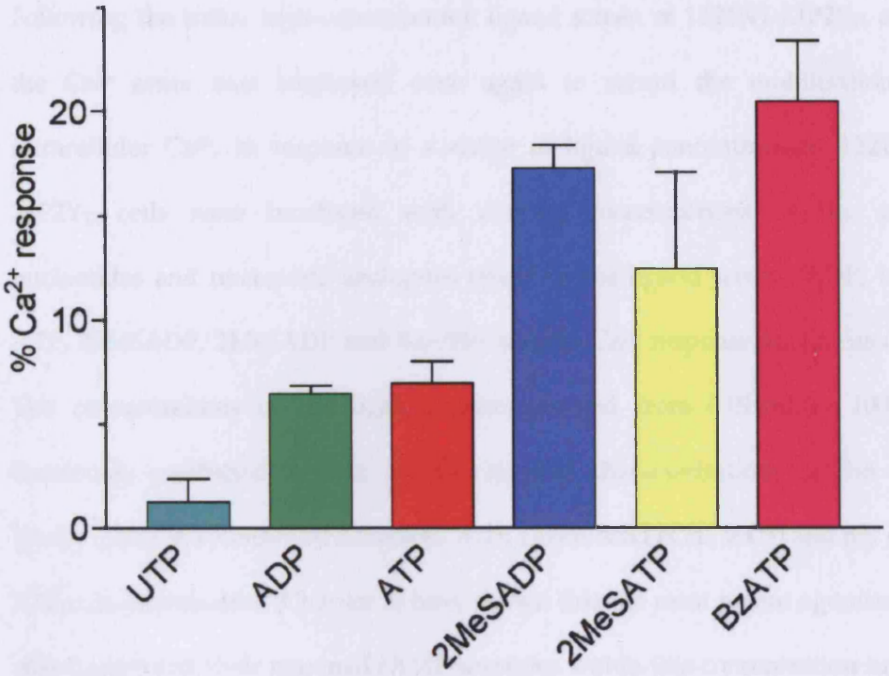

Figure 4.1

XlP2Y$_{11}$ is activated by nucleotides, producing a Ca^{2+} response.

Several nucleotide analogues were screened for their ability to induce a Ca^{2+} response in 1321N1 human astrocytoma cells stably expressing XlP2Y$_{11}$. Ca^{2+} mobilisation was measured after the addition of: UTP, ATP, 2MeSATP, 2MeSADP, BzATP (each at 100 μM) and 1mM ADP. Results are expressed as a percentage of the Ca^{2+} response to a supramaximal concentration of carbachol (1mM) and represent the mean ± s.e.m. of at least three different experiments, each performed in triplicate. The data shown are control response deducted.

4.2.2 Concentration-response of nucleotides on Ca^{2+} mobilisation in 1321N1- $XlP2Y_{11}$ cells.

Following the initial high-concentration ligand screen of 1321N1-$XlP2Y_{11}$ cells, the Ca^{2+} assay was employed once again to record the mobilisation of intracellular Ca^{2+}, in response to a range of ligand concentrations. 1321N1-$XlP2Y_{11}$ cells were incubated with varying concentrations of the same nucleotides and nucleotide analogues tested in the ligand screen (ADP, UTP, ATP, 2MeSADP, 2MeSADP and BzATP) and the Ca^{2+} response was measured. The concentrations of the ligands tested ranged from 0.01µM to 100µM. Previously published agonist pharmacological characterisations of the P2Y family (King & Townsend-Nicholson, 2003; Lazarowski et al., 2003) and my own $P2Y_{11}$ characterisation (Chapter 3) have shown that the most potent agonists are able to generate their maximal cAMP response within this concentration range. This holds true for $hP2Y_{11}$ (Communi et al., 2001; Qi et al., 2001[a]) and $cP2Y_{11}$ (Zambon et al., 2001).

Figure 4.2 shows the concentration-responses of Ca^{2+} mobilisation to: ADP, UTP, ATP, 2MeSATP, 2MeSADP and BzATP. The data displayed in Figure 4.2 are representative experiments taken from one of the 3 independent experiment performed for each ligand. The curves generated by non-linear regression analysis are shown fitted to ATP (◆), 2MeSATP, (■) 2MeSADP (▲) and BzATP (▼). Curves have not been fitted to the UTP (□) and ADP (△) representative experiments, which are shown with lines connecting the individual data points.

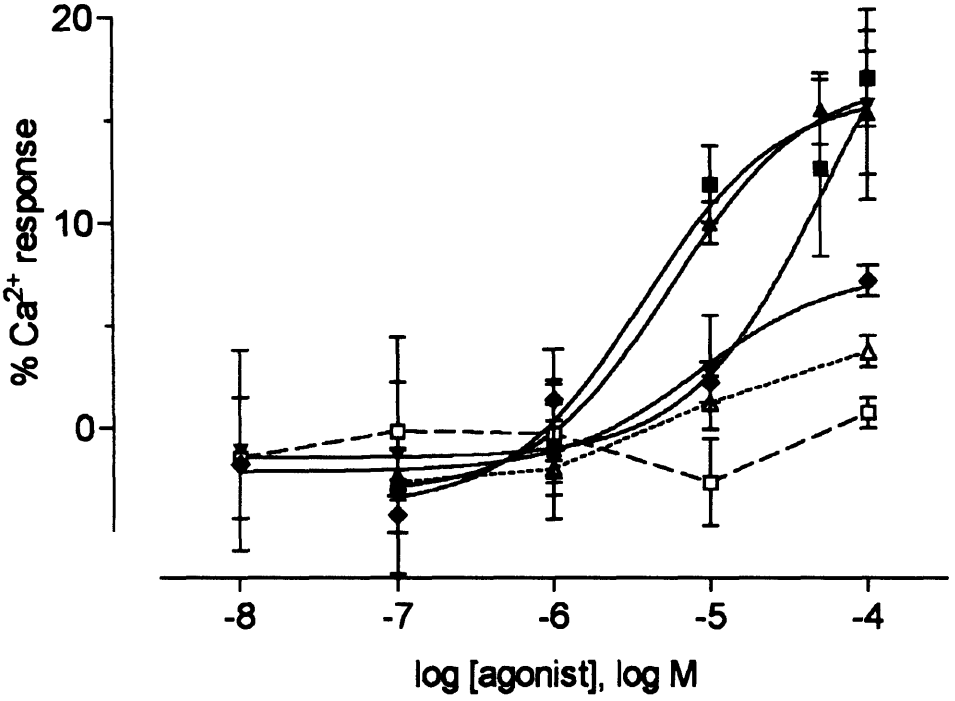

Figure 4.2

Concentration-response curves of Ca^{2+} mobilisation following nucleotide activation of 1321N1 human astrocytoma cells stably expressing the $XlP2Y_{11}$ receptor.

The Ca^{2+} response to increasing concentrations of nucleotides was measured in cultured cells as described in the Materials and Methods: UTP (□), ADP (△), ATP (◆), 2MeSATP (■), 2MeSADP (▲) and BzATP (▼). Results are expressed as a percentage of the Ca^{2+} response to a supramaximal concentration of carbachol (1mM). The data are the mean ± s.e.m. of one representative experiment of three performed.

Each of the ligands tested were successful in eliciting a Ca^{2+} response in a concentration-dependent manner, with increasing concentrations of ligands able to mobilise increasing amounts of Ca^{2+}. Consistent with previous P2Y receptor characterisations (Marteau et al., 2003; Communi et al., 2001), Figure 4.2 shows that the maximal Ca^{2+} response is achieved over approximately 2 to 2.5 log units of ligand concentration. Curves are not fitted to the Ca^{2+} responses generated by ADP and UTP, because a maximal response is not reached in the range of ligands tested.

The calculated EC_{50} values for ATP (2.54 $\pm$ 1.06 μM), 2MeSATP (1.96 $\pm$ 0.92 μM), 2MeSADP (7.49 $\pm$ 1.52 μM) and BzATP (42.51 $\pm$ 11.58 μM) (shown in Table 4.1), allowing the following Ca^{2+} response agonist potency order to be formed for the $XlP2Y_{11}$ receptor:

ATP ≈ 2MeSATP > 2MeSADP > BzATP >> ADP

4.3 The effect of nucleotides on cAMP accumulation in 1321N1 human astrocytoma cells stably expressing the $XlP2Y_{11}$ receptor.

Having shown in section 4.2, that 1321N1-$XlP2Y_{11}$ cells were able to produce an intracellular Ca^{2+} response following treatment with nucleotides, the ability of these cells to generate a cAMP response was investigated. 1321N1 cells stably expressing the $XlP2Y_{11}$ receptor were incubated with the nucleotides and nucleotide analogues (ADP, UTP, ATP, 2MeSADP, 2MeSADP and BzATP) used

in the characterisation of the 1321N1-XlP2Y_{11} Ca^{2+} response (Chapter 4.2.1 and 4.2.2) and *de novo* cAMP production was quantified.

4.3.1 XlP2Y_{11} is activated by nucleotides, producing a cAMP response.

Figure 4.3 shows the percentage cAMP response of 1321N1 human astrocytoma cells stably expressing XlP2Y_{11} following ten-minute incubations with: UTP, ATP, 2MeSATP, 2MeSADP, BzATP (each added to a final concentration of 10μM) and ADP (added to a final concentration of 1mM). The results are expressed as a percentage of the response produced after a ten-minute incubation in the presence of 10μM isoproterenol.

The normalised cAMP responses produced by UTP (5.4 ± 2.23 %), ATP (10.1 ± 1.48 %), 2MeSADP (8.4 ± 1.22 %), 2MeSATP (13.0 ± 1.02 %) and BzATP (12.0 ± 2.90 %) are all significantly different from the cAMP accumulation produced by the PBS/negative vehicle control, (*, $p < 0.05$, by ANOVA with Tukey's post test), whereas the minimal cAMP response generated by incubation with ADP (0.2 ± 0.09 %) exhibits no statistically significant difference from the PBS control.

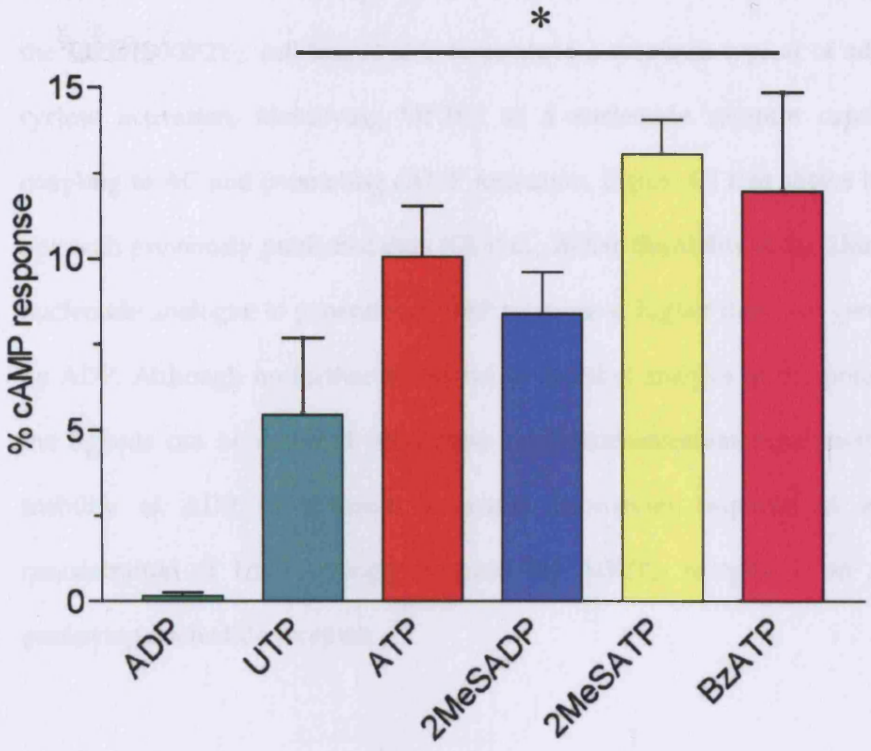

Figure 4.3

XlP2Y$_{11}$ is activated by nucleotides, producing a cAMP response.

Nucleotide analogues were screened for their ability to induce a cAMP response in 1321N1 human astrocytoma cells stably expressing XlP2Y$_{11}$. *De novo* cAMP production was determined after incubation with 100μM of each of: UTP, ATP, 2MeSATP, 2MeSADP, BzATP and 1mM ADP. Results are expressed as a percentage of the cAMP response to a supramaximal concentration of isoproterenol (10μM), and represent the mean ± s.e.m. of three different experiments, each performed in triplicate. *, $p < 0.05$, by ANOVA with Tukey's post test. The data shown are control response deducted.

These data show that, in response to the addition of extracellular nucleotides, the 1321N1-XlP2Y_{11} cell line is able to produce a response typical of adenylyl cyclase activation, identifying XlP2Y_{11} as a nucleotide receptor capable of coupling to AC and promoting cAMP formation. Figure 4.3 also shows that, in line with previously published data (Qi et al., 2001[a]), the ability of the 2MeSADP nucleotide analogue to generate a cAMP response is higher than that generated by ADP. Although no further inferences or detailed analysis of the potency of the ligands can be deduced from these single concentration experiments, the inability of ADP to generate a second messenger response at a final concentration of 1mM strongly suggests the XlP2Y_{11} receptor is an ATP - preferring nucleotide receptor.

4.3.2 Nucleotides produce a concentration-dependent cAMP response in 1321N1-XlP2Y_{11} cells.

In order to further examine the signalling ability of the XlP2Y_{11} receptor, the cAMP assay was employed to record the accumulation of *de novo* cAMP production in 1321N1-XlP2Y_{11} cells in response to a range of ligand concentrations. The cells were incubated with the same nucleotides and nucleotide analogues used in the ligand screen of Section 4.3.1 (ADP, UTP, ATP, 2MeSADP, 2MeSADP and BzATP) and cAMP accumulation was measured.

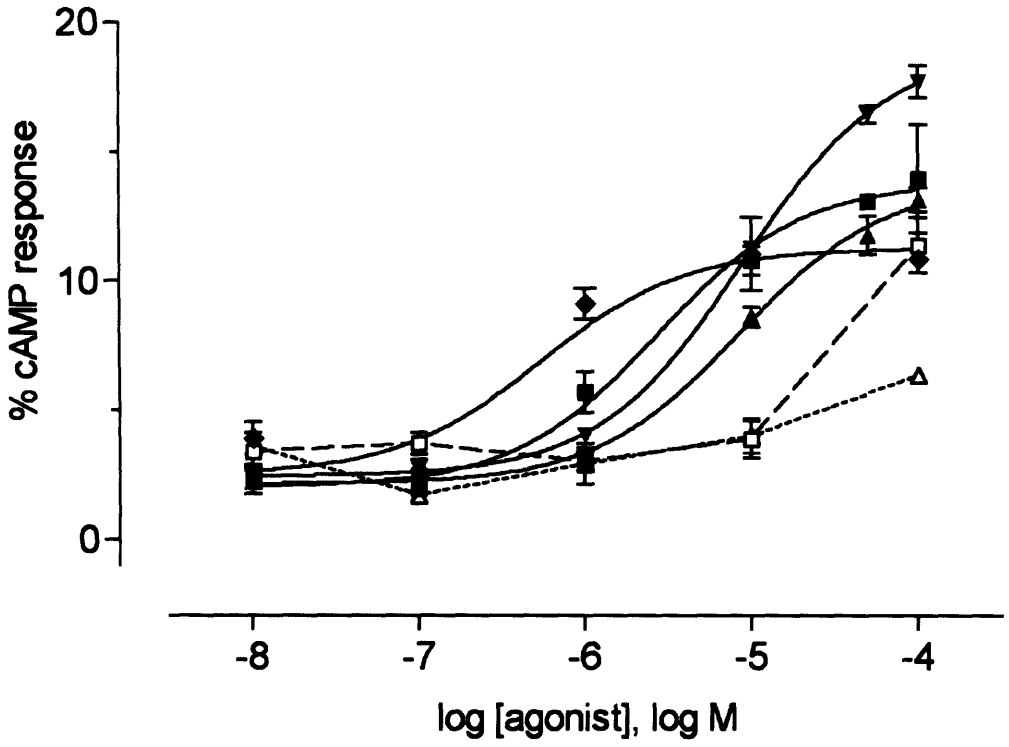

Figure 4.4

Concentration-response curves of the cAMP response following nucleotide activation of 1321N1 human astrocytoma cells stably expressing the XlP2Y$_{11}$ receptor.

The cAMP response to increasing concentrations of nucleotides was measured following incubation with: UTP (□), ATP (◆), 2MeSATP (■), 2MeSADP (▲), BzATP (▼) and ADP (△). Results are expressed as a percentage of the cAMP response to a supramaximal concentration of isoproterenol (10μM). The data are the mean ± s.e.m. of one representative experiment of three to five performed for each ligand.

In order to replicate the range of concentrations used in the Ca^{2+} concentration-response experiments (Section 4.2.2), the concentrations of the ligands tested ranged from 0.01μM to 100μM (log values: -8 to -4).

Figure 4.4 shows the percentage cAMP response of 1321N1-XlP2Y_{11} cells following ten-minute incubation with increasing concentrations of: ADP, UTP, ATP, 2MeSATP, 2MeSADP, BzATP. The results are normalised to the response obtained after a ten-minute incubation in the presence of 10μM isoproterenol. The data displayed are representative experiments taken from one of the three to five independent experiment performed for each ligand. Non-linear regression analysis was performed for each set of ligand data. The curves have been fitted to the results for ATP (◆), 2MeSATP (■), 2MeSADP (▲), and BzATP (▼) in Figure 4.4. Curves have not been fitted to the UTP (□) and ADP (△) experiments, which are shown with lines connecting the individual data points.

Although a curve may be fitted to the representative UTP experiment shown in Figure 4.4, the other independent UTP experiments exhibited large fluctuations in the percentage cAMP response generated across all concentrations (data not shown). The experiment shown in Figure 4.4 has a relatively high cAMP response at the 100μM (log value -4) ligand concentration, which supports the previously recorded UTP response in the high-concentration ligand screen (Figure 4.3) - found to be significantly different from the PBS control. Curves are not fitted to the cAMP responses generated by ADP, because a maximal response is not reached in the range of ligands tested. Each of the ligands tested elicited a concentration-dependent cAMP response. Consistent with previous

Nucleotide	Ca^{2+} mobilisation EC_{50} (μM)	$Log\ EC_{50}$
ATP	2.5	-5.60 ± 0.19
2MeSATP	2.0	-5.71 ± 0.22
ADP		ND[a] ± ND
2MeSADP	7.5	-5.13 ± 0.08
BzATP	42.5	-4.37 ± 0.12
UTP		ND ± ND

Table 4.1

EC_{50} values of nucleotides able to elicit a Ca^{2+} response in 1321N1 human astrocytoma cells stably expressing the $XlP2Y_{11}$ receptor.

EC_{50} values were calculated following non-linear regression analysis of the Ca^{2+} concentration-response data obtained for each ligand. Results are expressed as the mean EC_{50} value (in μM), and log EC_{50} ± s.e.m., of three to four independent experiments, each performed in triplicate. [a]ND, not determined, indicates that an EC_{50} value could not be calculated.

characterisations (Marteau et al., 2003; Communi et al., 2001) and my own pharmacological characterisation in section 4.2.2, the concentration range of ligand required to elicit a maximal cAMP response for each of the concentration-response curves is achieved over approximately 2 to 2.5 log units.

As with the Ca^{2+} responses experiments, incubation of 1321N1-XlP2Y_{11} cells with nucleotides produces concentration-dependent cAMP responses. The calculated EC_{50} values for ATP (1.0μM, log EC_{50} = -6.02 ± 0.01) 2MeSATP (1.7μM, log EC_{50} = -5.76 ± 0.11) 2MeSADP (12.6μM, log EC_{50} = -4.90 ± 0.10) and BzATP (15.6μM, log EC_{50} = -4.81 ± 0.12) (also shown in Table 4.2) can be used to create a cAMP response agonist potency order for the XlP2Y_{11} receptor:

ATP ≥ 2MeSATP > 2MeSADP ≥ BzATP >> ADP

Nucleotide	*Cyclic AMP accumulation* EC_{50} (μM)	Log EC_{50}
ATP	1.0	-6.02 ± 0.01
2MeSATP	1.7	-5.76 ± 0.11
ADP		ND[a] ± ND
2MeSADP	12.6	-4.90 ± 0.10
BzATP	15.6	-4.81 ± 0.12
UTP		ND ± ND

Table 4.2

EC_{50} values of nucleotides able to elicit cAMP accumulation in 1321N1 human astrocytoma cells stably expressing the $XlP2Y_{11}$ receptor.

EC_{50} values were calculated following non-linear regression analysis of the cAMP concentration-response data obtained for each ligand. Results are expressed as the mean ± s.e.m. of three to four independent experiments, each performed in triplicate. [a]ND, not determined, indicates that an EC_{50} value could not be calculated.

4.3 Summary

The Ca^{2+} mobilisation assay was initially employed to characterise the intracellular second messenger response generated by the $XlP2Y_{11}$ receptor, in response to high concentrations of: UTP, ATP, 2MeSATP, 2MeSADP, BzATP (each at 100μM final concentration) and ADP (at a final concentration of 1mM). The ligands were chosen and used at concentrations shown previously to elicit an intracellular Ca^{2+} response at $P2Y_{11}$ receptors (Qi et al., 2001[a]; Zambon et al. 2001). The initial high-concentration ligand screening experiments undertaken in 1321N1-$XlP2Y_{11}$ cells revealed that several of these ligands were able to generate a second messenger signalling response in the form of Ca^{2+} release from intracellular stores. Following this initial screening, concentration-response curves were generated, providing a more detailed pharmacological profile of the receptor. These investigations revealed the activated $XlP2Y_{11}$ receptor was able to induce concentration dependent Ca^{2+} responses when stably expressed in the 1321N1 cells with a rank order of potency equal to:

ATP ≈ 2MeSATP > 2MeSADP > BzATP >> ADP

The ability of the receptor to activate the cAMP second messenger signalling pathway was also investigated. The initial ligand screening experiments revealed that, in addition to Ca^{2+} mobilisation, the activated *Xenopus* receptor could also generate cAMP in response to the same ligands used in the Ca^{2+} mobilisation experiments. Subsequent agonist concentration-response studies revealed the cAMP accumulation to be concentration-dependent. Analysis of the concentration-response curves allowed the determination of the EC_{50} values,

enabling the construction of a cAMP response agonist potency order for the $XlP2Y_{11}$ receptor:

ATP ≥ 2MeSATP > 2MeSADP ≥ BzATP >> ADP

Both the cAMP and Ca^{2+} second messenger responses reveal ATP and 2MeSATP to be more efficacious than ADP and 2MeSADP. The similarities between the agonist efficacies and potencies of the $XlP2Y_{11}$ receptor responses in the different signalling pathways (and a comparison with previously published $P2Y_{11}$ data) are shown in Chapter 6.

When expressed in human astrocytoma 1321N1 cells, the $XlP2Y_{11}$ receptor can be activated by nucleotides and nucleotide analogues, to generate two different second messenger responses - mobilisation of Ca^{2+} from intracellular stores and an increase in the production of cAMP. The data in this chapter represent the first pharmacological characterisation of a non-mammalian $P2Y_{11}$ receptor orthologue, defined as such by (1) its response to nucleotides and (2) its ability to activate dual signalling pathways.

Chapter 5

Antagonism of the XlP2Y$_{11}$ receptor.

5.1 Introduction

As outlined in Chapter 1, relatively few selective antagonists exist compared to the range of P2Y agonists. The use of selective agonists, and the complex activity profiles generated by multiple non-selective antagonists, can be used for the pharmacological profiling and the subsequent discrimination between P2Y purinoceptor family subtypes.

As described in Chapter 4, when stably expressed in 1321N1 human astrocytoma cells, the XlP2Y$_{11}$ receptor has been shown to be a selective purinoceptor, capable of generating both cAMP and Ca^{2+} second messenger signals in response to the presence of various nucleotides and nucleotide analogues. This chapter seeks to examine the ability of known P2Y antagonists to inhibit XlP2Y$_{11}$-mediated second messenger responses. The cAMP

accumulation and Ca^{2+} mobilisation assays have been employed to identify the extent to which $XlP2Y_{11}$ responses are able to be inhibited by known P2Y receptor antagonists.

As outlined in Chapters 1 and 4, to date, only human and canine orthologues of the $P2Y_{11}$ receptor have been cloned and a pharmacological characterisation with agonists and antagonists performed. Therefore, the work described in this chapter represents the first antagonist characterisation of a non-mammalian $P2Y_{11}$ receptor orthologue. Previous studies on the $P2Y_{11}$ receptor, both human ($hP2Y_{11}$) and canine ($cP2Y_{11}$), have shown these receptor orthologues to possess very similar antagonist sensitivities (Zambon et al., 2001; Qi et al., 2001[b]). The work in this chapter will therefore endeavour to identify whether the $XlP2Y_{11}$ receptor possess a similar antagonist profile to its human and canine counterparts.

5.2 The effect of antagonists on cAMP accumulation in 1321N1-$XlP2Y_{11}$ cells.

In order to assess the ability of several ligands to act as antagonists, the cAMP assay was employed to record the accumulation of *de novo* cAMP production in 1321N1 cells stably expressing the $XlP2Y_{11}$ receptor. The ability of 2MeSATP (a ligand previously shown in chapter 4 to act as an agonist of the $XlP2Y_{11}$ receptor) to generate cAMP was recorded in the presence of these ligands.

The ability of an antagonist to inhibit a second messenger response can be assessed with a greater degree of accuracy and confidence when an efficacious agonist is used (allowing clear visualisation of the decrease in agonist response). Correspondingly, the ability of an antagonist to shift an agonist induced concentration-response curve is easier to visualise when used in conjunction with a potent activator of the second messenger response. The ability of 2MeSATP to potently and efficaciously activate the $XlP2Y_{11}$ receptor makes this agonist an ideal candidate to study the ability of antagonists to inhibit $XlP2Y_{11}$-mediated cAMP responses.

The ligands selected for this pharmacological study were used in previous antagonist characterisations of the purinoceptor family (as outlined in Chapter 1) and in characterisations of the human and canine $P2Y_{11}$ receptors (Communi et al., 1999; Qi et al., 2001[b]; Zambon et al., 2001)(Chapter 3). Potent antagonists of the $hP2Y_{11}$ and $cP2Y_{11}$ receptors have been shown, in previous characterisations (Suramin and Reactive Blue 2) (Qi et al., 2001[b]) and my own antagonist studies (Suramin and Reactive Red) (Chapter 3), to generate substantial second messenger inhibition when used at concentrations of approximately 100μM, whereas less effective antagonists have been shown to elicit a smaller agonist inhibitions when used at much higher concentrations. Taking this into account, high concentrations (1mM final concentrations) were used in the initial experiments in order to screen the ligands for any potential antagonist ability.

5.2.1 Antagonists inhibit cAMP accumulation induced by agonist activation of the $XlP2Y_{11}$ receptor.

1321N1 human astrocytoma cells stably expressing the $XlP2Y_{11}$ were pre-incubated with several different P2 receptor antagonists. PPADS, Suramin, Phenol Red, Reactive Blue and Reactive Red were each used initially at 1mM final concentration, whilst the highest concentration of Acid Blue able to be used was 10μM (due to the solubility of this compound). Following antagonist preincubation, the ability of 2MeSATP (at a final concentration of 10μM) to generate *de novo* cAMP production was determined. By comparing the agonist-induced response, in the presence of antagonist, to that of the agonist alone, the ability of the ligands to inhibit the second messenger response was determined. Previous experiments, in Chapter 4, have shown that 10μM 2MeSATP induces a cAMP response equivalent to approximately 12 percent of the response produced by 10μM isoproterenol.

Figure 5.1 shows the percentage inhibition of the 2MeSATP induced cAMP response following pre-incubation with PPADS, Suramin, Phenol Red, Reactive Blue, Reactive Red (added to 1mM final concentrations) and Acid Blue (added to a 10μM final concentration). The 2MeSATP control response (data not shown) induced a response equal to 14.01 $\pm$ 1.97 percent of the 10μM isoproterenol response. The raw data obtained for the antagonists were transformed from the percentage cAMP response obtained to show the percentage inhibition of the 2MeSATP response generated by each of the ligands. Reactive Red, Reactive Blue, Phenol Red and Suramin were each able to inhibit the 2MeSATP response.

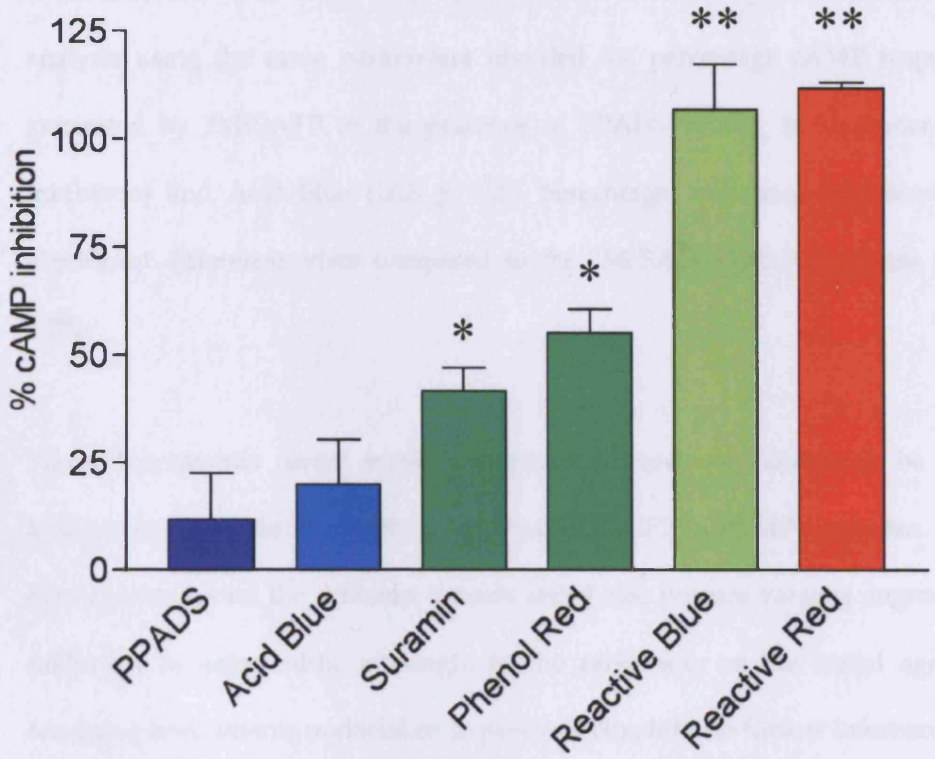

Figure 5.1

Antagonists inhibit cAMP accumulation produced by 2MeSATP activation of $XlP2Y_{11}$.

Several ligands were screened for their ability to inhibit cAMP accumulation produced by 2MeSATP activation of $XlP2Y_{11}$. Following pre-incubation with: PPADS, Suramin, Phenol Red, Reactive Blue, Reactive Red (each at 1mM final concentration) and Acid Blue (10μM final concentration), *de novo* cAMP production was measured after incubation with 10μM of 2MeSATP. Results are expressed as a percentage inhibition of the cAMP response to 10μM 2MeSATP and represent the mean ± s.e.m. of three different experiments, each performed in triplicate. **, $p < 0.01$; *, $p < 0.05$; compared with control response, by ANOVA with Tukey's post test.

Suramin (41.6 ± 5.50 percentage inhibition), Phenol Red (55.1 ± 5.6 percentage inhibition), Reactive Blue (106.9 ± 10.4 percentage inhibition) and Reactive Red (110.8 ± 1.5 percentage inhibition) all show a significant difference in responses to the 2MeSATP control ($p > 0.05$, by ANOVA with Tukey's post test). Statistical analysis using the same parameters revealed the percentage cAMP response generated by 2MeSATP in the presence of PPADS (11.6 ± 10.84 percentage inhibition) and Acid Blue (18.8 ± 10.31 percentage inhibition) possessed no significant difference when compared to the 2MeSATP control response ($p < 0.05$).

These experiments reveal several compounds, previously shown to be P2Y antagonists, are able to inhibit agonist-induced $XlP2Y_{11}$ cAMP responses. The experiments reveal the different ligands tested also possess varying degrees of inhibition as antagonists, although, in the same way as the initial agonist screening experiments undertaken in previous chapters, no further inferences or detailed analysis of the potency of the ligands can be deduced from these single concentration experiments.

5.2.2 Antagonists inhibit the cAMP responses of the $XlP2Y_{11}$ receptor in a concentration-dependent manner.

In order to further examine the ability of the ligands shown to act as antagonists of cAMP response generated by $XlP2Y_{11}$, the effect of various concentrations of each antagonist upon *de novo* cAMP production generated by 10μM 2MeSATP

was assessed following 30-minute pre-incubation with increasing concentrations of: Reactive Blue, Reactive Red, Suramin and Acid Blue. Reactive Blue and Reactive Red were chosen for further study in these experiments because they were the only antagonists to induce complete inhibition of the 2MeSATP response in the initial antagonist screening experiments (Section 5.2.1). Suramin was used in these concentration-response experiments because of its inability to completely antagonise the 2MeSATP (whereas previous studies have shown Suramin to be one of the strongest $hP2Y_{11}$ and $cP2Y_{11}$ antagonists)(Communi et al., 1999; Qi et al., 2001[b]). Acid blue was selected because it had been shown to generate minimal antagonism in the initial screening experiments - and was used as a negative control in this and subsequent experiments. In the same way as the antagonist high-concentration screen (Section 5.2.1), 2MeSATP was used in these experiments at a concentration of 10μM in order to assess the ability of the antagonists to decrease the cAMP response. The antagonists were used at final concentrations ranging from 10nM to 5mM. The relative insolubility of Acid Blue prevented its use at concentrations higher than 10μM.

Figure 5.2 shows the concentration-response curves of the different antagonists in the cAMP assay. The results have been normalised to the supramaximal isoproterenol-induced cAMP response generated in the 1321N1-$XlP2Y_{11}$ cells. The data displayed are a representative experiments taken from one of at least three independent experiments performed. The antagonists at their highest concentrations, elicit similar inhibitions of the 2MeSATP response to those recorded in the high-concentration antagonist experiments. The cAMP response

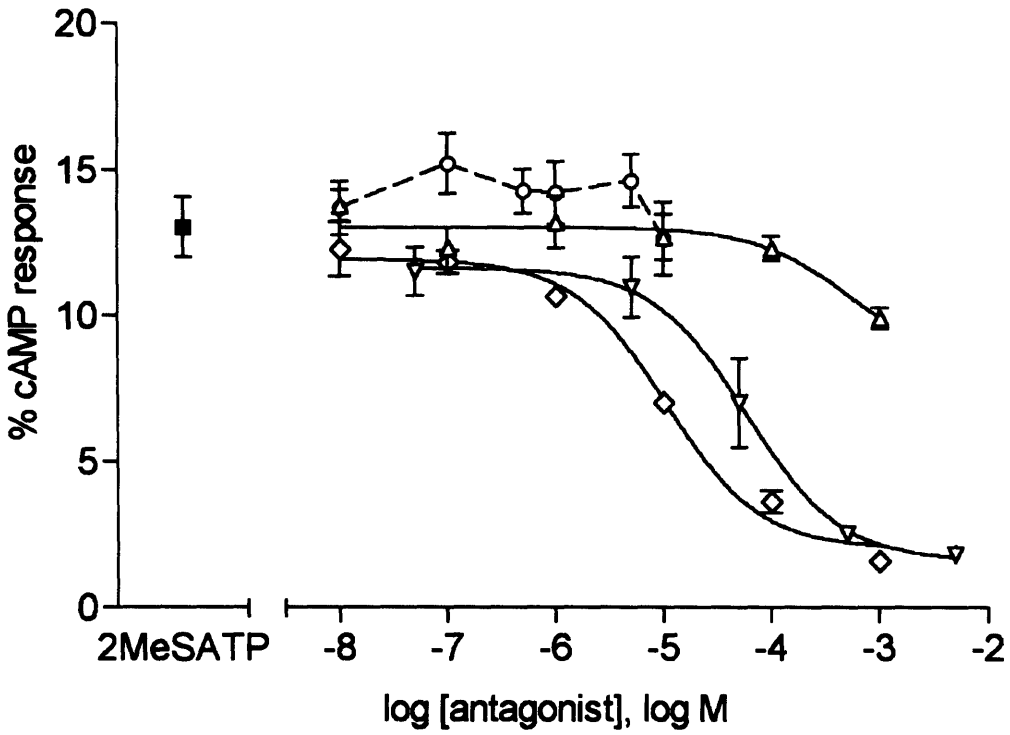

Figure 5.2

Inhibition curves for antagonists on cAMP accumulation generated by 2MeSATP, in 1321N1 human astrocytoma cells stably expressing the XlP2Y_{11} receptor.

Following pre-incubation with increasing concentrations of antagonists (Reactive Blue, ◇; Reactive Red, ▽; Suramin, △; and Acid Blue, ○) the cAMP response was measured after incubation with 10μM final concentration 2MeSATP. The cAMP response of 2MeSATP (10μM final concentration), in the absence of any antagonist, is also shown (■).Results are expressed as a percentage of the cAMP response to a supramaximal concentration of isoproterenol (10μM). The data are the mean ± s.e.m. of one representative experiment of 3 independent experiments performed.

recorded for 2MeSATP alone, shown in Figure 5.2, is typical of the response induced by this agonist (approximately 12 percent of the isoproterenol response). Non-linear regression analysis was undertaken for each set of data in Figure 5.2 and the curves are shown fitted to the responses of 2MeSATP in the presence of increasing concentrations of Reactive Blue (◇), Reactive Red (▽) and Suramin (△). A curve has not been fitted to the cAMP responses of 2MeSATP in the presence of Acid Blue (○) - shown with a connecting line. The data points shown are the mean ± s.e.m. of one representative experiment of three independent experiments performed.

Within the range of concentrations tested, Reactive Blue and Reactive Red are able to fully antagonise the cAMP response generated by 2MeSATP. The percentage cAMP response created by the addition of 10μM 2MeSATP is reduced to a basal level, shown by statistical analysis to be indistinguishable from the response generated by the PBS control alone (p value < 0.01 by Student's two-tailed paired *t*-test). The effect of increasing concentrations of Suramin is less pronounced; the reduction in the 2MeSATP cAMP response at 1mM of the agonist allows non-linear regression analysis to fit a curve, although maximum inhibition is clearly not reached at this concentration. The effect of increasing concentrations of Acid Blue produced a negligible decrease in the 2MeSATP cAMP response. The data obtained in the Acid Blue experiments were limited by the relative insolubility of the compound, which prevented the use of a wider range of concentrations, and a curve could not be fitted to these data.

The non-linear regression analysis undertaken on each of the 3 independent concentration-response experiments gave the following mean IC_{50} values: Reactive Blue, 13.2μM (log IC_{50} = -4.88 ± 0.05); Reactive Red, 100.7μM (log IC_{50} = -4.00 ± 0.02)(Table 5.1). The IC_{50} values for Suramin were not able to be calculated from these data. It can be seen from both Figure 5.2 and Table 5.1, that three of the antagonists elicit a concentration-dependent inhibition of the cAMP response in 1321N1-XlP2Y_{11} cells. The degree of this inhibition and the concentration of ligand required to elicit a half-maximal inhibitory response give the following antagonist potency order for XlP2Y_{11}-mediated cAMP responses:

Reactive Blue > Reactive Red >> Suramin

5.2.3 Antagonists modify the 2MeSATP induced cAMP concentration-response of XlP2Y_{11}.

In order to determine the nature of the antagonism of Reactive Blue, Reactive Red and Suramin, a series of experiments were conducted to determine the potency of 2MeSATP and the shape of the 2MeSATP concentration-response curve in the presence of a fixed concentration of each antagonist.

Figure 5.3 shows the cAMP response of 1321N1 human astrocytoma cells stably expressing XlP2Y_{11} after a 10-minute incubation with 2MeSATP in the presence of 500μM Reactive Blue, 100μM Reactive Red, 500μM Suramin or 1μM Acid

Blue. The data displayed are from a representative experiment performed for each ligand. Non-linear regression analysis was undertaken for each set of data. The curves generated by the analysis are shown fitted to the responses of increasing concentrations of 2MeSATP in the presence of fixed concentrations of various ligands. The 2MeSATP concentration response (--■--) in the absence of antagonist is also shown in Figure 5.3. The data points shown for each ligand are the mean ± s.e.m. of one representative experiment of three independent experiments performed.

Figure 5.3 shows that Suramin, Reactive Blue and Reactive Red were able to affect a rightward shift of the 2MeSATP concentration-response curve. The right-shift of the concentration-response curve is more pronounced in the presence of Suramin and Reactive Blue. However, the maximum agonist response in these experiments was not reached at the highest concentration of 2MeSATP used.

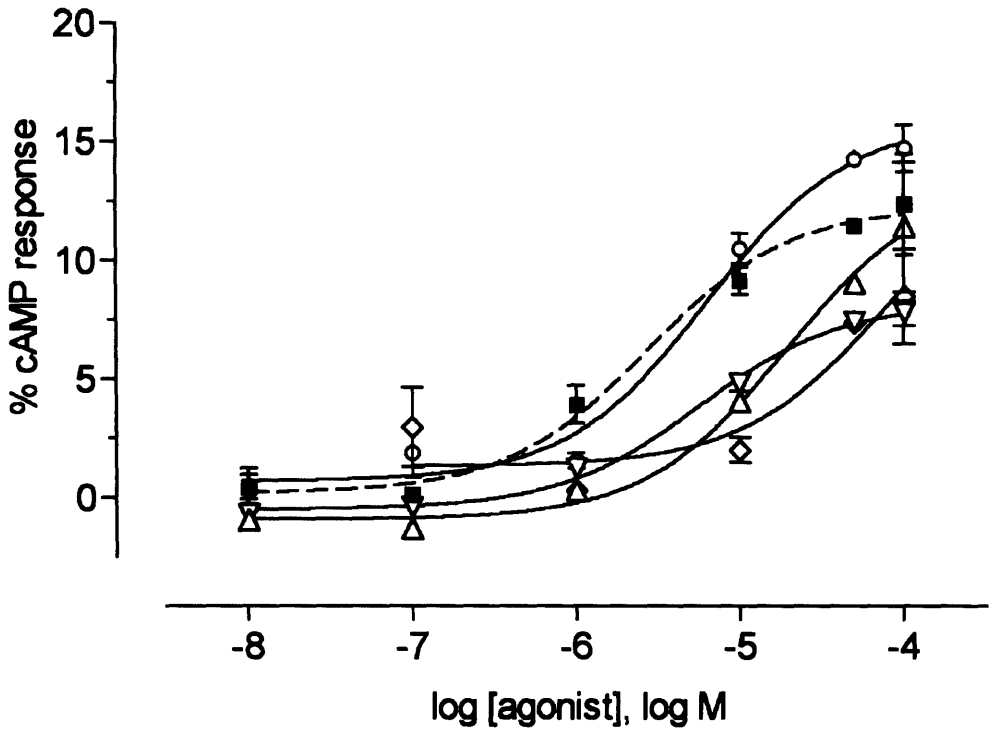

Figure 5.3

Concentration-response curves of 2MeSATP on cAMP accumulation in 1321N1 human astrocytoma cells stably expressing the XlP2Y_{11} receptor, in the presence of antagonists.

Following pre-incubation with fixed concentrations of antagonists (500μM Reactive Blue, ◇; 100μM Reactive Red, ▽; 500μM Suramin, △ and 1μM Acid Blue, ○) the cAMP response was measured after incubation with increasing concentrations of 2MeSATP. 2MeSATP concentration-response curve without antagonist is also shown (--■--). Results are expressed as a percentage of the cAMP response to a supramaximal concentration of isoproterenol (10μM). The data are the mean ± s.e.m. of one representtative experiment of 3 independent experiments performed. Analysis shows a significant difference between i) the EC50's of Suramin, Reactive Blue and Reactive Red and the curve generated by 2MeSATP alone, ii) the maximal response generated by 100μM 2MeSATP in the presence of 100μM Reactive Red, and iii) the response generated by 0.1μM 2MeSATP in the presence of 500μM Reactive Blue ($p < 0.05$, by ANOVA with Tukey's post-test).

5.3 Investigating antagonism of Ca^{2+} mobilisation in 1321N1-XlP2Y_{11} cells.

Having demonstrated that various ligands are able to act as antagonists upon the agonist-induced cAMP response of the XlP2Y_{11} receptor, the ability of these same ligands to inhibit the receptor's ability to induce Ca^{2+} mobilisation was investigated. In accordance with the previous experiments, 2MeSATP was selected as the agonist used to elicit the second messenger response.

5.3.1 Suramin and Reactive Red are unable to inhibit Ca^{2+} mobilisation from the XlP2Y_{11} receptor.

The initial approach to these studies was the same as that employed in section 5.2.1, with each antagonist tested initially at 1mM final concentration. Figure 5.4 shows the Ca^{2+} response of 1321N1 human astrocytoma cells stably expressing XlP2Y_{11} after the addition of the 2MeSATP alone (at a final concentration of 10μM), and in the presence of Suramin and Reactive Red. The results are expressed as a percentage Ca^{2+} response, and have been normalised to the Ca^{2+} mobilisation produced by 1mM carbachol. Results shown are the means $\pm$ s.e.m. of three different experiments each performed in triplicate.

Surprisingly, these data show that there is no major inhibition of the agonist-induced Ca^{2+} response in the presence of either Suramin or Reactive Red. Nor is there any potentiation of the 2MeSATP response. There is no significant difference between the Ca^{2+} responses in the presence or absence of the

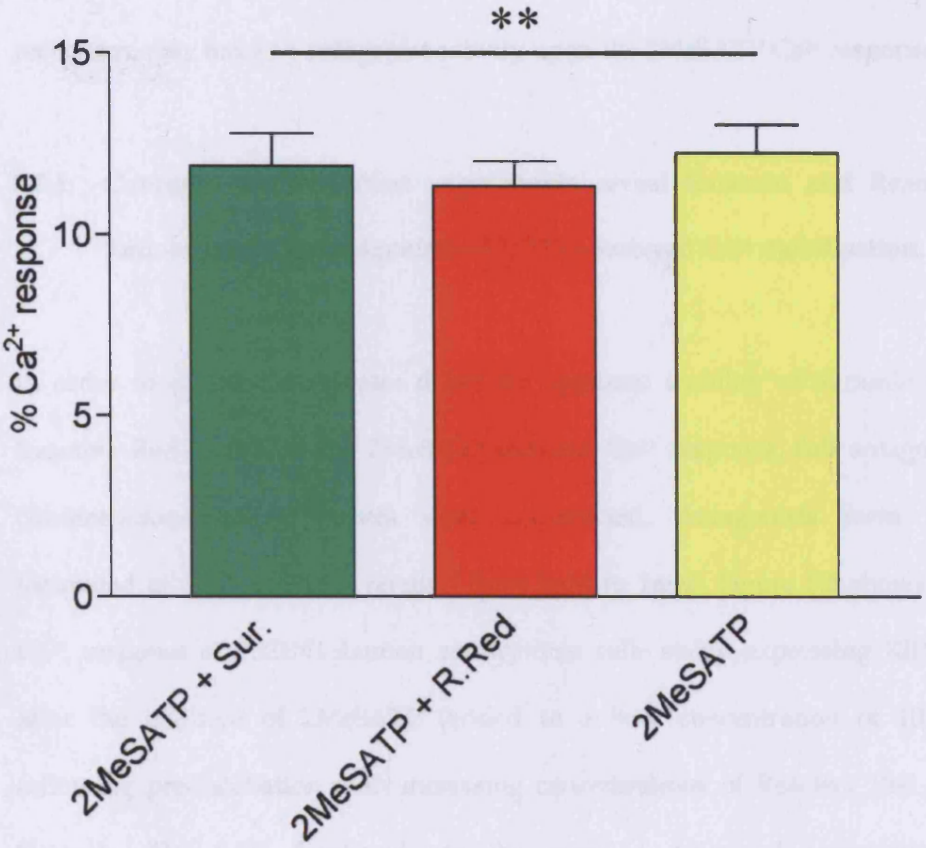

Figure 5.4

Antagonists do not inhibit Ca^{2+} mobilisation produced by 2MeSATP activation of $XlP2Y_{11}$.

Suramin and Reactive Red were screened for their ability to inhibit Ca^{2+} mobilisation generated by 2MeSATP activation of $XlP2Y_{11}$. Following pre-incubation with Suramin and Reactive Red (each at 1mM final concentration), Ca^{2+} mobilisation was measured following the addition of 10μM final concentration of 2MeSATP. Results are expressed as a percentage of the Ca^{2+} response to a supramaximal concentration of carbachol (1mM). Results are the mean ± s.e.m. of three different experiments, each performed in triplicate. **, $p < 0.01$, compared with control (not shown), Student's t-test.

antagonists (p value > 0.01 by a Student's *t*-test). Although previous studies have shown that these ligands were able to inhibit agonist-induced cAMP responses, they have no antagonist activity upon the 2MeSATP Ca^{2+} response.

5.3.2 Concentration-inhibition experiments reveal Suramin and Reactive Red do not act as antagonists of $XlP2Y_{11}$ induced Ca^{2+} mobilisation.

In order to examine in greater detail the apparent inability of Suramin and Reactive Red to inhibit the 2MeSATP-induced Ca^{2+} response, full antagonist concentration-response curves were constructed. Antagonists were pre-incubated at concentrations ranging from 1nM to 1mM. Figure 5.5 shows the Ca^{2+} response of 1321N1 human astrocytoma cells stably expressing $XlP2Y_{11}$ after the addition of 2MeSATP (added to a final concentration of 10μM) following pre-incubation with increasing concentrations of Reactive Red and Suramin. The data displayed are the mean ± s.e.m. of representative experiments taken from the 3 independent experiments performed for each ligand.

Increasing concentrations of Suramin and Reactive Red are unable to elicit any substantial reduction in the Ca^{2+} response generated by 2MeSATP. Analysis reveals that no significant difference exists between any of the data points, suggesting that the Suramin and Reactive Red do not act as antagonists of the Ca^{2+} signalling generated by 2MeSATP (one-way analysis of variance, $p > 0.05$).

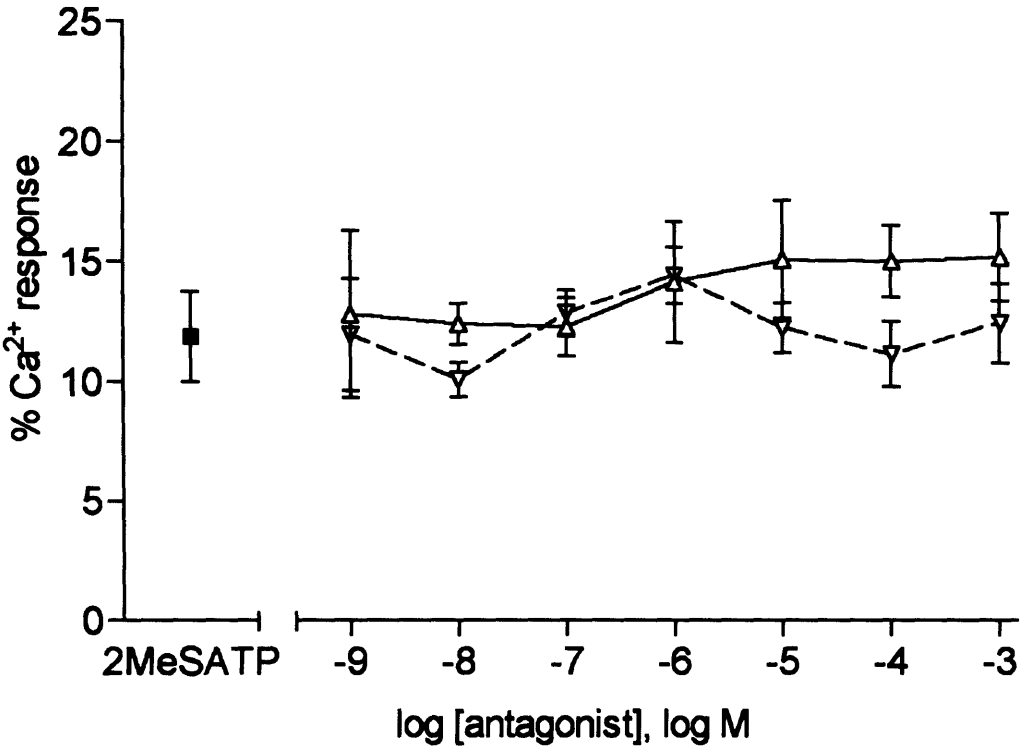

Figure 5.5

Lack of antagonism on Ca^{2+} mobilisation generated by 2MeSATP, in 1321N1 human astrocytoma cells stably expressing the $XlP2Y_{11}$ receptor.

Following pre-incubation with increasing concentrations of antagonists (Reactive Red, ▽; and Suramin, --△--), Ca^{2+} mobilisation was measured after the addition of 10μM final concentration 2MeSATP. Results are expressed as a percentage of the Ca^{2+} response to a supramaximal concentration of carbachol (1mM). The data are the mean ± s.e.m. of one representative experiment of three performed.

Antagonists	*IC_{50} (μM)*	*Log IC_{50}*	*Kd (μM)*
Reactive Blue	13.1	-4.88 ± 0.05	4.9 ± 1.8
Reactive Red	100.7	-4.00 ± 0.02	21.6 ± 4.5
Suramin	[a]ND		82.8 ± 27.3
Acid Blue	ND		ND

Table 5.1

IC_{50} and Kd values for antagonists used on 1321N1 human astrocytoma cells stably expressing the XlP2Y_{11} receptor.

IC_{50} values were calculated from linear regression curve analysis of the antagonist concentration-response experiments performed in the presence of a fixed concentration of 2MeSATP. Kd values were calculated as described in Materials and Methods. Results are expressed as the mean IC_{50}, and log of the mean IC_{50} ± s.e.m., of 3 independent experiments, each performed in triplicate. [a]ND, not determined, indicates that the low response generated could not be used to calculate an IC_{50} value.

5.4 Summary

In order to determine the antagonism at $XlP2Y_{11}$ of several compounds previously shown to act as P2Y receptor antagonists, the cAMP assay was employed. These experiments successfully identified antagonists of the cAMP second messenger response, with Reactive Red and Reactive Blue as the most efficacious antagonists, followed by Phenol Red and Suramin.

Concentration-inhibition experiments were then performed and the antagonists tested were shown to inhibit the production of cAMP in a concentration-dependent manner. Reactive Blue was shown to be the most potent antagonist, followed by Reactive Red. While Suramin was able to antagonise the cAMP response (although to a much lesser extent than Reactive Blue and Reactive Red) Acid Blue was unable to elicit any inhibition. The IC_{50} values calculated for the full antagonists were in the micromolar range (Reactive Blue: 13.1μM, log IC_{50} = -4.88 ± 0.05; Reactive Red: 100.7μM, log IC_{50} = -4.00 ± 0.02).

To determine the nature of the antagonism, each of these four ligands was included at a fixed concentration in 2MeSATP concentration-response curves. Reactive Blue, Reactive Red and Suramin were all found to shift the agonist induced concentration-response curve to the right. Although Acid Blue did not significantly shift the agonist induced concentration-response curve, the maximal height of the curve was higher than that of agonist alone, suggesting that Acid Blue may potentiate the agonist-induced response at higher concentrations. Unfortunately, the solubility of this ligand did not permit these experiments to be performed. Reactive Red was also found to reduce the

maximal height of the agonist-induced curve, suggesting the possibility of this ligand acting as a non-competitive antagonist at the $XlP2Y_{11}$ receptor. Concentration-response curves performed in the presence of Reactive Blue and Suramin were unable to reach a maximum within the range of concentrations tested. The significantly right-shifted curve generated by the presence of Reactive Blue was also noticeable for its higher basal level of cAMP accumulation at low concentrations of agonist, suggesting Reactive Blue may act as a partial agonist.

Since the different antagonists were not used at the same concentrations in these experiments the corresponding Kd values were calculated for each antagonist (shown in Table 5.1). Reactive Blue (log IC_{50}, -4.88 $\pm$ 0.05; Kd, 4.9 $\pm$ 1.6 μM) was found to be the most potent antagonist, followed by Reactive Red (log IC_{50}, -4.00 $\pm$ 0.02; Kd, 21.6 $\pm$ 4.5 μM) and then Suramin (Kd, 82.8 $\pm$ 27.3 μM).

The ability of these antagonists to block $XlP2Y_{11}$-mediated activation of the Ca^{2+} second-messenger signalling pathway was investigated. Initially, the Ca^{2+} response was determined in the presence of high concentrations of Suramin and Reactive Red, but no inhibition was observed. The subsequent concentration-response curves for these two antagonists did not show any significant decrease in the agonist-induced Ca^{2+} second messenger response, despite the ability of these ligands to antagonise cAMP signalling through $XlP2Y_{11}$.

Chapter 6

Discussion.

6.1 Introduction

The work presented in this thesis describes the pharmacological characterisation of the human $P2Y_{11}$ ($hP2Y_{11}$) and the *Xenopus laevis* $P2Y_{11}$ ($XlP2Y_{11}$) receptors. Previous studies have shown the $hP2Y_{11}$ receptor and its canine ($cP2Y_{11}$) receptor orthologue are activated by extracellular nucleotides, promoting intracellular cAMP production, Ca^{2+} mobilisation and IP accumulation (Communi et al., 1997 & 1999; Qi et al., 2001[a]; Qi et al., 2001[b]; White et al., 2003) responses typical of phospholipase C and adenylyl cyclase activation (Streb et al., 1983; Danchin, 1993). I have shown in the present work that both the $hP2Y_{11}$ and the novel *Xenopus laevis* P2Y receptors are activated by extracellular nucleotides and nucleotide analogues, to mobilise intracellular Ca^{2+} and produce cAMP.

The ligand potencies and dual signal pathway activation lead me to conclude that XlP2Y$_{11}$ is the *Xenopus laevis* orthologue of the P2Y$_{11}$ receptor. This conclusion is supported further by the antagonist profiles that I have determined for the hP2Y$_{11}$ and XlP2Y$_{11}$ receptors. This chapter presents a comparison of my agonist and antagonist data, both with each other, and with the previously published data for P2Y$_{11}$ receptor orthologues, from the perspective of both ligand activation and second messenger production. This chapter is therefore an opportunity to analyse, evaluate and assess the previous research into the role of this receptor.

6.2 Determination of agonist potencies at the XlP2Y$_{11}$ and hP2Y$_{11}$ receptors.

The pharmacological data obtained for the hP2Y$_{11}$ and XlP2Y$_{11}$ receptors, previously presented separately in Chapters 3, 4 and 5, are shown in Table 6.1. The agonist log EC_{50} values and intrinsic activities (IA), determined using the Ca^{2+} and cAMP assays are shown for both receptors, together with the ratios of the EC_{50} values gained for agonist-induced cAMP accumulation to the Ca^{2+} mobilisation EC_{50} values, in order to compare the magnitude of the two different second messenger responses.

The potency orders previously presented in Chapters 3 and 4 (shown below) reveal that ATP, when compared to ADP, more potently activates both the hP2Y$_{11}$ and XlP2Y$_{11}$ receptors. The ATP and BzATP EC_{50} ratios of 1321N1-XlP2Y$_{11}$ cells (0.40; 0.37, respectively) and 1321N1-hP2Y$_{11}$ cells (ATP ratio: 0.67;

BzATP ratio: 0.16) indicate that both agonists are more potent activators of the cAMP accumulation response in each of the two cell lines. Analysis of the 2-thioether-substituted potencies reveals 2MeSATP conforms to this above observation, activating cAMP responses more potently than Ca^{2+} mobilisation, however, contrary to all of the agonists tested on $hP2Y_{11}$ and $XlP2Y_{11}$, 2MeADP more potently activates Ca^{2+} mobilisation. Analysis of these EC_{50}'s values also reveals ATP is equipotent with and 6-fold less potent than BzATP, in terms of Ca^{2+} mobilisation response and cAMP accumulation response, respectively at the $hP2Y_{11}$ receptor, whereas the same ligand is 16-fold more potent than BzATP in both cAMP and Ca^{2+} responses at the $XlP2Y_{11}$ receptor. These observations can be seen in the rank order of potency for these $P2Y_{11}$ receptor orthologues, summarised below.

$hP2Y_{11}$: **BzATP > ATP > α,β-meATP = β,γ-meATP**

$XlP2Y_{11}$: **ATP ≥ 2MeSATP > 2MeSADP ≥ BzATP >> ADP**

The Clustal W alignment of the $hP2Y_{11}$, $cP2Y_{11}$ and $XlP2Y_{11}$ coding sequences (shown in Chapter 1) was undertaken in order to examine the percentage identity exhibited between these receptors and showed that $XlP2Y_{11}$ possesses approximately 40 percent identity to $hP2Y_{11}$ and approximately 32 percent to $cP2Y_{11}$ amino acid sequences. As previously outlined, studies have shown that the human $P2Y_4$ receptor (Communi et al., 1996; Communi and Boeynams, 1997) and its rat orthologue, $rP2Y_4$ (Bogdanov et al., 1998), possess distinctly altered agonist and antagonist pharmacology, despite sharing approximately 80 percent sequence identity. Considering the low sequence identity observed when comparing the $XlP2Y_{11}$ sequence against the human and canine $P2Y_{11}$

orthologues, the ability of the receptor to induce similar second messenger responses to both the $hP2Y_{11}$ and $cP2Y_{11}$ receptor activation is surprising.

The low sequence identity between the $hP2Y_{11}$ and $XlP2Y_{11}$ amino acid sequences (32 percent identity) suggests that the conservation of key residues in specific locations is crucial to the preservation of the $hP2Y_{11}$-like agonist responses of the $XP2Y_{11}$ receptor. The positively charged basic amino acid residues found in the plasma membrane-extracellular interface of transmembrane domain 6 (TM6) regions in P2Y receptors are predicted through their interaction with phosphate moieties, to bind and stabilise extracellular nucleotide agonists (Erb et al., 1995; Jiang et al., 1997; Qi et al., 2001[b]) and the $hP2Y_{11}$ residues, ^{262}His and ^{265}Arg, and their equivalents in the $cP2Y_{11}$ amino acid sequence have been shown to dictate the ATP versus ADP selectivity exhibited by each of these receptors (Qi et al., 2001[b]). $XlP2Y_{11}$ contains the identical residues when compared with the $hP2Y_{11}$ receptor, notably ^{262}His and ^{265}Arg ($XlP2Y_{11}$ equivalent positions: equivalent positions ^{241}His and ^{245}Arg) (shown in Figure 6.1), and is different from $cP2Y_{11}$ at these residues. This is likely to account for the preference of the $XlP2Y_{11}$ receptor for ATP , rather than ADP.

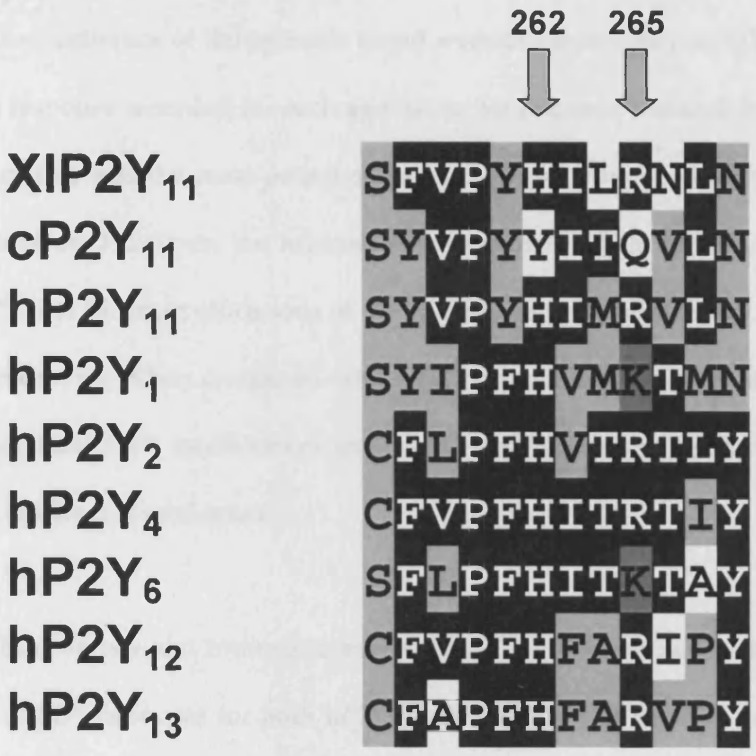

Figure 6.1

Partial amino acid sequence alignment of transmembrane domain 6 in P2Y receptors reveals XIP2Y$_{11}$ contains basic residues at residues 241 and 244.

Clustal W alignment of partial amino acid sequences of transmembrane domain 6 of multiple P2Y receptors. Conserved residues are shaded black. Similar residues are shaded in gray. Numbered residues denote hP2Y$_{11}$ residues predicted to contribute to the ATP versus ADP selectivity of hP2Y$_{11}$ and cP2Y$_{11}$ receptors.

6.3 Determination of agonist efficacies at the XlP2Y$_{11}$ and hP2Y$_{11}$ receptors.

The intrinsic activities of the agonists tested were calculated by normalising the maximal response recorded for each agonist to the response induced by 100μM ATP, since this was the most potent of the non-synthetic nucleotides tested on these receptors. However, the intrinsic activity presented in Table 6.1 reveal, that ATP is not the most efficacious of the agonists tested on either the hP2Y$_{11}$ or XlP2Y$_{11}$ receptors. When compared with ATP, both cell lines produce similar or higher maximal Ca^{2+} mobilisation and cAMP accumulation responses to the synthetic nucleotide analogues.

The log EC_{50} values and intrinsic activities of UTP are not shown as the UTP-induced cAMP responses for both hP2Y$_{11}$ and XlP2Y$_{11}$, and the Ca^{2+} responses for XlP2Y$_{11}$, were found to be indistinguishable from the vehicle control. Similarly, the EC_{50} values for ADP-induced cAMP accumulation responses are not shown for either receptor; however, the observation that ADP generates a Ca^{2+} response significantly different from the control in 1321N1-XlP2Y$_{11}$ cells warrants the inclusion of its intrinsic activity in Table 6.1. The table reveals that ADP can generate Ca^{2+} mobilisation levels equivalent to approximately 40 percent of the Ca^{2+} mobilisation induced by 100μM ATP. ADP's inability to reach a maximum Ca^{2+} response within the range of concentrations used does not permit an EC_{50} value to be calculated.

	Ca^{2+} mobilisation		*Cyclic AMP accumulation*		Ratio[b]
Nucleotide	*Log EC_{50}*	IA (%)[a]	*Log EC_{50}*	IA (%)	
hP2Y$_{11}$ receptor					
ATP	-5.07 ± 0.03	100	-5.24 ± 0.07	100	0.67
ADP			ND[c]	ND	
BzATP	-5.26 ± 0.10	97.1 ± 3.2	-6.05 ± 0.06	96.3 ± 2.6	0.16
UTP			ND	ND	
α,β-meATP			-4.64 ± 0.07	116.7 ± 7.2	
β,γ-meATP			-4.61 ± 0.14	110.3 ± 0.9	
XlP2Y$_{11}$ receptor					
ATP	-5.06 ± 0.19	100	-6.02 ± 0.01	100	0.40
ADP	ND	40.5 ± 13.1	ND	ND	
BzATP	-4.37 ± 11.6	178.0 ± 35.4	-4.81 ± 0.12	153.4 ± 28.0	0.37
UTP	ND	ND	ND	ND	
2MeSATP	-5.71 ± 0.22	170.0 ± 29.6	-5.76 ± 0.11	126.0 ± 14.5	0.85
2MeSADP	-5.13 ± 0.08	180.0 ± 17.7	-4.90 ± 0.10	121.0 ± 10.0	1.68

Table 6.1

Comparison of agonist activities in 1321N1-hP2Y$_{11}$ and 1321N1-XlP2Y$_{11}$cells.

hP2Y$_{11}$ and XlP2Y$_{11}$ receptor log EC_{50} data from the agonist-induced Ca^{2+} and cAMP responses of 1321N1-hP2Y$_{11}$ and 1321N1-XlP2Y$_{11}$ cells. Data are expressed as the mean, ± s.e.m of three to five independent experiments, each performed in triplicate. [a]IA, intrinsic activity, shows the percentage agonist responses normalised to the maximal response of 100μM ATP. [b]Ratio, shows the ratio of EC_{50} for cAMP accumulation to EC_{50} for Ca^{2+} mobilisation. [c]ND, indicates responses were not determined.

Despite the consistencies between the two cell lines, key differences exist between the intrinsic activities of the agonists at the human $P2Y_{11}$ receptor when compared with the *Xenopus laevis* $P2Y_{11}$ receptor. Table 6.1 reveals that the maximal responses produced by BzATP are much higher at the $XlP2Y_{11}$ receptor (Ca^{2+} IA, 178 ± 35.4; cAMP IA, 153.4 ± 28.0) than at the $hP2Y_{11}$ receptor (Ca^{2+}IA, 97.1 ± 3.2; cAMP IA, 96.3 ± 2.6 percent).

6.4 Comparison of the agonist-induced responses of $XlP2Y_{11}$ and $hP2Y_{11}$ with previously published data.

The previously published $P2Y_{11}$ receptor agonist activities (Qi et al., 2001[b]) are listed in Table 6.2 to highlight key differences between these data and my own pharmacological characterisations of the $hP2Y_{11}$ and $XlP2Y_{11}$ receptors. Although these data were obtained from $hP2Y_{11}$ and $cP2Y_{11}$ orthologues stably expressed in CHO-K1 cell lines, as opposed to the 1321N1 cell line, these data were selected for comparison as both functional assays were performed in the same cell line (Qi et al., 2001[b]).

The log EC_{50} values for agonist-induced cAMP and IP accumulation responses are shown, together with the ratio of these EC_{50} values (cAMP accumulation to IP accumulation) for each agonist. The agonist intrinsic activities are also shown. The data for $hP2Y_{11}$ are normalised to the maximal response of 300μM ATP and the canine $P2Y_{11}$ data are normalised to 100μM ADP. Although agonist log EC_{50} values and intrinsic activities cannot be directly compared between different cell lines, previous characterisations in 1321N1- and CHO-K1 cells have revealed the

agonist potency orders calculated for the receptors remain the same in the different cell lines (Communi et al., 1999; Qi et al., 2001[b]). The differences in the second messenger signalling ability as a function of both receptor subtype and cell line used is discussed further in section 6.7.

Evaluation of the XlP2Y_{11} agonist results is not possible through direct comparison with previous work on this receptor, as I am the first to characterise this novel receptor. Although, as previously stated, direct comparison of the EC_{50} and intrinsic activities values cannot be undertaken between different cell lines, analysis and inferences can be gained by comparing the order of agonist potency. The 1321N1-XlP2Y_{11} data presented in Table 6.1 and Table 6.2 reveal 2MeSATP and 2MeSADP to be more potent than their non-synthetic analogues, ATP and ADP, in terms of both Ca^{2+} mobilisation and cAMP accumulation responses. XlP2Y_{11} possesses the same ATP > 2MeSATP and ADP > 2MeSATP selectivity possessed by the hP2Y_{11} receptor (ATP > 2MeSATP >> ADP > 2MeSADP) (Communi et al., 1997 & 1999). The XlP2Y_{11} data is more like hP2Y_{11} in terms of ATP and ADP responses and differs substantially from the previously published cP2Y_{11} data for these agonists, which possess a selectivity of 2MeSADP ~ 2MeSATP >> ADP > ATP (Zambon et al., 2001; Qi et al., 2001[b]).

Direct comparison of the hP2Y_{11} data presented in this thesis is, however, possible due to previous Ca^{2+} and cAMP characterisations of the receptor in 1321N1 cells. The first published example of cAMP accumulation in 1321N1-hP2Y_{11} cells gives an EC_{50} value of 130 $\pm$ 10 μM for ATP (Qi et al., 2001[a]). By direct comparison, the 1321N1-hP2Y_{11} cAMP investigations presented in Chapter 3 and Table 6.2 show ATP to be 23-fold more potent than previously

	Ca^{2+} *mobilisation* [d]		*Cyclic AMP accumulation* [d]		Ratio[b]
Nucleotide	*Log* EC_{50}	IA (%)[a]	*Log* EC_{50}	IA (%)	
hP2Y$_{11}$ receptor					
ATP	-5.07 ± 0.03	100	-5.24 ± 0.07	100	0.67
BzATP	-5.26 ± 0.10	97.1 ± 3.2	-6.05 ± 0.06	96.3 ± 2.6	0.16
α,β-meATP			-4.64 ± 0.07	116.7 ± 7.2	
β,γ-meATP			-4.61 ± 0.14	110.3 ± 0.9	
XlP2Y$_{11}$ receptor					
ATP	-5.06 ± 0.19	100	-6.02 ± 0.01	100	0.40
ADP	ND	40.5 ± 13.1	ND	ND	
BzATP	-4.37 ± 11.6	178.0 ± 35.4	-4.81 ± 0.12	153.4 ± 28.0	0.37
2MeSATP	-5.71 ± 0.22	170.0 ± 29.6	-5.76 ± 0.11	126.0 ± 14.5	0.85
2MeSADP	-5.13 ± 0.08	180.0 ± 17.7	-4.90 ± 0.10	121.0 ± 10.0	1.68

	IP accumulation		*Cyclic AMP accumulation*		Ratio
Nucleotide	*Log* EC_{50}	IA (%)	*Log* EC_{50}	IA (%)	
Human P2Y$_{11}$ receptor *					
ATP	-5.44 ± 0.15	100	-4.20 ± 0.11	100	17.3
ADP	-4.30 ± 0.19	60.2 ± 4.3	ND	ND	ND
2MeSATP	-5.62 ± 0.07	99.4 ± 8.2	-4.58 ± 0.06	99.4 ± 5.5	11
2MeSADP	-4.84 ± 0.10	60.5 ± 6.0	ND	ND	ND
Canine P2Y$_{11}$ receptor *					
ATP	-4.48 ± 0.19	96.8 ± 9.3	-4.12 ± 0.17	94.8 ± 9.3	2.3
ADP	-5.21 ± 0.10	100	-4.96 ± 0.15	100	1.8
2MeSATP	-6.24 ± 0.08	66.2 ± 3.5	-5.66 ± 0.08	74.9 ± 5.0	3.9
2MeSADP	-7.10 ± 0.05	102 ± 6.8	-6.80 ± 0.08	84.0 ± 2.5	2.0

Table 6.2

Comparison of agonist activities in 1321N1-hP2Y$_{11}$, 1321N1-XlP2Y$_{11}$, CHO-hP2Y$_{11}$ and CHO-cP2Y$_{11}$ cells.

hP2Y$_{11}$ and XlP2Y$_{11}$ receptor EC_{50} data show the responses of agonists in 1321N1-hP2Y$_{11}$ and 1321N1-XlP2Y$_{11}$ cells. Data are expressed as the mean, ± s.e.m of three to five independent experiments, each performed in triplicate. * Human and canine P2Y$_{11}$ receptor data (taken from Qi et al., 2001[b]) show the activities of nucleotides in CHO-hP2Y$_{11}$ and CHO-cP2Y$_{11}$ cells, data are mean ± S.D. from three to six separate experiments. [a] IA, intrinsic activity, shows the percentage agonist responses, normalised to the maximal response of 100μM ATP (hP2Y$_{11}$ and XlP2Y$_{11}$), 300μM ATP (* hP2Y$_{11}$) and 100μM ADP (* cP2Y$_{11}$). [b] Ratio, shows the ratio of EC_{50} for cAMP accumulation to EC_{50} for Ca^{2+} mobilisation (hP2Y$_{11}$ and XlP2Y$_{11}$), and EC_{50} for cAMP accumulation to IP accumulation (hP2Y$_{11}$ and cP2Y$_{11}$). [c] ND, indicates responses were not determined. [d]Data taken from Table 6.1.

determined. In addition, although the EC_{50} values were not presented, previous studies have reported that agonist potencies for cAMP accumulation recorded in 1321N1-$hP2Y_{11}$ and 1321N1-$cP2Y_{11}$ cells are lower than the potencies recorded for both receptors in CHO cells (presented in Table 2) (Qi et al., 2001[b]). suggesting that the previously reported cAMP EC_{50} value for ATP in 1321N1-$hP2Y_{11}$ cells would be greater than 62.4 $\pm$ 15.6 µM. The ATP EC_{50} value presented in Chapter 3 for the 13121N1-$hP2Y_{11}$ cells is, therefore, at least 11-fold more potent than this previous cAMP investigation. These data reveal the 1321N1-$hP2Y_{11}$ cells used throughout this thesis are more efficient at inducing cAMP accumulation than the 1321N1-$hP2Y_{11}$ cells used in previous studies.

Less information is available to permit direct comparison of the Ca^{2+} EC_{50} values obtained for the 1321N1-$hP2Y_{11}$ cells in Chapter 3. Initial single-concentration pharmacological studies on the $hP2Y_{11}$ receptor reported, in addition to generating IP and cAMP accumulation, that ATP also induced intracellular Ca^{2+} mobilisation (Communi et al., 1997). Further inspection of the receptor's pharmacological profile, achieved through concentration-response experiments, revealed that ATP (as well as ADP, and both 2-thioether analogues) was able to produce concentration-dependent Ca^{2+} responses (Qi et al., 2001[b]). Although EC_{50} values were not presented in either study, visual inspection of the published graphs shows that half-maximal ATP-induced Ca^{2+} response are achieved at approximately 10µM. Subsequent investigations into UTP- and ATP-induced Ca^{2+} responses of the $hP2Y_{11}$ receptor (White et al., 2001) have yielded EC_{50} values for ATP which may be directly compared to the 1321N1-$hP2Y_{11}$ data presented in Chapter 3. The EC_{50} value, presented as log: -4.9 $\pm$ 0.13,

is of a similar magnitude as the log EC_{50} value determined for ATP in Chapter 3 (-5.24 ± 0.07).

Comparing the $hP2Y_{11}$ and $XlP2Y_{11}$ receptor data presented in this thesis, with previously published $hP2Y_{11}$ and $cP2Y_{11}$ data highlights a number of inconsistencies. Firstly, while previously published studies initially revealed, that ATP possessed an EC_{50} value of 38 ± 7 μM for IP accumulation in 1321N1-$hP2Y_{11}$ cells (Communi et al., 1997), subsequent studies using 1321N1-$hP2Y_{11}$ cells have shown the IP EC_{50} value for ATP to vary from 65 ± 12 μM (Communi et al., 2001) to 8.5 ± 0.1 μM (Qi et al., 2001[a]). Similarly, ATP-induced cAMP accumulation EC_{50} values for CHO-$hP2Y_{11}$ cells have been shown to range from 17.4 ± 6.1 (Communi et al., 1999) to 62.4 ± 15.6 (Qi et al., 2001[a]). My own work has led to the calculation of an EC_{50} value of 5.7μM for cAMP response at the $hP2Y_{11}$ receptor. These discrepancies, which can arise in the same laboratory, may be a function of the techniques and methods used to determine second messenger responses. They may also relate to receptor density, as described in section 6.5.

6.5 Problems associated with comparing ligand intrinsic activities and potencies.

As mentioned in sections 6.3 and 6.4, the direct comparison of agonist intrinsic activities and EC_{50} values cannot be undertaken between different cell lines. Agonist intrinsic activities and EC_{50} values are determined by receptor number and differences in receptor expression levels between cell lines may affect these

values (Kenakin et al., 1997). Despite this, it has been shown, however, that the order of agonist potency in cells with different receptor expression levels remains the same (Qi et al., 2001[b]). Different receptor expression levels between the 1321N1-hP2Y_{11} cells used in Chapter 3 of this thesis, and those used to produce the previously published cAMP accumulation data, may account for some of the differences in intrinsic activities and EC_{50}. As no appropriate radiolabelled compounds have been described for the hP2Y_{11} receptor, it is not yet possible to accurately determine P2Y_{11} receptor density in any given cell line. It must also be noted, that in terms of second messenger signalling, the intrinsic activities and EC_{50} values recorded in Ca^{2+} responses cannot be compared with the IP or cAMP values (and vice versa). It is only possible to compare the efficiency of coupling to the different second messenger pathways. In this regard, it is difficult to analyse the results of the XlP2Y_{11} receptor as the efficacies of coupling to the mammalian $G_{s\alpha}$ and $G_{q/11\alpha}$ proteins are unknown.

6.5.1 Agonist interconversion.

As outlined in Chapter 1, the presence and turnover of extracellular agonists by ATP-generating and ATP-consuming extracellular pathways can govern the duration and magnitude of intracellular signalling responses (Zimmerman, 1992; Lazarowski et al., 1997). The stepwise bi-directional interconversion of ATP, ADP and AMP (and the ability of Ecto-5'-nucleotidase and Adenosine Deaminase to sequentially degrade AMP into Adenosine and Inosine), must be taken into consideration when interpreting the agonists responses of the hP2Y_{11} and XlP2Y_{11} receptors.

It may be possible that the Ca^{2+} mobilisation and cAMP production caused by agonists such as ATP are in fact produced by the downstream products of the agonists' ectonuclease degradation. However, the lack of any signaling responses recorded for ADP in both pharmacological assays suggests very little ADP is converted to ATP. The similarity of the responses recorded in the Ca^{2+} assay (which records the intracellular response in real-time - giving any ecto-enzymes very little incubation time with the agonists) to those recorded in the cAMP responses also confirms that little or no agonist interconversion occurred in relation to ATP and ADP.

6.6 Determination of antagonist potencies at the XlP2Y$_{11}$ and hP2Y$_{11}$ receptors.

The inhibition of several antagonists at the hP2Y$_{11}$ and XlP2Y$_{11}$ receptors are listed in Table 6.3, which summarises the log IC_{50} values and intrinsic affinity (presented as percentage inhibition of agonist-induced responses), previously presented separately in Chapters 3 and 5. IC_{50}'s have not been calculated for antagonists that either exhibited minimal inhibition throughout the range of antagonist concentrations tested, or were unable to develop maximal antagonism of the agonist-induced response within this concentration range.

Previous studies of the hP2Y$_{11}$ and cP2Y$_{11}$ receptors that have examined the signalling responses induced by non-specific antagonists have shown that Suramin and Reactive Blue inhibit IP and cAMP responses in 1321N1-hP2Y$_{11}$

cells, CHO-hP2Y$_{11}$ cells (Communi et al., 1999), and CHO-cP2Y$_{11}$ cells (Qi et al., 2001[b]). In line with the previously published cP2Y$_{11}$ and hP2Y$_{11}$ data, Reactive Blue fully inhibits the cAMP response in 1321N1-XlP2Y$_{11}$ cells (Table 6.3). This full inhibition of cAMP responses by Reactive Blue has also ben shown for the hP2Y$_{11}$ and cP2Y$_{11}$ receptors (Qi et al., 2001[b]), however, a separate study has reported Reactive Blue only produces a partial inhibition of activated hP2Y$_{11}$ receptors (Communi et al., 1999). Reactive Red, an antagonist of both agonist-induced cAMP accumulation and Ca^{2+} mobilisation responses generated by the hP2Y$_{11}$ receptor, is only able to act as an antagonist upon the cAMP response of the XlP2Y$_{11}$ receptor. Similarly, Suramin, shown to fully inhibit the Ca^{2+} response in 1321N1-hP2Y$_{11}$ cells, is unable to reduce agonist-induced Ca^{2+} mobilisation in 1321N1-XlP2Y$_{11}$ and is only partially able to inhibit the agonist promoted cAMP responses within this cell line.

Suramin, shown in Chapter 3 to act as an antagonist on 1321N1-hP2Y$_{11}$ cells, is in agreement with previous studies, where the ligand has been shown to inhibit IP and cAMP responses in 1321N1-hP2Y$_{11}$ and CHO-hP2Y$_{11}$ cells (Communi et al., 1999), and in CHO-cP2Y$_{11}$ cells (Qi et al., 2001[b]). The inability of Suramin to inhibit Ca^{2+} mobilisation and its partial ability to inhibit cAMP accumulation in 1321N1-XlP2Y$_{11}$ cells differs from other P2Y$_{11}$ orthologues studies, where Suramin has been shown to act as a full antagonist (Communi et al., 1999, Qi et al., 2001[b]).

	Ca^{2+} mobilisation		*Cyclic AMP accumulation*	
antagonist	*Log IC_{50}*	IA (%)[a]	*Log IC_{50}*	IA (%)[a]
$hP2Y_{11}$ receptor				
Reactive Red	-3.57 ± 0.17	94.5 ± 1.8	-5.76 ± 0.07	97.4 ± 1.0
Suramin	-4.55 ± 0.15	96.2 ± 1.7		
Acid Blue	ND[b]	2.6 ± 2.2		
Phenol Red	ND	10.3 ± 7.1		
$XlP2Y_{11}$ receptor				
Reactive Red	ND	8.6 ± 6.4	-4.00 ± 0.02	97.7 ± 7.8
Suramin	ND	7.4 ± 6.0	ND	37.2 ± 6.8
Acid Blue			ND	15.6 ± 9.3
Reactive Blue			-4.88 ± 0.05	96.3 ± 10.6

Table 6.3

Antagonism of responses in 1321N1-$hP2Y_{11}$ and 1321N1-$XlP2Y_{11}$ cells.

Log IC_{50} values were calculated after non-linear regression analysis of the antagonist concentration-inhibition experiments. Results are expressed as the mean, ± s.e.m. of three independent experiments, each performed in triplicate. [a] IA, intrinsic affinity, are normalised to show the maximal percentage inhibition of second messenger responses achieved by the antagonist within the range of concentrations tested. [b]ND, not determined, indicates that the responses generated could not be used to calculate an IC_{50} value.

These data suggest a stronger or more efficient coupling of the agonist-activated $XlP2Y_{11}$ receptor, in the presence of antagonist, to the pathways involved in Ca^{2+} release. Alternatively, previous investigations have suggested that UTP and ATP may induce Ca^{2+} mobilisation in 1321N1-hP2Y11 cells by means of different agonist induced pathways (White et al., 2001). The $XlP2Y_{11}$ receptor, in the presence of Suramin, and other antagonists, may be able to promote pathway selective inhibition of second messenger responses - highlighting further complexities involved in the agonist binding and signal induction of the activated $P2Y_{11}$ receptor. However, the small degree of inhibition induced by suramin in 1321N1-$hP2Y_{11}$ and the lack of any recordable inhibition in the 1321N1-$XlP2Y_{11}$ cells may also simply reflect an impure Suramin source.

6.7 Signal transduction of the $XlP2Y_{11}$ and $hP2Y_{11}$ receptors.

Although previous studies of the signalling ability of the $hP2Y_{11}$ and $cP2Y_{11}$ receptors have examined the potency and efficacy of agonists in promoting second messenger signal transduction, the differences in the maximum IP, cAMP and Ca^{2+} responses produced by the most efficacious ligands for each receptor have not been discussed (Zambon et al., 2001; Qi et al., 2001[b]). However, these studies have recorded similar maximal Ca^{2+} mobilisations for both $hP2Y_{11}$ and $cP2Y_{11}$. Antagonist studies have shown that the maximal agonist responses generated by the $cP2Y_{11}$ receptor in both IP and cAMP accumulation assays are higher than those produced by the $hP2Y_{11}$ receptor (Qi et al., 2001[b]). The IP and cAMP responses induced by ADP in the 1321N1-$cP2Y_{11}$ cells are approximately 25 and 40 percent higher (in cAMP and IP accumulation,

respectively) than the maximal responses induced by ATP in the 1321N1-hP2Y_{11} cells.

As my experimental results were normalised to an endogenous control, the degree of the functional response of the XlP2Y_{11} and hP2Y_{11} receptors may be compared directly. A comparison of the ATP-induced cAMP responses is shown in Figure 6.2. These data were presented in Chapters 3 and 4. ATP is only able to induce a cAMP response in the 1321N1-XlP2Y_{11} cells that is approximately one third (30.5 $\pm$ 3.8 percent) of the response seen in 1321N1-hP2Y_{11} cells. Analysis of the Ca^{2+} responses induced by ATP in both 1321N1-hP2Y_{11} and 1321N1-XlP2Y_{11} cells reveals a similar difference in ATP efficacy between the cell lines (data not shown), with ATP inducing a Ca^{2+} maximal response in the 1321N1-XlP2Y_{11} cells that is approximately 23.5 $\pm$ 1.9 percent of the maximal response recorded in the 1321N1-hP2Y_{11} cells.

That the XlP2Y_{11} receptor is unable to induce second messenger responses as strong as those produced by the hP2Y_{11} receptor in both cAMP and Ca^{2+} pathways may be indicative of the receptor's signalling ability. It may also reflect differences in receptor expression levels in the two cell lines. It should also be noted that there are inherent differences between *Xenopus laevis* and human G proteins, which may lead to a reduced coupling efficiency for the amphipian XlP2Y_{11} receptor when expressed in the mammalian 1321N1 cells.

References.

Abbracchio MP, Boeynaems J M, Barnard E A, Boyer J L, Kennedy C, Miras-Portugal M T, King B F, Gachet C, Jacobson K A, Weisman G A and Burnstock G (2003) Characterization of the UDP-Glucose Receptor (Re-Named Here the P2Y14 Receptor) Adds Diversity to the P2Y Receptor Family. *Trends Pharmacol Sci* **24**: pp 52-55.

Abbracchio MP, Burnstock G, Boeynaems J M, Barnard E A, Boyer J L, Kennedy C, Miras-Portugal M T, King B F, Gachet C, Jacobson K A and Weisman G A (2005) The Recently Deorphanized GPR80 (GPR99) Proposed to Be the P2Y15 Receptor Is Not a Genuine P2Y Receptor. *Trends Pharmacol Sci* **26**: pp 8-9.

Adrian K, Bernhard M K, Breitinger H G and Ogilvie A (2000) Expression of Purinergic Receptors (Ionotropic P2X1-7 and Metabotropic P2Y1-11) During Myeloid Differentiation of HL60 Cells. *Biochim Biophys Acta* **1492**: pp 127-138.

Arenzana-Seisdedos F, Fernandez B, Dominguez I, Jacque J M, Thomas D, Diaz-Meco M T, Moscat J and Virelizier J L (1993) Phosphatidylcholine Hydrolysis Activates NF-Kappa B and Increases Human Immunodeficiency Virus Replication in Human Monocytes and T Lymphocytes. *J Virol* **67**: pp 6596-6604.

Bailey MA, Imbert-Teboul M, Turner C, Srai S K, Burnstock G and Unwin R J (2001) Evidence for Basolateral P2Y(6) Receptors Along the Rat Proximal Tubule: Functional and Molecular Characterization. *J Am Soc Nephrol* **12**: pp 1640-1647.

Balboa MA, Firestein B L, Godson C, Bell K S and Insel P A (1994) Protein Kinase C Alpha Mediates Phospholipase D Activation by Nucleotides and Phorbol Ester in Madin-Darby Canine Kidney Cells. Stimulation of Phospholipase D Is Independent of Activation of Polyphosphoinositide-Specific Phospholipase C and Phospholipase A2. *J Biol Chem* **269**: pp 10511-10516.

Balogh J, Wihlborg A K, Isackson H, Joshi B V, Jacobson K A, Arner A and Erlinge D (2005) Phospholipase C and CAMP-Dependent Positive Inotropic Effects of ATP in Mouse Cardiomyocytes Via P2Y11-Like Receptors. *J Mol Cell Cardiol* **39**: pp 223-230.

Bean BP (1992) Pharmacology and Electrophysiology of ATP-Activated Ion Channels. *Trends Pharmacol Sci* **13**: pp 87-90.

Bell RM, Hannun Y A and Loomis C R (1986) Mechanism of Regulation of Protein Kinase C by Lipid Second Messengers. *Symp Fundam Cancer Res* **39**: pp 145-156.

Beltman J, Sonnenburg W K and Beavo J A (1993) The Role of Protein Phosphorylation in the Regulation of Cyclic Nucleotide Phosphodiesterases. *Mol Cell Biochem* **127-128**: pp 239-253.

Berridge MJ, Lipp P and Bootman M D (2000) The Versatility and Universality of Calcium Signalling. *Nat Rev Mol Cell Biol* **1**: pp 11-21.

Bogdanov YD, Dale L, King B F, Whittock N and Burnstock G (1997) Early Expression of a Novel Nucleotide Receptor in the Neural Plate of Xenopus Embryos. *J Biol Chem* **272**: pp 12583-12590.

Bogdanov YD, Wildman S S, Clements M P, King B F and Burnstock G (1998) Molecular Cloning and Characterization of Rat P2Y4 Nucleotide Receptor. *Br J Pharmacol* **124**: pp 428-430.

Boarder MR, Turner JT, Erb L, Weisman GA (1994) Classification of P2 purinoceptors. Not all G protein-coupled P2 purinoceptors can be classed as P2Y. *Trends Pharmacol Sci* **15**: pp 280-281.

Bosanac I, Alattia J R, Mal T K, Chan J, Talarico S, Tong F K, Tong K I, Yoshikawa F, Furuichi T, Iwai M, Michikawa T, Mikoshiba K and Ikura M (2002) Structure of the Inositol 1,4,5-Trisphosphate Receptor Binding Core in Complex With Its Ligand. *Nature* **420**: pp 696-700.

Bosanac I, Michikawa T, Mikoshiba K and Ikura M (2004) Structural Insights into the Regulatory Mechanism of IP3 Receptor. *Biochim Biophys Acta* **1742**: pp 89-102.

Bourne HR (1997) How Receptors Talk to Trimeric G Proteins. *Curr Opin Cell Biol* **9**: pp 134-142.

Bowler WB, Birch M A, Gallagher J A and Bilbe G (1995) Identification and Cloning of Human P2U Purinoceptor Present in Osteoclastoma, Bone, and Osteoblasts. *J Bone Miner Res* **10**: pp 1137-1145.

Bruzzone R (1990) The Molecular Basis of Enzyme Secretion. *Gastroenterology* **99**: pp 1157-1176.

Bultmann R and Starke K (1995) Reactive Red 2: a P2y-Selective Purinoceptor Antagonist and an Inhibitor of Ecto-Nucleotidase. *Naunyn Schmiedebergs Arch Pharmacol* **352**: pp 477-482.

Burnstock G (1972) Purinergic Nerves. *Pharmacol Rev* **24**: pp 509-581.

Burnstock G (1976) Purinergic Receptors. *J Theor Biol* **62**: pp 491-503.

Burnstock G and Kennedy C (1985) Is There a Basis for Distinguishing Two Types of P2-Purinoceptor? *Gen Pharmacol* **16**: pp 433-440.

Burnstock G (1989) Vascular Control by Purines With Emphasis on the Coronary System. *Eur Heart J* **10 Suppl F**: pp 15-21.

Casey PJ (1995) Protein Lipidation in Cell Signaling. *Science* **268**: pp 221-225.

Chen J and Iyengar R (1993) Inhibition of Cloned Adenylyl Cyclases by Mutant-Activated Gi-Alpha and Specific Suppression of Type 2 Adenylyl Cyclase Inhibition by Phorbol Ester Treatment. *J Biol Chem* **268**: pp 12253-12256.

Chen Y, Harry A, Li J, Smit M J, Bai X, Magnusson R, Pieroni J P, Weng G and Iyengar R (1997) Adenylyl Cyclase 6 Is Selectively Regulated by Protein Kinase A

Phosphorylation in a Region Involved in Galphas Stimulation. *Proc Natl Acad Sci U S A* **94**: pp 14100-14104.

Cheng AW, Kong L W, Tung E K, Siow N L, Choi R C, Zhu S Q, Peng B H and Tsim K W (2003) CDNA Encodes Xenopus P2Y(1) Nucleotide Receptor: Expression at the Neuromuscular Junctions. *Neuroreport* **14**: pp 351-357.

Chhatriwala M, Ravi R G, Patel R I, Boyer J L, Jacobson K A and Harden T K (2004) Induction of Novel Agonist Selectivity for the ADP-Activated P2Y1 Receptor Versus the ADP-Activated P2Y12 and P2Y13 Receptors by Conformational Constraint of an ADP Analog. *J Pharmacol Exp Ther* **311**: pp 1038-1043.

Choi SY and Kim K T (1997) Extracellular ATP-Stimulated Increase of Cytosolic CAMP in HL-60 Cells. *Biochem Pharmacol* **53**: pp 429-432.

Churchill GC and Galione A (2001) NAADP Induces Ca2+ Oscillations Via a Two-Pool Mechanism by Priming IP3- and CADPR-Sensitive Ca2+ Stores. *EMBO J* **20**: pp 2666-2671.

Clapham DE and Neer E J (1997) G Protein Beta Gamma Subunits. *Annu Rev Pharmacol Toxicol* **37**: pp 167-203.

Communi D, Pirotton S, Parmentier M and Boeynaems J M (1995) Cloning and Functional Expression of a Human Uridine Nucleotide Receptor. *J Biol Chem* **270**: pp 30849-30852.

Communi D, Motte S, Boeynaems J M and Pirotton S (1996) Pharmacological Characterization of the Human P2Y4 Receptor. *Eur J Pharmacol* **317**: pp 383-389.

Communi D, Parmentier M and Boeynaems J M (1996) Cloning, Functional Expression and Tissue Distribution of the Human P2Y6 Receptor. *Biochem Biophys Res Commun* **222**: pp 303-308.

Communi D, Govaerts C, Parmentier M and Boeynaems J M (1997) Cloning of a Human Purinergic P2Y Receptor Coupled to Phospholipase C and Adenylyl Cyclase. *J Biol Chem* **272**: pp 31969-31973.

Communi D and Boeynaems J M (1997) Receptors Responsive to Extracellular Pyrimidine Nucleotides. *Trends Pharmacol Sci* **18**: pp 83-86.

Communi D, Robaye B and Boeynaems J M (1999) Pharmacological Characterization of the Human P2Y11 Receptor. *Br J Pharmacol* **128**: pp 1199-1206.

Communi D, Suarez-Huerta N, Dussossoy D, Savi P and Boeynaems J M (2001) Cotranscription and Intergenic Splicing of Human P2Y11 and SSF1 Genes. *J Biol Chem* **276**: pp 16561-16566.

Conklin BR, Farfel Z, Lustig K D, Julius D and Bourne H R (1993) Substitution of Three Amino Acids Switches Receptor Specificity of Gq Alpha to That of Gi Alpha. *Nature* **363**: pp 274-276.

Conklin BR and Bourne H R (1993) Structural Elements of G Alpha Subunits That Interact With G Beta Gamma, Receptors, and Effectors. *Cell* **73**: pp 631-641.

Conklin BR, Herzmark P, Ishida S, Voyno-Yasenetskaya T A, Sun Y, Farfel Z and Bourne H R (1996) Carboxyl-Terminal Mutations of Gq Alpha and Gs Alpha That Alter the Fidelity of Receptor Activation. *Mol Pharmacol* **50**: pp 885-890.

Cooper DM, Karpen J W, Fagan K A and Mons N E (1998) Ca(2+)-Sensitive Adenylyl Cyclases. *Adv Second Messenger Phosphoprotein Res* **32**: pp 23-51.

Daly JW, Butts-Lamb P and Padgett W (1983) Subclasses of Adenosine Receptors in the Central Nervous System: Interaction With Caffeine and Related Methylxanthines. *Cell Mol Neurobiol* **3**: pp 69-80.

Danchin A (1993) Phylogeny of Adenylyl Cyclases. *Adv Second Messenger Phosphoprotein Res* **27**: pp 109-162.

de Rooij J, Zwartkruis F J, Verheijen M H, Cool R H, Nijman S M, Wittinghofer A and Bos J L (1998) Epac Is a Rap1 Guanine-Nucleotide-Exchange Factor Directly Activated by Cyclic AMP. *Nature* **396**: pp 474-477.

de Rooij J, Rehmann H, van Triest M, Cool R H, Wittinghofer A and Bos J L (2000) Mechanism of Regulation of the Epac Family of CAMP-Dependent RapGEFs. *J Biol Chem* **275**: pp 20829-20836.

Dean W, Santos F and Reik W (2003) Epigenetic Reprogramming in Early Mammalian Development and Following Somatic Nuclear Transfer. *Semin Cell Dev Biol* **14**: pp 93-100.

Dermott JM and Dhanasekaran N (2002) Determining Cellular Role of G Alpha 12. *Methods Enzymol* **344**: pp 298-309.

Dhanasekaran N and Dermott J M (1996) Signaling by the G12 Class of G Proteins. *Cell Signal* **8**: pp 235-245.

Dixon CJ, Hall J F, Webb T E and Boarder M R (2004) Regulation of Rat Hepatocyte Function by P2Y Receptors: Focus on Control of Glycogen Phosphorylase and Cyclic AMP by 2-Methylthioadenosine 5'-Diphosphate. *J Pharmacol Exp Ther* **311**: pp 334-341.

Douglas WW and Poisner A M (1962) On the Mode of Action of Acetylcholine in Evoking Adrenal Medullary Secretion: Increased Uptake of Calcium During the Secretory Response. *J Physiol (Paris)* **162**: pp 385-392.

Downes GB and Gautam N (1999) The G Protein Subunit Gene Families. *Genomics* **62**: pp 544-552.

Drury AN and Szent-Gyorgyi A (1929) The Physiological Activity of Adenine Compounds with Especial Reference to their Action Upon the Mammalian Heart. *J Physiol* **68**: pp 213-237.

Dubyak GR and el Moatassim C (1993) Signal Transduction Via P2-Purinergic Receptors for Extracellular ATP and Other Nucleotides. *Am J Physiol* **265**: pp C577-C606.

Dunham TD and Farrens D L (1999) Conformational Changes in Rhodopsin. Movement of Helix f Detected by Site-Specific Chemical Labeling and Fluorescence Spectroscopy. *J Biol Chem* **274**: pp 1683-1690.

Erb L, Garrad R, Wang Y, Quinn T, Turner J T and Weisman G A (1995) Site-Directed Mutagenesis of P2U Purinoceptors. Positively Charged Amino Acids in Transmembrane Helices 6 and 7 Affect Agonist Potency and Specificity. *J Biol Chem* **270**: pp 4185-4188.

Evenas J, Malmendal A and Forsen S (1998) Calcium. *Curr Opin Chem Biol* **2**: pp 293-302.

Evenas J, Malmendal A, Thulin E, Carlstrom G and Forsen S (1998) Ca2+ Binding and Conformational Changes in a Calmodulin Domain. *Biochemistry* **37**: pp 13744-13754.

Farahbakhsh ZT, Ridge K D, Khorana H G and Hubbell W L (1995) Mapping Light-Dependent Structural Changes in the Cytoplasmic Loop Connecting Helices C and D in Rhodopsin: a Site-Directed Spin Labeling Study. *Biochemistry* **34**: pp 8812-8819.

Farrens DL, Altenbach C, Yang K, Hubbell W L and Khorana H G (1996) Requirement of Rigid-Body Motion of Transmembrane Helices for Light Activation of Rhodopsin. *Science* **274**: pp 768-770.

Feinstein PG, Schrader K A, Bakalyar H A, Tang W J, Krupinski J, Gilman A G and Reed R R (1991) Molecular Cloning and Characterization of a Ca2+/Calmodulin-Insensitive Adenylyl Cyclase From Rat Brain. *Proc Natl Acad Sci U S A* **88**: pp 10173-10177.

Filtz TM, Li Q, Boyer J L, Nicholas R A and Harden T K (1994) Expression of a Cloned P2Y Purinergic Receptor That Couples to Phospholipase C. *Mol Pharmacol* **46**: pp 8-14.

Fimia GM and Sassone-Corsi P (2001) Cyclic AMP Signalling. *J Cell Sci* **114**: pp 1971-1972.

Frelin C, Breittmayer J P and Vigne P (1993) ADP Induces Inositol Phosphate-Independent Intracellular Ca2+ Mobilization in Brain Capillary Endothelial Cells. *J Biol Chem* **268**: pp 8787-8792.

GAARDER A, JONSEN J, LALAND S, HELLEM A and OWREN P A (1961) Adenosine Diphosphate in Red Cells As a Factor in the Adhesiveness of Human Blood Platelets. *Nature* **192**: pp 531-532.

Galione A, Patel S and Churchill G C (2000) NAADP-Induced Calcium Release in Sea Urchin Eggs. *Biol Cell* **92**: pp 197-204.

Gao BN and Gilman A G (1991) Cloning and Expression of a Widely Distributed (Type IV) Adenylyl Cyclase. *Proc Natl Acad Sci U S A* **88**: pp 10178-10182.

Gearing KL, Barnes A, Barnett J, Brown A, Cousens D, Dowell S, Green A, Patel K, Thomas P, Volpe F and Marshall F (2003) Complex Chimeras to Map Ligand Binding Sites of GPCRs. *Protein Eng* **16**: pp 365-372.

Gordon JL (1986) Extracellular ATP: Effects, Sources and Fate. *Biochem J* **233**: pp 309-319.

Gu C and Cooper D M (1999) Calmodulin-Binding Sites on Adenylyl Cyclase Type VIII. *J Biol Chem* **274** : pp 8012-8021.

Guerini D, Coletto L and Carafoli E (2005) Exporting Calcium From Cells. *Cell Calcium* **38**: pp 281-289.

Hall A (1992) Signal Transduction Through Small GTPases--a Tale of Two GAPs. *Cell* **69**: pp 389-391.

Hannun YA, Loomis C R and Bell R M (1985) Activation of Protein Kinase C by Triton X-100 Mixed Micelles Containing Diacylglycerol and Phosphatidylserine. *J Biol Chem* **260**: pp 10039-10043.

Haraguchi K and Rodbell M (1991) Carbachol-Activated Muscarinic (M1 and M3) Receptors Transfected into Chinese Hamster Ovary Cells Inhibit Trafficking of Endosomes. *Proc Natl Acad Sci U S A* **88**: pp 5964-5968.

Harden TK, Boyer J L and Nicholas R A (1995) P2-Purinergic Receptors: Subtype-Associated Signaling Responses and Structure. *Annu Rev Pharmacol Toxicol* **35**: pp 541-579.

Harnett KM and Biancani P (2003) Calcium-Dependent and Calcium-Independent Contractions in Smooth Muscles. *Am J Med* **115 Suppl 3A**: pp 24S-30S.

Heise C E, O'Dowd B F, Figueroa D J, Sawyer N, Nguyen T, Im D S, Stocco R, Bellefeuille J N, Abramovitz M, Cheng R, Williams D L Jr, Zeng Z, Liu Q, Ma L, Clements M K, Coulombe N, Liu Y, Austin CP, George S R, O'Neill GP, Metters K M, Lynch K R, Evans JF (2000) Characterization of the Human Cysteinyl Leukotriene 2 Receptor. *J Biol Chem* **275**: pp 30531-30536.

Hellevuo K, Yoshimura M, Mons N, Hoffman P L, Cooper D M and Tabakoff B (1995) The Characterization of a Novel Human Adenylyl Cyclase Which Is Present in Brain and Other Tissues. *J Biol Chem* **270**: pp 11581-11589.

Herold CL, Li Q, Schachter J B, Harden T K and Nicholas R A (1997) Lack of Nucleotide-Promoted Second Messenger Signaling Responses in 1321N1 Cells Expressing the Proposed P2Y Receptor, P2y7. *Biochem Biophys Res Commun* **235**: pp 717-721.

Hokin MR and Hokin L E (1953) Enzyme Secretion and the Incorporation of P32 into Phospholipides of Pancreas Slices. *J Biol Chem* **203**: pp 967-977.

Hopkins AL and Groom C R (2002) The Druggable Genome. *Nat Rev Drug Discov* **1**: pp 727-730.

Houslay MD (1998) Adaptation in Cyclic AMP Signalling Processes: a Central Role for Cyclic AMP Phosphodiesterases. *Semin Cell Dev Biol* **9**: pp 161-167.

Inbe H, Watanabe S, Miyawaki M, Tanabe E and Encinas J A (2004) Identification and Characterization of a Cell-Surface Receptor, P2Y15, for AMP and Adenosine. *J Biol Chem* **279**: pp 19790-19799.

Iwami G, Kawabe J, Ebina T, Cannon P J, Homcy C J and Ishikawa Y (1995) Regulation of Adenylyl Cyclase by Protein Kinase A. *J Biol Chem* **270**: pp 12481-12484.

Jacob C, Cottrell G S, Gehringer D, Schmidlin F, Grady E F and Bunnett N W (2005) C-Cbl Mediates Ubiquitination, Degradation, and Down-Regulation of Human Protease-Activated Receptor 2. *J Biol Chem* **280**: pp 16076-16087.

Jacobowitz O, Chen J, Premont R T and Iyengar R (1993) Stimulation of Specific Types of Gs-Stimulated Adenylyl Cyclases by Phorbol Ester Treatment. *J Biol Chem* **268**: pp 3829-3832.

Janssens R, Communi D, Pirotton S, Samson M, Parmentier M and Boeynaems J M (1996) Cloning and Tissue Distribution of the Human P2Y1 Receptor. *Biochem Biophys Res Commun* **221**: pp 588-593.

Jensik PJ, Holbird D, Collard M W and Cox T C (2001) Cloning and Characterization of a Functional P2X Receptor From Larval Bullfrog Skin. *Am J Physiol Cell Physiol* **281**: pp C954-C962.

Jiang Q, Guo D, Lee B X, Van Rhee A M, Kim Y C, Nicholas R A, Schachter J B, Harden T K and Jacobson K A (1997) A Mutational Analysis of Residues Essential for Ligand Recognition at the Human P2Y1 Receptor. *Mol Pharmacol* **52**: pp 499-507.

Johnson RA and Salomon Y (1991) Assay of Adenylyl Cyclase Catalytic Activity. *Methods Enzymol* **195**: pp 3-21.

Jones EA (2005) Xenopus: a Prince Among Models for Pronephric Kidney Development. *J Am Soc Nephrol* **16**: pp 313-321.

Jordan BA and Devi L A (1999) G-Protein-Coupled Receptor Heterodimerization Modulates Receptor Function. *Nature* **399**: pp 697-700.

Kasri NN, Sienaert I, Parys J B, Callewaert G, Missiaen L, Jeromin A and De Smedt H (2003) A Novel Ca2+-Induced Ca2+ Release Mechanism in A7r5 Cells Regulated by Calmodulin-Like Proteins. *J Biol Chem* **278**: pp 27548-27555.

Kaupmann K, Malitschek B, Schuler V, Heid J, Froestl W, Beck P, Mosbacher J, Bischoff S, Kulik A, Shigemoto R, Karschin A and Bettler B (1998) GABA(B)-Receptor Subtypes Assemble into Functional Heteromeric Complexes. *Nature* **396**: pp 683-687.

Kennedy C, Qi A D, Herold C L, Harden T K and Nicholas R A (2000) ATP, an Agonist at the Rat P2Y(4) Receptor, Is an Antagonist at the Human P2Y(4) Receptor. *Mol Pharmacol* **57**: pp 926-931.

Kurose H (2003) Galpha12 and Galpha13 As Key Regulatory Mediator in Signal Transduction. *Life Sci* **74**: pp 155-161.

Lazarowski ER, Homolya L, Boucher RC, Harden TK (1997) Identification of an ecto-nucleoside diphosphokinase and its contribution to interconversion of P2 receptor agonists. *J Biol Chem* **272**: pp 20402-20407.

Liu M and Simon M I (1996) Regulation by CAMP-Dependent Protein Kinease of a G-Protein-Mediated Phospholipase C. *Nature* **382**: pp 83-87.

Lustig KD, Conklin B R, Herzmark P, Taussig R and Bourne H R (1993) Type II Adenylylcyclase Integrates Coincident Signals From Gs, Gi, and Gq. *J Biol Chem* **268**: pp 13900-13905.

Lynch K R, O'Neill G P, Liu Q, Im D S, Sawyer N, Metters K M, Coulombe N, Abramovitz M, Figueroa D J, Zeng Z, Connolly B M, Bai C, Austin C P,

Chateauneuf A, Stocco R, Greig G M, Kargman S, Hooks S B, Hosfield E, Williams D L Jr, Ford-Hutchinson A W, Caskey C T, Evans J F (1999). Characterization of the Human Cysteinyl Leukotriene CysLT1 receptor. *Nature* **399**: pp 789-793.

Malcuit C, Kurokawa M and Fissore R A (2005) Calcium Oscillations and Mammalian Egg Activation. *J Cell Physiol.*

Marshall FH, Jones K A, Kaupmann K and Bettler B (1999) GABAB Receptors - the First 7TM Heterodimers. *Trends Pharmacol Sci* **20**: pp 396-399.

Marteau F, Le Poul E, Communi D, Communi D, Labouret C, Savi P, Boeynaems J M and Gonzalez N S (2003) Pharmacological Characterization of the Human P2Y13 Receptor. *Mol Pharmacol* **64**: pp 104-112.

Mellor EA, Maekawa A, Austen KF, Boyce JA (2001) Cysteinyl Leukotriene Receptor 1 is also a Pyrimidinergic Receptor and is Expressed by Human Mast Cells. *Proc Natl Acad Sci U S A* **98**: pp 7964-7969.

Mellor EA, Frank N, Soler D, Hodge MR, Lora JM, Austen KF, Boyce JA (2003) Expression of the type 2 receptor for cysteinyl leukotrienes (CysLT2R) by human mast cells: Functional distinction from CysLT1R.. *Proc Natl Acad Sci U S A* **100**: pp 11589-11593.

Michell RH (1975) Inositol Phospholipids and Cell Surface Receptor Function. *Biochim Biophys Acta* **415**: pp 81-47.

Milligan G, Parenti M and Magee A I (1995) The Dynamic Role of Palmitoylation in Signal Transduction. *Trends Biochem Sci* **20**: pp 181-187.

Nakamura E, Uezono Y, Narusawa K, Shibuya I, Oishi Y, Tanaka M, Yanagihara N, Nakamura T and Izumi F (2000) ATP Activates DNA Synthesis by Acting on P2X Receptors in Human Osteoblast-Like MG-63 Cells. *Am J Physiol Cell Physiol* **279**: pp C510-C519.

Neer EJ (1995) Heterotrimeric G Proteins: Organizers of Transmembrane Signals. *Cell* **80**: pp 249-257.

Nguyen TD, Meichle S, Kim U S, Wong T and Moody M W (2001) P2Y(11), a Purinergic Receptor Acting Via CAMP, Mediates Secretion by Pancreatic Duct Epithelial Cells. *Am J Physiol Gastrointest Liver Physiol* **280**: pp G795-G804.

Olah ME and Stiles G L (1992) Adenosine Receptors. *Annu Rev Physiol* **54**: pp 211-225.

Patel K, Barnes A, Camacho J, Paterson C, Boughtflower R, Cousens D and Marshall F (2001) Activity of Diadenosine Polyphosphates at P2Y Receptors Stably Expressed in 1321N1 Cells. *Eur J Pharmacol* **430**: pp 203-210.

Paterson JM, Smith S M, Simpson J, Grace O C, Sosunov A A, Bell J E and Antoni F A (2000) Characterisation of Human Adenylyl Cyclase IX Reveals Inhibition by Ca(2+)/Calcineurin and Differential MRNA Plyadenylation. *J Neurochem* **75**: pp 1358-1367.

Post SR, Jacobson J P and Insel P A (1996) P2 Purinergic Receptor Agonists Enhance CAMP Production in Madin-Darby Canine Kidney Epithelial Cells Via an Autocrine/Paracrine Mechanism. *J Biol Chem* **271**: pp 2029-2032.

[a] Qi AD, Kennedy C, Harden T K and Nicholas R A (2001) Differential Coupling of the Human P2Y(11) Receptor to Phospholipase C and Adenylyl Cyclase. *Br J Pharmacol* **132**: pp 318-326.

[b] Qi AD, Zambon A C, Insel P A and Nicholas R A (2001) An Arginine/Glutamine Difference at the Juxtaposition of Transmembrane Domain 6 and the Third Extracellular Loop Contributes to the Markedly Different Nucleotide Selectivities of Human and Canine P2Y11 Receptors. *Mol Pharmacol* **60**: pp 1375-1382.

Ralevic V and Burnstock G (1998) Receptors for Purines and Pyrimidines. *Pharmacol Rev* **50**: pp 413-492.

Salomon Y, Londos C and Rodbell M (1974) A Highly Sensitive Adenylate Cyclase Assay. *Anal Biochem* **58**: pp 541-548.

Schnurr M, Toy T, Stoitzner P, Cameron P, Shin A, Beecroft T, Davis I D, Cebon J and Maraskovsky E (2003) ATP Gradients Inhibit the Migratory Capacity of Specific Human Dendritic Cell Types: Implications for P2Y11 Receptor Signaling. *Blood* **102**: pp 613-620.

Schwartz TW (1994) Locating Ligand-Binding Sites in 7TM Receptors by Protein Engineering. *Curr Opin Biotechnol* **5**: pp 434-444.

Scrivens M and Dickenson J M (2005) Pharmacological Effects Mediated by UDP-Glucose That Are Independent of P2Y14 Receptor Expression. *Pharmacol Res* **51**: pp 533-538.

Simon MI, Strathmann M P and Gautam N (1991) Diversity of G Proteins in Signal Transduction. *Science* **252**: pp 802-808.

Simon V, Robin M T, Legrand C and Cohen-Tannoudji J (2003) Endogenous G Protein-Coupled Receptor Kinase 6 Triggers Homologous Beta-Adrenergic Receptor Desensitization in Primary Uterine Smooth Muscle Cells. *Endocrinology* **144**: pp 3058-3066.

Slakey LL, Gordon E L and Pearson J D (1990) A Comparison of Ectonucleotidase Activities on Vascular Endothelial and Smooth Muscle Cells. *Ann N Y Acad Sci* **603**: pp 366-378.

Snyder SH and Pasternak G W (2003) Historical Review: Opioid Receptors. *Trends Pharmacol Sci* **24**: pp 198-205.

Stephan CC and Sastry B V (1992) Characterization of the Subtype of Muscarinic Receptor Coupled to the Stimulation of Phosphoinositide Hydrolysis in 132-1N1 Human Astrocytoma Cells. *Cell Mol Biol (Noisy -le-grand)* **38**: pp 701-712.

Streb H, Irvine R F, Berridge M J and Schulz I (1983) Release of Ca2+ From a Nonmitochondrial Intracellular Store in Pancreatic Acinar Cells by Inositol-1,4,5-Trisphosphate. *Nature* **306**: pp 67-69.

Strobaek D, Christophersen P, Dissing S and Olesen S P (1996) ATP Activates K and Cl Channels Via Purinoceptor-Mediated Release of Ca2+ in Human Coronary Artery Smooth Muscle. *Am J Physiol* **271**: pp C1463-C1471.

Suh BC, Kim T D, Lee I S and Kim K T (2000) Differential Regulation of P2Y(11) Receptor-Mediated Signalling to Phospholipase C and Adenylyl Cyclase by Protein Kinase C in HL-60 Promyelocytes. *Br J Pharmacol* **131**: pp 489-497.

Sunahara RK, Dessauer C W, Whisnant R E, Kleuss C and Gilman A G (1997) Interaction of Gsalpha With the Cytosolic Domains of Mammalian Adenylyl Cyclase. *J Biol Chem* **272**: pp 22265-22271.

Sutherland EW (1970) On the Biological Role of Cyclic AMP. *JAMA* **214**: pp 1281-1288.

Tang WJ and Gilman A G (1991) Type-Specific Regulation of Adenylyl Cyclase by G Protein Beta Gamma Subunits. *Science* **254**: pp 1500-1503.

Taussig R, Tang W J, Hepler J R and Gilman A G (1994) Distinct Patterns of Bidirectional Regulation of Mammalian Adenylyl Cyclases. *J Biol Chem* **269**: pp 6093-6100.

Taylor SS, Knighton D R, Zheng J, Ten Eyck L F and Sowadski J M (1992) Structural Framework for the Protein Kinase Family. *Annu Rev Cell Biol* **8**: pp 429-462.

Taylor SS, Knighton D R, Zheng J, Ten Eyck L F and Sowadski J M (1992) CAMP-Dependent Protein Kinase and the Protein Kinase Family. *Faraday Discuss* pp 143-152.

Tesmer JJ, Sunahara R K, Gilman A G and Sprang S R (1997) Crystal Structure of the Catalytic Domains of Adenylyl Cyclase in a Complex With Gsalpha.GTPgammaS. *Science* **278**: pp 1907-1916.

Tesmer JJ, Sunahara R K, Fancy D A, Gilman A G and Sprang S R (2002) Crystallization of Complex Between Soluble Domains of Adenylyl Cyclase and Activated Gs Alpha. *Methods Enzymol* **345**: pp 198-206.

Torres B, Zambon A C and Insel P A (2002) P2Y11 Receptors Activate Adenylyl Cyclase and Contribute to Nucleotide-Promoted CAMP Formation in MDCK-D(1) Cells. A Mechanism for Nucleotide-Mediated Autocrine-Paracrine Regulation. *J Biol Chem* **277**: pp 7761-7765.

Tulapurkar ME, Schafer R, Hanck T, Flores R V, Weisman G A, Gonzalez F A and Reiser G (2005) Endocytosis Mechanism of P2Y2 Nucleotide Receptor Tagged With Green Fluorescent Protein: Clathrin and Actin Cytoskeleton Dependence. *Cell Mol Life Sci* **62**: pp 1388-1399.

van Calker D, Muller M and Hamprecht B (1978) Adenosine Inhibits the Accumulation of Cyclic AMP in Cultured Brain Cells. *Nature* **276**: pp 839-841.

van der WL, Adams D J, Luttrell B M, Conigrave A D and Morris M B (2000) Pharmacological Characterisation of the P2Y11 Receptor in Stably Transfected Haematological Cell Lines. *Mol Cell Biochem* **213**: pp 75-81.

van der WL, Conigrave A D and Morris M B (2000) Signal Transduction and White Cell Maturation Via Extracellular ATP and the P2Y11 Receptor. *Immunol Cell Biol* **78**: pp 369-374.

Vignali R, De Lucchini S, Kablar B and Barsacchi G (1994) Genetic Control of Development in Xenopus Laevis. *Genetica* **94**: pp 235-248.

von K, I and Wetter A (2000) Molecular Pharmacology of P2Y-Receptors. *Naunyn Schmiedebergs Arch Pharmacol* **362**: pp 310-323.

Wayman GA, Impey S and Storm D R (1995) Ca2+ Inhibition of Type III Adenylyl Cyclase in Vivo. *J Biol Chem* **270**: pp 21480-21486.

Webb TE, Henderson D, King B F, Wang S, Simon J, Bateson A N, Burnstock G and Barnard E A (1996) A Novel G Protein-Coupled P2 Purinoceptor (P2Y3) Activated Preferentially by Nucleoside Diphosphates. *Mol Pharmacol* **50**: pp 258-265.

Wedegaertner PB, Chu D H, Wilson P T, Levis M J and Bourne H R (1993) Palmitoylation Is Required for Signaling Functions and Membrane Attachment of Gq Alpha and Gs Alpha. *J Biol Chem* **268**: pp 25001-25008.

Wei J, Zhao A Z, Chan G C, Baker L P, Impey S, Beavo J A and Storm D R (1998) Phosphorylation and Inhibition of Olfactory Adenylyl Cyclase by CaM Kinase II in Neurons: a Mechanism for Attenuation of Olfactory Signals. *Neuron* **21**: pp 495-504.

Whisnant RE, Gilman A G and Dessauer C W (1996) Interaction of the Two Cytosolic Domains of Mammalian Adenylyl Cyclase. *Proc Natl Acad Sci U S A* **93**: pp 6621-6625.

White AA and Zenser T V (1971) Separation of Cyclic 3',5'-Nucleoside Monophosphates From Other Nucleotides on Aluminum Oxide Columns. Application to the Assay of Adenyl Cyclase and Guanyl Cyclase. *Anal Biochem* **41**: pp 372-396.

White PJ, Webb T E and Boarder M R (2003) Characterization of a Ca2+ Response to Both UTP and ATP at Human P2Y11 Receptors: Evidence for Agonist-Specific Signaling. *Mol Pharmacol* **63**: pp 1356-1363.

Wong SK (2003) G Protein Selectivity Is Regulated by Multiple Intracellular Regions of GPCRs. *Neurosignals* **12**: pp 1-12.

Xing M, Firestein B L, Shen G H and Insel P A (1997) Dual Role of Protein Kinase C in the Regulation of CPLA2-Mediated Arachidonic Acid Release by P2U Receptors in MDCK-D1 Cells: Involvement of MAP Kinase-Dependent and -Independent Pathways. *J Clin Invest* **99** : pp 805-814.

Yang CM, Tsai Y J, Pan S L, Tsai C T, Wu W B, Chiu C T, Luo S F and Ou J T (1997) Purinoceptor-Stimulated Phosphoinositide Hydrolysis in Madin-Darby Canine Kidney (MDCK) Cells. *Naunyn Schmiedebergs Arch Pharmacol* **356**: pp 1-7.

Yau KW (1994) Cyclic Nucleotide-Gated Channels: an Expanding New Family of Ion Channels. *Proc Natl Acad Sci U S A* **91**: pp 3481-3483.

Yoshioka K, Saitoh O and Nakata H (2001) Heteromeric Association Creates a P2Y-Like Adenosine Receptor. *Proc Natl Acad Sci U S A* **98**: pp 7617-7622.

Yoshioka K, Hosoda R, Kuroda Y and Nakata H (2002) Hetero-Oligomerization of Adenosine A1 Receptors With P2Y1 Receptors in Rat Brains. *FEBS Lett* **531**: pp 299-303.

Zambon AC, Brunton L L, Barrett K E, Hughes R J, Torres B and Insel P A (2001) Cloning, Expression, Signaling Mechanisms, and Membrane Targeting of P2Y(11) Receptors in Madin Darby Canine Kidney Cells. *Mol Pharmacol* **60**: pp 26-35.

Zhang G, Liu Y, Ruoho A E and Hurley J H (1997) Structure of the Adenylyl Cyclase Catalytic Core. *Nature* **386**: pp 247-253.

Zheng Y, Liu H, Coughlin J, Zheng J, Li L and Stone J C (2005) Phosphorylation of RasGRP3 on Threonine 133 Provides a Mechanistic Link Between PKC and Ras Signaling Systems in B Cells. *Blood* **105**: pp 3648-3654.

Zimmerman H (1992) 5'-Nucleotidase: Molecular Structure and Functional Aspects. *Biochem J* **285**: pp 345-365.